AN INVESTIGATION OF SOME HEAT TRANSFER AND GAS FLOW PROBLEMS RELEVANT TO MINIATURE REFRIGERATORS

Thesis submitted for the degree of

Doctor of Philosophy

at Oxford University

Trinity Term 1985

ANNA HELENA ORLOWSKA

KEBLE COLLEGE

Pamięci ojca poswięcam

AN INVESTIGATION OF SOME HEAT TRANSFER AND GAS FLOW PROBLEMS RELEVANT TO MINIATURE REFRIGERATORS

Thesis submitted for the degree of

Doctor of Philosophy

Trinity Term 1985

A.H. ORLOWSKA KEBLE COLLEGE

ABSTRACT

The performance of regenerative miniature refrigerators is governed by heat transfer and pressure drop losses, particularly in the regenerator.

Steady flow experiments have been performed on various regenerator matrices at cryogenic temperatures and heat transfer from helium gas to the matrix, and pressure drop across the matrix have been determined. These data have been found to be in reasonable agreement with data obtained by other workers using transient flow techniques.

In order to determine the applicability of such data to the performance of a cooling engine, experimental methods have been developed to measure the performance and losses in a working Stirling-cycle miniature refrigerator. These techniques have led to the analysis of pressure drop and shuttle heat transfer losses, regenerator efficiency, and to the measurement of other losses in the refrigerator.

An energy balance is performed on the machine.

These novel techniques, which allow the factors determining poor performance of a working refrigerator to be measured in situ, may be applied profitably to other cyclic machines.

ACKNOWLEDGEMENTS

I would like to thank Dr. G. Davey for his supervision during this work, and Dr. C.A. Bailey for the interest he has shown.

There have been many others for whose help I am grateful. In particular, Robert Breen and Dr. Neil Richardson have always offered advice and encouragement and the help of Messrs John Barton, Bryan Skinner, and Ted Tallis has been invaluable.

Finally I would like to thank Mrs Takas', John Mooney and Sue Blake for their help with illustrations, photographs, and tables, respectively.

I have been supported during this study by the S.E.R.C., who funded this research, and also by R.S.R.E., Malvern.

CONTENTS

NOMENCLATURE

A_f	frontal area
A_{fl}	flow area
A_s	surface area
A_w	wall surface area
c	heat capacity
D	diameter
D_h	hydraulic diameter
f	frequency
g	acceleration due to gravity
h	heat transfer coefficient
I	current
I_e	regenerator inefficiency
L	length
L_d	displacer length
m	mass
$\dot{m}$	mass flow rate
P	pressure
Q,q	heat flow
Q_s	shuttle heat transfer
Q_T	total refrigeration
r	radius
R	gas constant
R	electrical resistance
S	displacer stroke
S	entropy
T	temperature

t	width of gap between wall and displacer
V	volume
v	velocity
W	work
W_g	Power available to produce refrigeration
W_{ir}	Losses due to irreversible compression
W_{tot}	total input power

ϵ	regenerator efficiency
η	refrigeration efficiency
λ	penetration depth
μ	viscosity
ρ	density
σ	matrix porosity
τ	time interval

Nu	Nusselt number = $D_h h/k_g$
Re	Reynolds number = $D_h \rho v/\mu$
Pr	Prandtl number = $c_p \mu/k_g$
St	Stanton number = $h/\rho c_p v$

Subscripts

c	cold end
d	displacer
g	gas
h	hot end
in	inlet
ir	irreversible
m	matrix

out	outlet
w	wall

CHAPTER 1

INTRODUCION

1.1 GENERAL INTRODUCTION

There are many systems which can be devised in order to produce a refrigeration effect, [1]. Of these, the predominant means of obtaining temperatures down to about -40°C for both industrial and domestic applications has been the vapour compression cycle machine. Very low (cryogenic) temperatures, below 100K, have in the past been achieved using large scale gas liquefaction plant, the history and development of which have been chronicled by Walker [2], and others, [3,4]. The liquid cryogens produced have then been the source of cooling most often used for laboratory and other applications. In recent years, the development of electronic devices which dissipate small amounts of heat (less than 5W) at low temperatures has called for a new generation of miniature closed-cycle refrigerators, producing a few watts of cooling and requiring only an external power supply. These may be required to operate in remote enviroments such as satellites, or need to be portable for many civil and military applications.

The research described here includes an investigation of the actual, rather than ideal, working cycle of one such closed-cycle cooler, the Stirling-cycle refrigerator, and examines the important role of heat transfer processes on the performance of such a machine.

This work will concentrate on coolers providing refrigeration in the range 8K to 120K, the temperatures required for the satisfactory operation of many semiconducting and some superconducting devices. It will therefore exclude dilution refrigerators and magnetic refrigerators which operate in the milli-Kelvin range, [5], together with thermoelectric and vapour-compression devices, [6], which operate at temperatures only tens of degrees below ambient.

1.2 REFRIGERATION REQUIREMENTS

The demand for coolers to provide small amounts of refrigeration at low temperatures has expanded rapidly in recent years in the fields of space and military sciences, medical diagnosis and treatment, geological and meteorological monitoring, magnetically levitated vehicles, data processing and a wide range of basic research experiments. The majority of applications involve cooling small electronic devices although there are also applications requiring the direct cooling of a material for purposes other than to enhance its electrical properties.

The operating temperature required for an electronic device is dictated by the material from which it is made. Semiconducting devices require cooling in order to reduce thermally induced excitation and obtain a better signal to noise ratio. Superconducting devices require refrigeration to a temperature below the appropriate superconducting transition temperature in order to operate.

Although advances in materials technology are continuously raising acceptable operating temperatures, for both semiconductors and superconductors, [7,8], it is unlikely that it will be possible to dispense with cryogenic refrigeration in the forseeable future.

1.2.1 Remote Cooling Applications

In considering cryogenic cooling for space applications there are many problems that need to be overcome. Structural strength is of great importance as combined thrust and vibration loads in excess of 20g's can be experienced during launch. There is need for reliabilty far higher than required in the laboratory. Typical experiments can cost several millions of dollars and take many years to prepare, so there must be a very high chance of a successful mission to justify the investment of time and money, [9]. Weight, size, and power consumption are also severely constrained.

The increasing number of space instruments that require cryogenic cooling to accomplish their objectives include devices for earth observation, atmospheric science, gamma ray, X-ray and infra-red astronomy, [10]. Cryogenic cooling can be

necessary to provide the required detector response, and to reduce pre-amplifier noise and background radiation. A summary of present day and proposed space borne experiments which require refrigeration is given by Sherman, [11].

In addition to their use for earth observation in satellites, cooled infra-red sensors are also employed for geological surveys from aircraft and have successfully monitored effusive volcanism, detected hot spring activity, and distinguished a variety of geologic materials with physical and compositional differences, [12]. Nakano et al, [13], have reported that superconducting magnetometers, cooled by liquid helium, have been used on the ocean floor to measure the time variation of the earths geomagnetic field, an understanding of which could be employed in earthquake prediction.

Military sensors, for space, air or ground use, which can detect heat from various sources, both human and machine, using cooled infra-red semiconductor devices are of obvious importance in the fields of early warning systems, target identification and collision warning, among others. This kind of detector would also have a large number of civil uses, one of which could be the detection of people in smoke filled rooms by firefighters. These applications are discussed in more detail by Hudson and Hudson, [14], and Hayward, [15].

Many medical diagnostic techniques require cooled detectors. Two examples are thermography, the measurement of body temperature variations that may indicate cancer or cardiovascular problems, [16], and biomagnetism, the detection

of very small magnetic fields in the human body using a superconducting magnetometer, [17]. The technique of using cryogens to freeze small areas of diseased or damaged tissue is also increasingly used, [18]. Haarhuis, [19], describes the cooling needs of superconducting magnets used for Nuclear Magnetic Resonance (NMR) scanning in whole-body imaging.

Fujita et al, [20], describe the refrigeration system of the superconducting magnetically levitated (MAGLEV) vehicles in Japan, where miniature refrigerators are used to compensate for heat leak to the cryostats cooling the superconducting coils.

Very high performance could be obtained from data processing systems employing Josephson junctions that operate at 4.2K. Ultimate system performance would be significantly faster, due to the very fast switching times, short delay, and extremely low power dissipation offered by these junctions. Van der Hoeven and Anacker, [21], who discuss the cooling requirements for such systems state, "It is hoped that further work, specifically in the area of compressor/refrigerator design, efficiency, reliabilty and cost reduction, will be encouraged."

A number of devices, their general function, cooling requirement and operating temperatures are listed in Table (1.1).

The most commonly used methods of providing refrigeration at cryogenic temperatures for the applications outlined above will be discussed in the following chapter.

TABLE 1.1 Cryogenic cooling requirements for spacecraft applications, [22].

APPLICATION	DETECTOR TEMPERATURE K	REFRIGERATION LOAD W
Earth Observation (weather and pollution monitoring, earth resources)	10-100	10^{-3} to 10
Infra-red Astronomy	0.3-10	$(0.05\text{-}0.1)\times10^{-3}$
Radio Astronomy	>4	1
Magnetic Field Measurements	4	$(1\text{-}2)\times10^{-6}$
Superconducting Devices	1-15	wide range
Basic Research Experiments	0-10	< 0.1

CHAPTER 2

CRYOGENIC COOLING SYSTEMS

2.1 POSSIBLE COOLING SYSTEMS FOR REMOTE ENVIRONMENTS

The available methods of providing refrigeration in remote applications are

i) Direct radiation (to deep space)

ii) Stored refrigeration

iii) Open-cycle refrigeration

iv) Closed-cycle refrigeration

2.1.1 Direct Radiation

Radiant coolers offer a simple and reliable, passive, low weight method of cooling for space applications, but are only a practical solution when the cooling load temperature is relatively high. The size of the radiant cooler required increases rapidly with decreasing cooling load temperature, since the rate of heat transfer is proportional to the fourth power of this temperature. For example the same surface area is required to dissipate 1W of heat at 80K as nearly 200W at 300K. Typical operating temperatures for radiant coolers are

of the order of 100K, [23]. Although lower temperatures can theoretically be maintained against low loads, the constraints imposed on the spacecraft orientation together with the increasing radiator area required make this development impractical. However, these coolers have been developed succesfully for use with low dissipation infra-red detectors and are discussed by Donohoe et al, [24]. The application of radiant coolers to cool radiation shields for cryostat insulation in systems using liquid cryogen refrigeration is described by Kislov et al, [25].

2.1.2 Stored Cryogen Refrigeration

Stored refrigeration in the form of solid or liquid cryogens is the method of cooling most often used for laboratory experiments, cryogenic surgery, [18], and many space experiments. These systems have the advantages of simple design, high reliability, and the elimination of many zero gravity considerations. Temperatures between 48K and 63K can be reached with solid nitrogen, 13K to 24K with solid neon, and 8K to 13K with solid hydrogen. For lower temperatures liquid helium below 2.1K, the lambda point, has many properties such as high thermal conductivity and almost zero viscosity which make it the prime choice for cooling. Karr et al, [26], describe the cryogenic refrigeration system used to cool the infra-red telescope for the Shuttle SpaceLab 2 mission which employs liquid helium to provide cooling at temperatures in the range 2K to 60K at different heat stations.

Lifetimes of up to one year have been achieved with stored cryogen systems by reducing heat leaks to the instrument with well designed cryostats, [11], but these systems will always have the major disadvantages of weight and limited life.

Liquid cryogen cooling is adequate for much medical equipment at present used in laboratories such as the liquid helium cooled superconducting magnetic field detectors used in biomagnetism, and the liquid nitrogen cooled "cryoprobes" used in cryogenic surgery. There is no doubt that a greater number of people would benefit if a suitable portable closed-cycle cooler was to be developed and the equipment could be used outside the confines of a hospital.

2.1.3 Open-cycle Refrigeration

Open-cycle systems such as Joule-Thomson coolers, which use the fall in temperature experienced on expansion by a gas held below its inversion temperature, can produce very low temperatures and are at present used in many small scale applications, [15], and often as the principle means of refrigeration in large scale liquefaction plant. Expansion of nitrogen in a single-stage cooler can produce temperatures below 80K and further hydrogen and helium stages can reach temperatures below 3K, [22]. However, in common with stored cryogen systems, the performance of Joule-Thomson refrigerators is limited by storage capacity. The gas may be at a pressure of several hundred atmospheres and would require heavy storage cylinders. The level of reliability is high,

providing that there are no impurities in the gas which could freeze out and block the expansion valve. Higa and Wiebe, [27], describe Joule-Thomson coolers which together have operated for over one million hours, although some routine maintenance has been performed.

2.1.4 Closed-cycle Mechanical Refrigerators

The space craft constraints on weight and volume and the desire for lifetimes of five years or more for both space and other remote applications, point to closed-cycle mechanical refrigerators as the preferred, and sometimes the only possible, means of achieving cooling. These coolers reject heat at a high enough temperature for dissipation using practical radiant coolers, and can provide refrigeration over a wide range of temperatures.

The main drawbacks experienced with mechanical refrigerators are lack of reliability, the need for a power supply, and possible vibration, caused by reciprocating masses, which may prove unacceptable for some applications. Although these systems are more complex, because of moving parts, and therefore inherently less reliable than storage or open-cycle systems, in practice this may be of little consequence providing that the refrigerator can demonstrate a mean time between start up and failure several times greater than the endurance of a stored system. Naes and Nast, [28], reported in June 1980 that four mechanical refrigerators had been operating since February 1979 providing orbital cooling of two gamma-ray spectrometers. The systems had not failed,

although there had been some degradation of performance due to leakage of the helium working gas.

Much research effort has been concentrated on these problems in recent years as the demand for reliable mechanical closed-cycle miniature refrigerators has grown. Although a great deal of progress has been made, especially in the areas of reliability and vibration, many problems, including that of low efficiency, are still to be overcome.

Table (2.1) compares the useful operating ranges of the cooling systems described above. It must be noted that for the shorter missions, such as the 7 to 30 day Shuttle journeys, the stored cryogen systems listed in Table (2.1) could support greater refrigeration loads.

2.2 MINIATURE REFRIGERATORS

The refrigeration cycles employed in gas liquefaction plant such as the Claude and Hampson cycles described by, for example, Grenier, [29], are not always suitable for miniaturisation. In general this is because the conventional heat exchangers used would be both very difficult to manufacture on a miniature scale and vulnerable to blockage of the flow passages by any impurities in the working fluid. Other liquefaction cycles, such as the Brayton cycle, [6], also employ turbo-expanders which require very high operating speeds, (over 10^5rpm).

The most successful cryocoolers, the Stirling, Vuilleumier and Gifford-McMahon machines, employ regenerative cycles, requiring few moving parts at low temperature and using periodic heat exchangers known as regenerators.

2.2.1 Thermal Regenerators

The thermal regenerator is an energy storing device which connects two regions of different temperatures and therefore maintains a temperature gradient along its length. In operation, the gas flow through the regenerator is heated or cooled, depending on flow direction. The energy taken from the gas is stored in the regenerator packing (or matrix) and recovered by the gas flow in the reverse direction during the following part of the cycle. The heat capacity of the matrix is generally such that its temperature profile is only slightly altered by providing energy to the gas. In order to achieve this the regenerator consists of a porous material with a high ratio of surface area to volume, a high heat capacity, and a low conductivity in the direction of flow. Examples of regenerator materials are small bronze or lead spheres or stacked wire mesh screens made of stainless steel or bronze.

There are several advantages of regenerators over conventional heat exchangers for use in miniature refrigerators;

i) Size and efficiency - Regenerators can be made much smaller and more efficient than counterflow heat exchangers, [30]. For example overall efficiencies of 99% are necessary and can be achieved in a regenerator 5cm long, whereas it is difficult to achieve an efficiency of 97% in a very much larger counterflow heat exchanger.

ii) Construction and cost - Regenerator construction is much simpler than that of counterflow heat exchangers, which tend to involve small finned tubes or baffles, and therefore regenerators are considerably cheaper to make.

iii) Insensitivity to plugging - Thermal regenerators are much less sensitive to plugging from condensible impurities in the working gas than are conventional heat exchangers even though the gas flow passages are 10 to 20 times smaller in the regenerator. The reversing flow at varying pressure flushes the condensable impurities out of the matrix.

iv) Simplification - The use of regenerators can lead to the simplification of the design and construction of miniature refrigerators.

Thermal regenerators have been used as air preheaters in open hearth and blast furnaces for many years, [31], and at very high temperatures (>1000°C) in gas turbines, [32], but the operating speeds and efficiencies required for miniature refrigerator use are far greater than those acceptable for air preheating, while the space available is very limited. The theories of operation, and materials used, for these large scale regenerators are not always applicable to those used in

cryocoolers.

2.2.2 IDEAL REFRIGERATION

Consider the ideal representation of a refrigerator illustrated in Figure (2.1).

A quantity of heat, Q_1, is absorbed from the cold reservoir at temperature T_1. In accordance with the First Law and the principle of conservation of energy, Q_1, together with the heat equivalent of the work done, W, must be rejected to the hot reservoir (normally the surroundings) at temperature T_2. The Clausius statement of the Second Law states that no process is possible whose sole result is the transfer of heat from a colder to a hotter body, so that $W > 0$.

The performance of a refrigerator is usually expressed in terms of the Coefficient of Performance (COP), defined as the ratio of the heat lifted by the refrigerator to the work done.

$$COP = \frac{Q_1}{W} = \frac{Q_1}{Q_2 - Q_1}$$

The highest possible COP for a refrigerator operating between given temperatures will be that achieved by a system which executes a reversible cycle, as postulated by Carnot, [33], where,

$$\frac{Q_1}{Q_2-Q_1} = \frac{T_1}{T_2-T_1} \qquad (2\text{-}1)$$

The Carnot cycle, consisting of two isentropic and two isothermal processes, is shown in Figure (2.2). From the Second Law,

$$dQ_{rev} = TdS$$

hence, for the cycle,

$$Q_1 = T_1\Delta S$$

$$Q_2 = T_2\Delta S$$

and $W = (T_2-T_1)\Delta S$

hence

$$COP_{Carnot} = \frac{T_1}{T_2-T_1} \qquad (2\text{-}2)$$

It can be seen that the quantity of work neccesary per unit of refrigeration increases dramatically as the refrigeration temperature decreases. For the Carnot cycle system, with T_2= 300K, the work per unit refrigeration is 2 watts per watt at 100K, 29 watts per watt at 10K and 299 watts per watt at 1K.

The performance of the reversible ideal cycle is the standard by which other refrigeration cycles are normally judged, although in practice efficiencies fall well below these ideal figures.

2.2.3 The Stirling Cycle

If the isentropic processes of compression and expansion in the Carnot cycle are replaced by constant volume processes then it becomes the Stirling Cycle. This cycle was first devised as an engine by Stirling in 1816 and was reversed to produce a cooling machine by Kirk in 1874, [34].

A schematic diagram of an idealised Stirling cycle refrigerator is shown in Figure (2.3). It consists of two chambers, the compression space (at constant high temperature T_2), and the expansion space (at constant low temperature T_1), separated by a regenerator which acts as a heat store and maintains a temperature gradient along its length. In order to improve heat transfer from the compression and expansion spaces to the surroundings, hot and cold end heat exchangers adjacent to the cylinders are included. The working fluid, normally helium gas, is taken through the cycle by the reciprocating motion of a piston and a displacer, or in the earliest machines, [3], by two opposed pistons as shown in Figure (2.4). The ideal Stirling cycle consists of the following stages, illustrated in the diagrams for a two-piston machine in Figure (2.5), and in the P-V and T-S diagrams in Figure (2.6).

Step 1 - The gas, which is all in the compression (hot) space, is compressed by Piston A. Heat is dissipated to the surroundings, an isothermal process at temperature T_2.

Step 2 - Both pistons move, forcing the gas through the regenerator and into the expansion space (at the 'cold end'). Heat is transferred from the gas to the regenerator material, a constant volume process.

Step 3 -Piston B moves, the gas expands and heat is absorbed from the surroundings, an isothermal process at temperature T_1. This is the useful refrigeration in the cycle.

Step 4 - Both pistons move back, forcing the gas through the regenerator and into the compression space. Heat is transferred from the regenerator material to the gas, a constant volume process.

The cycle is repeated.

2.2.4 The Vuilleumier Cycle

The Vuilleumier cycle, Figure (2.7), is closely related to the Stirling cycle but has no mechanical compressor. Compression is brought about by thermal means, using a second displacer and regenerator and a heat source, usually electric. The transfer of gas at constant total volume between a heated and a cooled space, using the displacers to force it through the regenerators, causes the pressure to change. In order to achieve refrigeration the phase between the displacers is controlled so that the working gas is concentrated in the cold

end space when the pressure is decreasing from its maximum to its minimum value. Vuilleumier cycle machines can operate with no external source of work, but generally a small work input is provided to facilitate starting and maintain the required operating frequency. Because compression is provided by heating the working gas at constant volume, pressure ratios are limited and the cycle efficiency reduced.

2.2.5 The Gifford-McMahon Cycle

The Gifford-McMahon refrigerator, shown schematically in Figure (2.8), consists of a compressor and displacer separated by valves operating at ambient temperature. The operating cycle is as follows.

With the displacer in its lowest position, the inlet valve opens and the temperature of the gas in the compression space (V_c) rises due to isentropic compression. The displacer is then moved to its highest position, forcing the gas into the expansion space (V_e) through the regenerator. The inlet valve is then closed and the exhaust valve opened. The gas in V_e expands and its temperature falls, as it does work on the gas on the other side of the exhaust valve. The displacer then returns to its lowest position, forcing the cold gas partly into V_c and partly to the surroundings. The exhaust valve is closed and the cycle is repeated.

The main advantage of this system is that the valves effectively isolate the compressor and therefore remove the principle source of heat and vibration from the "cold finger" (that part of the refrigerator containing the displacer and

expansion space). Conventional oil lubricated compressors can be used for Gifford-McMahon machines where there is no danger of oil escaping to the cold end and contaminating the system, which precludes their use in Stirling or Vuilleumier refrigerators.

There are many other possible mechanical refrigerator systems such as the pulse tube, a comprehensive account of which is given by Richardson, [35], and other cycles discussed by Radebaugh, [1], and Walker, [2]. The cycles described above are those which are most widely used for commercial and laboratory mechanical cooling applications, and on which most research has concentrated. Chellis, [36], discusses these coolers and describes their relative advantages and disadvantages.

The efficiencies of some of the most commonly used commercially produced mechanical cooling systems are compared in Table (2.2). It can be seen that the Stirling cycle machines are in general lighter and more efficient than the Vuilleumier and Gifford-McMahon machines, but that the efficiencies of all these refrigerators are low.

2.3 THE DEVELOPMENT OF MINIATURE REFRIGERATORS

In the century or so since Kirk first reversed the Stirling engine and ran it as a refrigerator in 1874, there has been a great deal of development and progress in the effort to make smaller, more efficient and reliable machines which can reach, and give useful refrigeration at, ever lower

temperatures. The history of the first attempts to liquefy air and its constituent gases is given by many authors, including Kohler and Jonkers, [37], and Walker, [2]. This section will confine itself to a description of the major changes in the design of miniature refrigerators that have led to an improvement in their performance.

Early Stirling-cycle refrigerators employed two opposing pistons to produce the required volume variations in the cylinders. The replacement of this arrangement by a piston and displacer has eliminated the need for a cold end sealing mechanism. The pressure drop across a piston is large, so that a sliding seal arrangement must be provided in order to prevent gas from leaking past the piston and having a detrimental effect on the performance of the cooler. If a displacer is used the pressure drop accross it is much smaller and gas leaks can be kept acceptably low by having a narrow clearance gap between the displacer and the cylinder wall. This arrangement has the added advantage of reducing mechanical friction losses. The moving displacer does however introduce an additional thermal loss, the 'shuttle heat transfer' loss, which will be discussed in Chapter Three.

The development of the rhombic drive mechanism, described by Meijer, [38], which by using an arrangement of cranks and balance wheels gives the necessary phased movement to the piston and displacer and can eliminate unbalanced linear or angular forces, and its replacement by the linear drive mechanism, driving the piston and displacer separately, have significantly reduced problems of vibration and lubrication.

Linear drive is simpler, and therefore inherently more reliable than rhombic drive, and can lead to oil-free compressors using gas, [39], or magnetic, [40], bearings, or the flat spring suspension developed by Davey, [41]. Compressor efficiencies (defined here as the ratio between the power supplied to the gas, by the piston, to the electrical power supplied to the compressor) of up to 80% have been achieved.

Vibration at the cold end has been further minimised by the adoption of 'split-cycle' Stirling and Vuilleumier machines in which the compressor is separated from that part of the refrigerator which contains the displacer and regenerator, [42]. Gifford-McMahon machines have always had this advantage. The separation is limited by the dead volume of the link pipe between the cylinders as this has a detrimental effect on refrigerator performance, [43].

The design of cryocoolers has been greatly simplified by combining the displacer and regenerator in a single assembly. Either the regenerator matrix is contained within the displacer, [44], or a 'gap' regenerator is used, [45]. This employs no separate thermal store but forces the gas to flow through the annular gap between the displacer and the surrounding cylinder. The thermal capacity of the displacer and cylinder wall surfaces provides the regenerative mechanism.

Temperatures as low as 45K were reached by Kohler, [3], and other workers, using Stirling machines. Lower temperatures seemed unattainable until Prast, [46], developed a two stage expansion process using a stepped displacer. By expanding the gas in a number of stages and providing refrigeration at one or more intermediate levels, the cycle as a whole becomes more efficient. Prast states that the total COP relative to Carnot efficiency can be given by,

$$\eta_t = \eta_1 \eta_2 \qquad (2-3)$$

The lowest temperature achieved by the first two-stage Stirling machines was 12K, [46], and three-stage Stirling and Gifford-McMahon refrigerators have reached 8.5K and below, [44], [47]. Hung, [48], reports that, in China, a two stage Gifford-McMahon cooler has also reached 8.5K. An infinite-stage machine, with a conical displacer, has been suggested as the logical follower to these two-stage and three-stage coolers. Myrtle et al, [49], report on such a conical Stirling-cycle refrigerator which has reached 9K but at present this is not a practical device due to its size and slow rate of cool down.

The lowest temperature attainable by a regenerative refrigerator is limited by the heat capacity of the regenerator material. Metals, such as bronze or stainless steel, although adequate in regenerator matrices at temperatures down to 80K, have specific heats that follow the Debye model,

$$c_p \propto \left[\frac{T}{\theta_D}\right]^3 \qquad (2\text{-}4)$$

where θ_D is the Debye temperature of the metal, [5]. Clearly materials with a low Debye temperature are desirable for low temperature work. Lead, which has a Debye temperature of 83K, is the matrix material used in the coldest regenerators of the multiple stage machines. The discovery and development of rare earth compounds, such as europium sulphide, [44], which have specific heat anomalies in the 5K to 20K temperature range, may make lower refrigeration temperatures possible. Experiments with a matrix composed of GdRh and GdErRh, described by Nakashima et al, [50], have produced cooling to 3.74K. However, this temperature was not achieved in a working refrigerator but in apparatus which used boil-off gas from a liquid helium reservoir to cool gas to 10K before it entered the regenerator. The geometry of the matrix was not described. Zimmerman, [45], has reported on a Stirling cooler that has succeeded in liquefying helium using gap regeneration, however, at present this refrigerator has a low cooling capacity, is very large and therefore is not a practical alternative to the Joule-Thomson devices normally used in this range.

A compromise combined system, using a closed cycle refrigerator to cool gas which then passes through a Joule-Thomson expansion valve, such as those described by Vincent, [51], and Higa and Wiebe, [27], who use Gifford-McMahon coolers for the first stage, provides the most

practical solution presently available to the problem of refrigeration at temperatures below 5K.

The development work described above has been carried out over decades, but the best coolers available today are still only 5% efficient (where efficiency is defined as the useful refigeration obtained over the input power to the machine). The causes of this poor performance are not fully understood despite the fact that these devices are being developed commercially. Clearly there is scope for considerable further investigation of these machines, particularly in respect of the actual, rather than ideal, operating cycle, and the function of the heat exchange components, including the regenerator.

This study devotes particular attention to these areas and includes an investigation of the refrigerator energy balance.

Although the following chapters discuss mainly Stirling-Cycle refrigerators, most of the problems covered are common to, and the discussion relevant to, all small regenerative coolers.

TABLE 2.1 Spacecraft Cryogenic Cooling Techniques [52]

Cooling Method	Practical Temperature Range K	Usable Cooling Load for One Year Mission W
Radiant Coolers	70-100	0.01
Solid Stored Cryogens	10-90	0.8
Mechanical Coolers	4-100	0.3
Stored Liquid Helium	1.5-5.2	0.1

Figure 2.1 Ideal Refrigerator

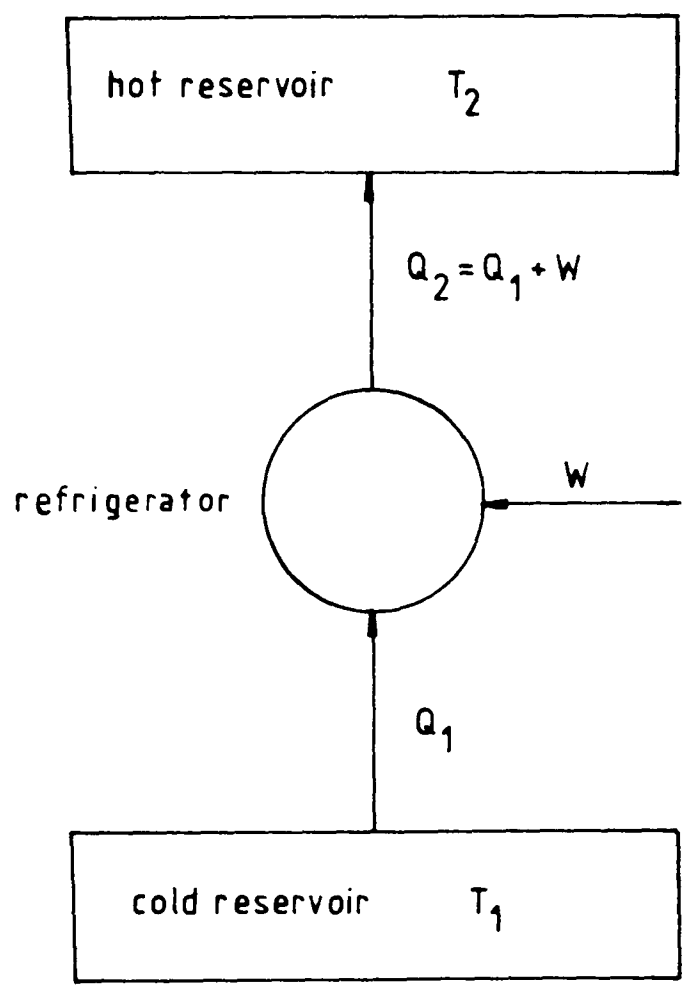

Figure 2.2 Carnot Cycle P-V and T-S Diagrams

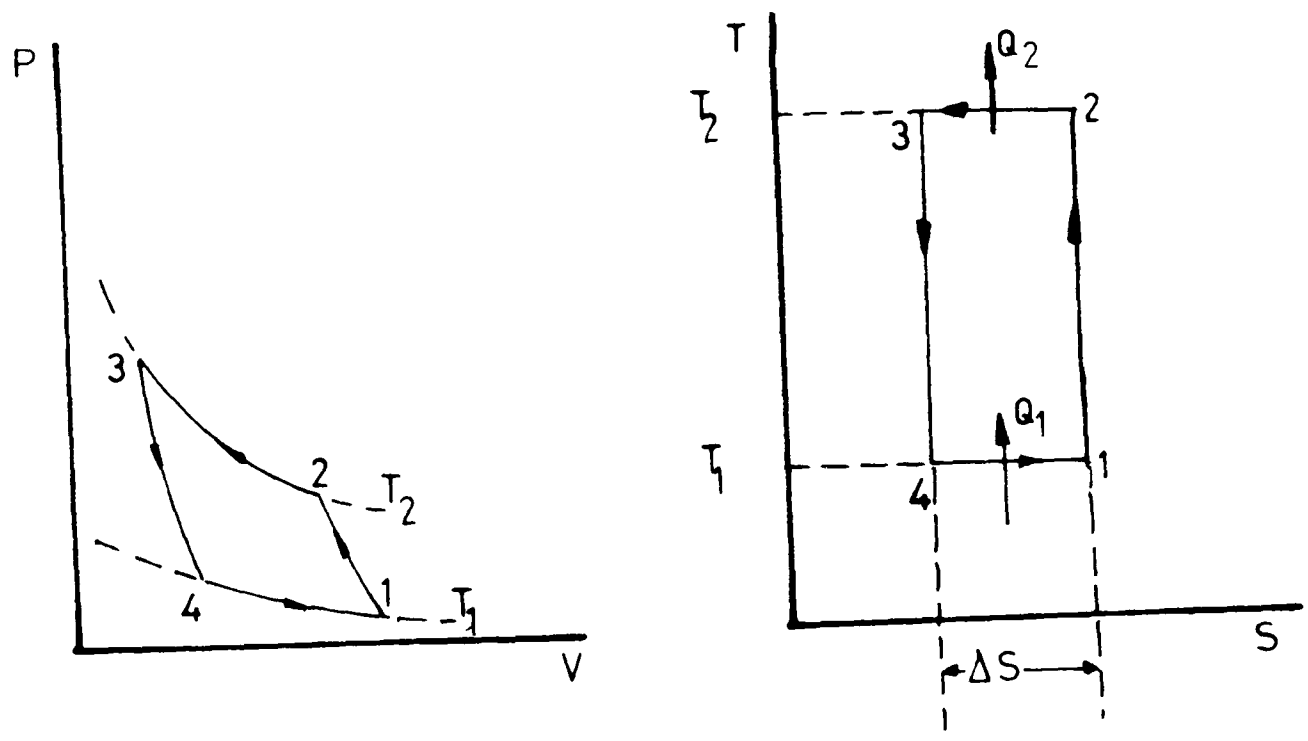

Figure 2.3 Stirling Cycle Refrigerator (piston-displacer)

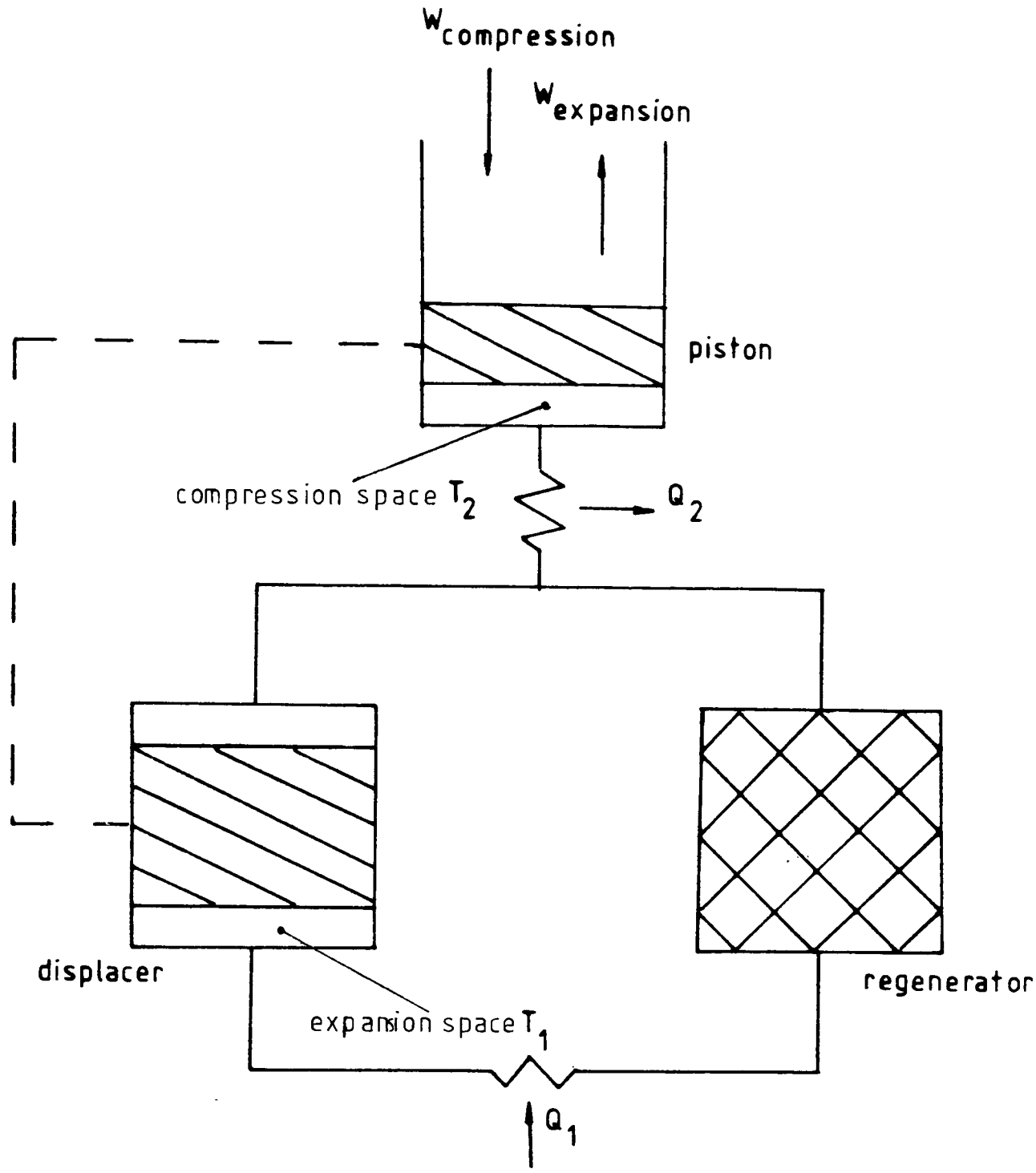

Figure 2.4 Stirling Cycle Refrigerator (two-piston)

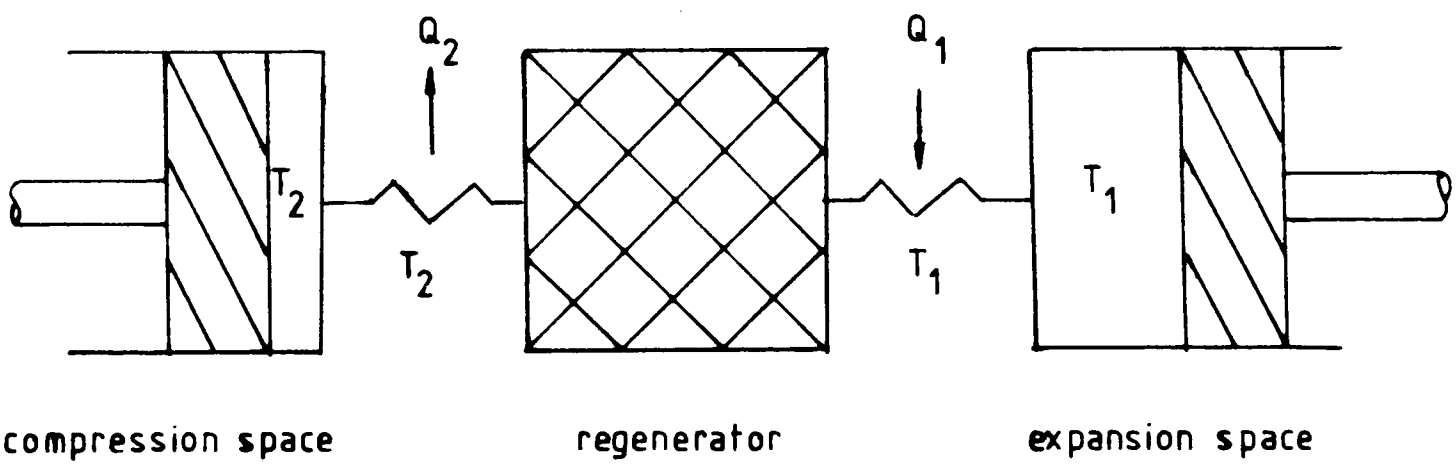

Figure 2.5 The Stirling Cycle

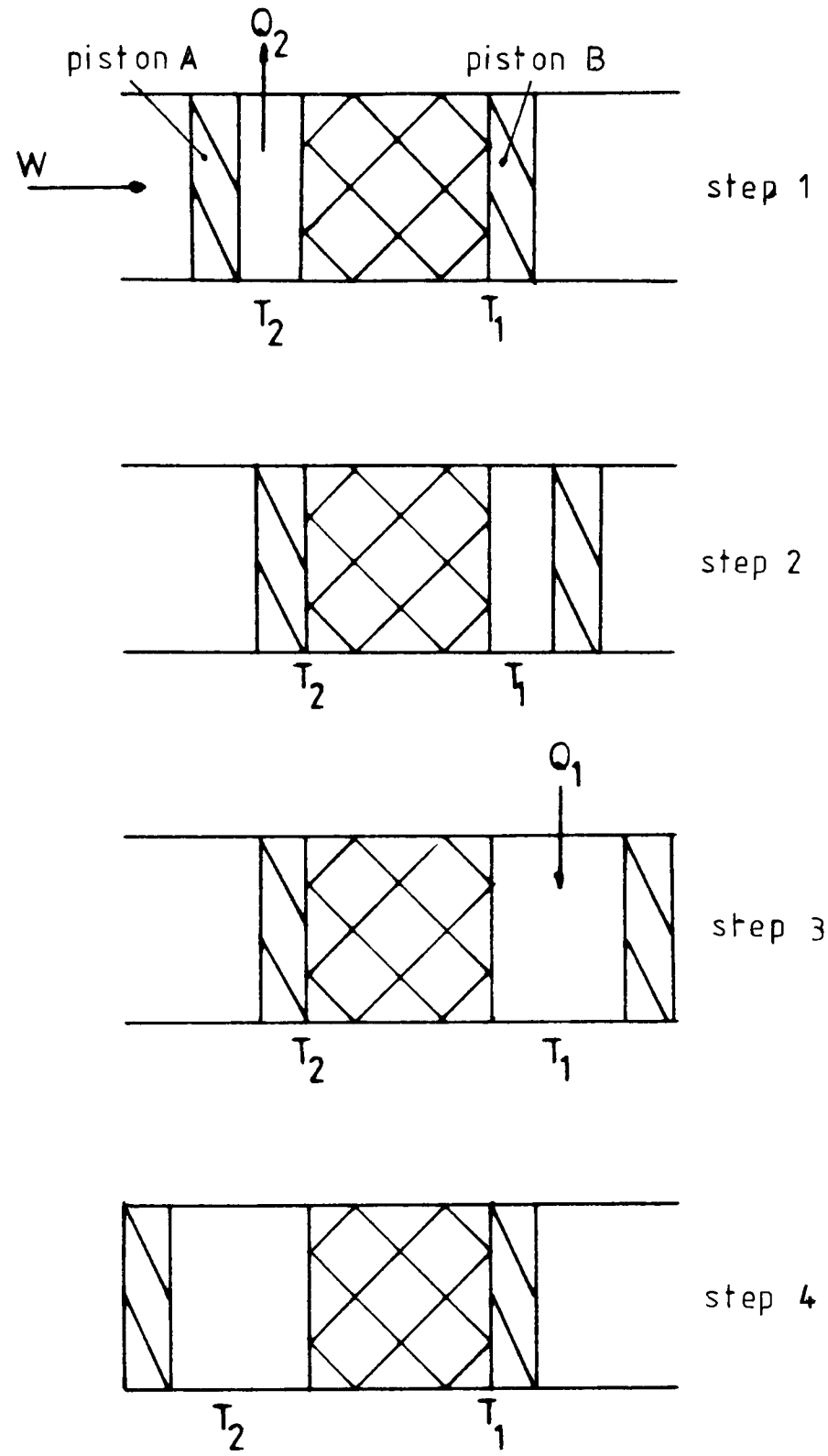

Figure 2.6 Stirling Cycle P-V and T-S Diagrams

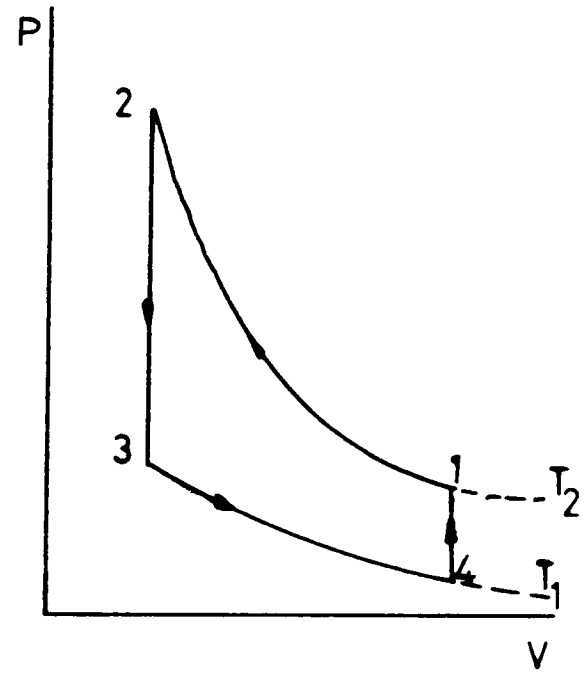

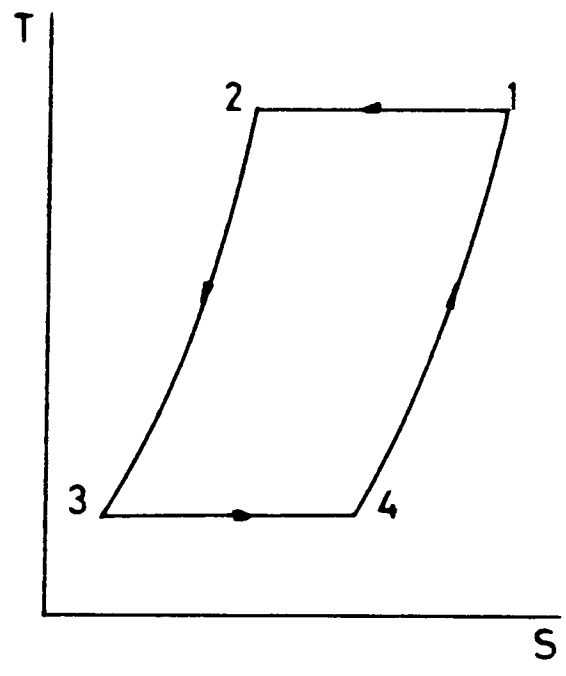

Figure 2.7 Vuilleumier Refrigerator

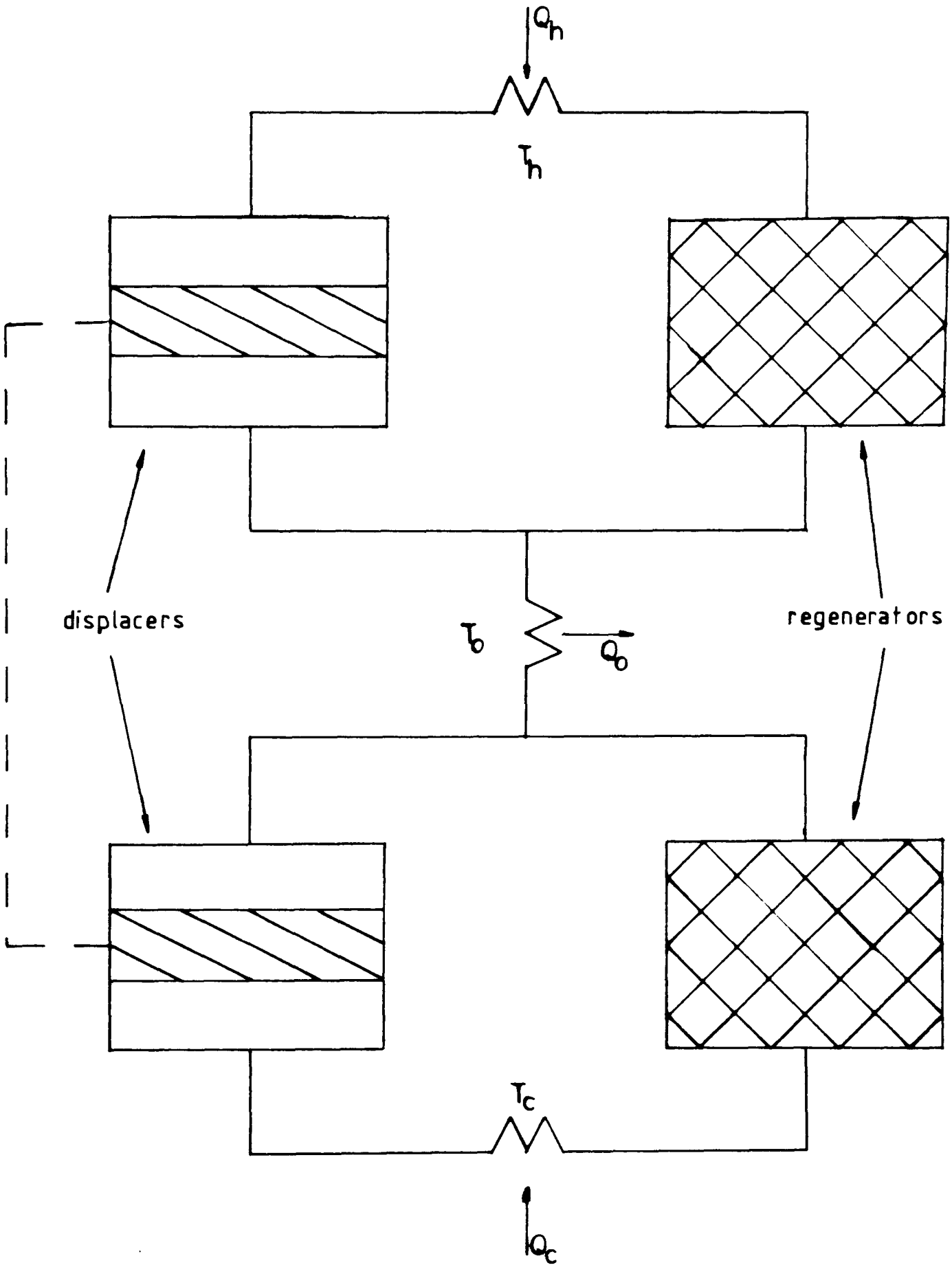

Figure 2.8 Gifford-McMahon Refrigerator

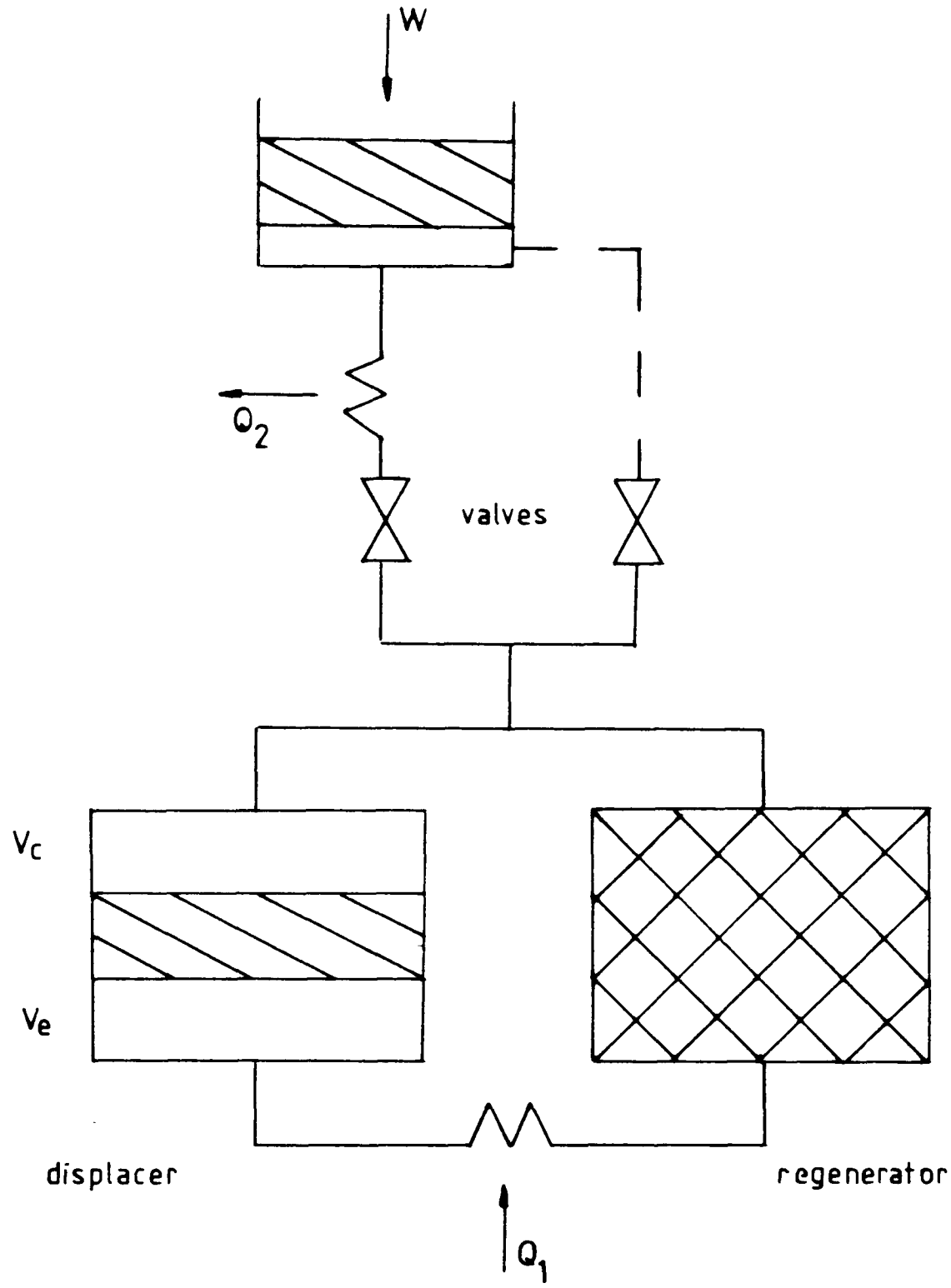

TABLE 2.2 Comparison of Small 77K refrigerators

(after Chellis [2])

CYCLE	POWER SOURCE	COOLING CAPACITY 77K (W)	SPEED (Hz)	WEIGHT (Kg)	INPUT POWER (W)	EFFICIENCY
STIRLING	400Hz ac	0.9	29.2	1.5	90	0.010
	400Hz ac	1.5	29.2	1.8	120	0.010
	28V dc	1.0	27.0	3.5	42	0.024
	400Hz ac	3.5	29.2	3.0	180	0.019
	400Hz ac	3.0	-	5.5	530	0.006
VUILLEUMIER	400Hz ac	2.0	10.0	6.4	340	0.006
	400Hz ac	1.0	10.0	2.9	125	0.008
	28V dc	1.0(85K)	-	3.2	120	0.008
	28V dc	1.0	7.5	2.8	90	0.011
GIFFORD-McMAHON	400Hz ac	5.0	5.6	6.8	575	0.009

CHAPTER 3

THE STIRLING CYCLE: ANALYSIS AND LOSSES

3.1 THE IDEAL CYCLE

Consider the P-V and T-S diagrams for an ideal Stirling cycle refrigerator in Figure (2-6).

Stage one - Isothermal compression at temperature T_2 (From point 1 to point 2 on the diagrams).

Work is done on the gas,

$$W = P_1 V_1 \ln(V_{min}/V_{max})$$

From the First Law, this is the heat rejected to the surroundings

$$P_1 V_1 \ln(V_{min}/V_{max}) = RT_2 \ln(V_{min}/V_{max})$$

$$= W = Q$$

and the change in entropy,

$$S_1 - S_2 = R\ln(V_{min}/V_{max})$$

Stage Two - Constant volume regenerative cooling process (Point 2 to point 3 on the diagrams). Heat is transferred from the working fluid to the regenerator matrix. No work is done and there is a decrease in the internal energy and entropy of the fluid.

Heat transferred = $C_v(T_2 - T_1)$

Change in entropy = $S_3 - S_2 = Cv\ln(T_1/T_2)$

Stage Three - Isothermal expansion at temperature T_1 (Point 3 to point 4 on the diagrams). Heat is supplied to the fluid from the surroundings and work is done by the fluid.

Heat transferred = Work done

$= P_3V_3\ln(V_{max}/V_{min})$

$= RT_1\ln(V_{max}/V_{min})$

and the change in entropy = $R\ln(V_{max}/V_{min})$

Stage Four - Constant volume regenerative heat transfer process. Heat is transferred to the working fluid from the regenerator matrix, raising the fluid temperature from T_1 to T_2 (Point 4 to point 1 on the diagrams).

Heat transferred = $Q = C_v(T_2 - T_1)$

Change in entropy = $S_1 - S_4 = C_v\ln(T_2/T_1)$

The COP of the refrigerator is given by,

$$\text{COP} = (\text{Heat lifted})/(\text{Work done})$$

$$= \frac{RT_1 \ln(V_{max}/V_{min})}{RT_2 \ln(V_{max}/V_{min}) - RT_1 \ln(V_{max}/V_{min})}$$

$$= T_1/(T_2 - T_1) \qquad (3\text{-}1)$$

which is the same as the Carnot COP for a refrigerator working between the same temperatures.

Obviously the working fluid in a real Stirling-cycle cooler cannot all be instantaneously in either the compression space or the expansion space, as required by the ideal model, as there will always be fluid in the flow channels of the regenerator and the link pipe between the cylinders. For this reason the fluid cannot all be in the same thermodynamic state (except when the machine is not working and is at ambient temperature). It is therefore not possible to represent the state of the fluid on one P-V diagram and separate diagrams for the compression space and the expansion space are usually drawn.

The effect of the dead volume on the performance of the machine is to reduce the volume compression ratio, V_{max}/V_{min}, and the pressure ratio, P_{max}/P_{min}.

It is not impossible to achieve the discontinuous piston and displacer motions assumed in the ideal Stirling cycle, but very elaborate mechanisms are necessary. For this reason simple harmonic motion is almost universally used in practical working refrigerators. The variation of piston and displacer movement with time can be seen in Figure (3.1), and the effect that the simple harmonic movement and dead volume have on the P-V diagrams for the compression space and the expansion space is shown in Figure (3.2).

The area of the P-V diagrams is the work done by the gas or on the gas. The difference between the areas of the compression space and expansion space diagrams is the net work of the cycle. In a refrigerator the compression space work, the work done on the gas, is greater than the expansion space work, the work done by the gas (i.e. the refrigeration effect), so work must be supplied to the cycle (thus obeying the Second Law).

3.1.1 The Schmidt Analysis

The classical analysis of the Stirling refrigerator cycle was given by Schmidt in 1871, [53,54]. Simple harmonic motion of the piston and displacer were assumed and a dead volume was allowed for. Expressions for the heat transferred in the expansion and compression spaces, the mass distribution and the mean cycle pressure were derived in terms of the swept volume ratio, the temperature ratio, the phase angle between the motions of piston and displacer, and the dead volume ratio.

In deriving these expressions the following assumptions were made.

i) Perfect regeneration

ii) The instantaneous pressure is the same throughout the system

iii) The working fluid is an ideal gas

iv) The mass of the working fluid remains constant

v) Volume variations in the working spaces occur sinusoidally

vi) There are no temperature gradients in the heat exchangers

vii) The cylinder wall and piston temperatures remain constant

viii) There is perfect mixing of the cylinder contents

ix) The speed of the machine is constant

x) Steady-state conditions are established

The Schmidt analysis is described in detail in Appendix 1.

It can be seen that all heat transfer processes are assumed to be 100% efficient and that no pressure losses are taken into account. The Schmidt analysis is therefore still an analysis of an ideal cycle and gives the same COP as the Carnot cycle (equation (A-16)). Although useful as a preliminary design tool, the Schmidt analysis cannot be used to predict the performance of a refrigerator. Actual performance will be much lower than that predicted by the analysis because of the losses, mainly heat transfer losses,

that are present in all practical Stirling-cycle cryocoolers. Efficiencies of about 10% of Carnot are the highest that have been attained, to date, for miniature refrigerators working at 80K and below.

3.2 NON-IDEALITIES IN STIRLING-CYCLE OPERATION

3.2.1 Non-isothermal Compression And Expansion

The condition of isothermal compression and expansion assumed in the Schmidt analysis requires either infinite rates of heat transfer in the working spaces or an infinite time for the heat transfer process to take place. In practice a Stirling-cycle refrigerator runs at speeds between 15Hz and 60Hz so that conditions in the cylinders are probably closer to adiabatic than isothermal. Halpern and Shtrikman, [55], give the heat diffusion length, the distance through which a gas temperature fluctuation will spread in a time τ, as

$$L = \sqrt{(\tau k_g/\rho_g c_g)}$$

For a typical system with helium at 10 bar pressure and at 273K, operating at 40Hz, this gives the heat diffusion length for one quarter cycle as 0.03cm. At lower temperatures L is even smaller. These values are so much smaller than the dimensions of a working chamber that the gas in such a chamber will expand and be compressed almost adiabatically, with heat transfer taking place almost exclusively in the specially designed heat exchangers which adjoin the working spaces.

The effect of adiabatic compression and expansion on the performance of the cycle has been analysed by many authors including Finkelstein, [56].

Finkelstein specified that the processes of compression and expansion, in the cylinders, could occur anywhere between the ideal cases of isothermal and adiabatic, so,

$$PV^n = \text{constant}$$

where $1 \leq n \leq \gamma$.

The model assumed that infinite heat transfer, and therefore isothermal conditions, prevailed in the hot and cold heat exchangers, and retained all the other assumptions of the Schmidt analysis.

Closed form solutions were not obtained for any case except the isothermal, where they corresponded exactly with those of the Schmidt analysis. Numerical analysis was used to obtain solutions for other cases and a sample solution for one case, that with a temperature ratio (T_2/T_1) of 2.0 and a Carnot COP of 1.0, was presented. With adiabatic compression and expansion the COP was reduced to 0.543. Walker and Khan, [57], presented numerical solutions for a number of other cases. Rios et al, [58], show that when adiabatic processes are assumed, the COP is strongly dependent on the dead volume, phase angle and pressure ratio of the system, and not just on temperature as in the ideal model.

The technique of Finkelstein has been used by Halpern and Shtrikman, [55], and extended to a system containing several working chambers. Numerical solutions for three chamber Stirling and Vuilleumier refrigerators have been given, and again shown to be dependent on the dead volume of the system, with the adiabatic processes yielding values of COP appreciably lower than those obtained assuming isothermal processes.

The assumption of non-isothermal compression and expansion leads to a more realistic model of a refrigerator, but there are many other non-ideal processes to be taken into account if a thorough understanding of the operation of a cooler is to be reached. These include imperfect heat transfer in the heat exchangers and regenerator, pressure drop in the system, and the finite heat capacity of the regenerator.

3.2.2 Regenerator Losses

Table (3.1) shows the predicted effect of regenerator inefficiency (the fraction of the heat load on the regenerator which is not stored) on the performance of a refrigerator which has no other losses, [43]. The effect of the refrigeration temperature is seen to be very pronounced. The thermal load on the regenerator in a machine producing 1 watt of useful refrigeration at 80K, with a pressure of 10 bar and a frequency of 40Hz, can be up to 100 watts. An increase in the overall efficiency of the regenerator of only 1% could therefore double the available refigeration, and hence the

COP, of the refrigerator.

The effect of finite rates of heat transfer is the most important influence on regenerator design. To achieve effective regeneration a very large surface area is required and is usually obtained by having the matrix material finely divided, usually in the form of wire mesh screens or small spheres.

The assumption that the temperature of the regenerator matrix at any point remains constant with time, which is used in both the ideal analysis and those discussed above, implies that the thermal capacity of the matrix is infinitely large compared to that of the gas passing through it. As the speed of the machine and the pressure of the working fluid increase, more gas passes through the regenerator and its heat capacity becomes significant compared with that of the matrix. This effect becomes increasingly important as lower temperatures are reached, because the specific heat of most regenerator materials decreases, while that of helium (the only gas that can be used below 20K) increases as the temperature is reduced. The regenerator thus reaches 'thermal saturation' and cannot heat or cool the gas effectively.

A dense packed regenerator which has a high heat capacity and large surface area will cause a large pressure drop in the gas passing through it. A more open geometry with a correspondingly lower pressure drop would however contain much dead volume, which would have a detrimental effect on performance. A compromise must therefore be made between the requirement for effective regeneration and that for negligible

pressure drop. At temperatures down to about 80K regenerator efficiencies of over 99% are usually achieved, but the performance of the regenerator is still the major problem to be overcome in order to reach lower temperatures.

The effect of the inefficiency of the regenerator on the system is to act as an additional heat load on the cold end of the refrigerator.

3.2.3 Heat Exchanger Losses

In the hot and cold end heat exhangers, as in the regenerator, it is important to have a large surface area for heat transfer, while minimising pressure drop and dead volume. In large refrigerators the hot end heat exchanger may be water-cooled but this is clearly not possible for cryocoolers designed for space use. The heat exchangers in miniature refrigerators often consist of annular passages. Chellis et al, [59], describe such a cold end heat exchanger and the efforts made to improve its performance by lengthening the ducts through which the gas is constrained to flow. As in the regenerator the improvement in heat transfer must be offset by the increase in pressure drop and dead volume.

The effect of imperfect heat exchange imposes an additional thermal load on the regenerator, and also has a detrimental effect on the COP of the machine. The gas inside the cold end must be significantly colder than the required refrigeration load temperature in order that the load be cooled (as the rate of heat transfer depends on the temperature difference between the gas and the wall).

3.2.4 Shuttle Heat Transfer

In machines where a displacer forces the gas to flow from the hot working space to the cold end an irreversible process takes place, which increases the apparent rate of heat conduction along the walls of the cylinder. This effect, the 'shuttle heat transfer loss', is caused by heat being transferred from the cylinder wall to the displacer at the hot end of the cylinder, carried by the displacer to the cold end and, there, transferred back to the wall.

Consider Figure (3.3a). An element, j, of the displacer is at temperature T_j and is opposite an element of the wall at the same temperature. When the displacer is moved towards the hot end of the cylinder, Figure (3.3b), the element at temperature T_j will be opposite an element of the wall at a higher temperature T_k. Heat will be transferred from the wall to the displacer across the clearance gap between them. The displacer then moves towards the cold end of the cylinder, Figure (3.3c), and the displacer element at T_j will be opposite a wall element at a lower temperature T_i. Heat will be transferred from the displacer to the wall. In this way heat is carried from the hot end of the cylinder to the cold end.

Shuttle heat transfer is not such an important source of loss in machines with two opposed pistons. The pistons move in cylinders which maintain small temperature gradients along their walls compared to the temperature gradient in a cylinder in which a displacer moves.

The shuttle heat transfer loss appears as an additional refrigeration load on the machine.

3.2.5 Conduction Losses

Heat leak from the surroundings to the cold end of the refrigerator can be minimised by the use of vacuum systems and insulation materials. There will also be a conduction loss from the hot end of the refrigerator to the cold end, through the walls of the cylinders, the displacer material, and the working gas, and an axial conducion loss through the regenerator matrix.

These effects also appear as an extra refrigeration load.

3.2.6 The Effect Of Pressure Drop And Dead Volume

The effect of pressure drop losses, caused by fluid friction in the regenerator, heat exchangers and dead volume (such as the pipe linking compressor and displacer units in split-cycle machines), is to lower the pressure ratio available.

The work done by the gas against the fluid friction will be manifest as heat in the refrigerator. At the regenerator cold end this will be an extra refrigeration load on the cooler, and at the hot end of the refrigerator it will adversly affect the maximum possible efficiency given by Carnot (which depends on the temperature of the hot and cold ends).

3.3 MODELS OF STIRLING-CYCLE PERFORMANCE

There are two ways in which the losses described above have been incorporated into Stirling-cycle analyses in the literature.

The first, used by Finkelstein, [60], involves deriving a set of partial differential equations describing the processes encountered in the refrigerator, and, in order to allow for the variation of temperature and physical properties with location, dividing the system into control volumes sufficiently small for accurate treatment of the system variables. The machine parts must also be subdivided so that the heat flow through them can be accounted for. Finkelstein, describes such a network of nodes, and the computer program needed to solve the equations for each time increment at each location. The analysis requires a correlation between mass flow and heat transfer in the regenerator matrix (such as the Reynolds-Nusselt number relationships given by Walker and Vasishta, [61]), and a knowledge of the dependence of pressure drop on mass flow, heat transfer coefficients in the heat exchangers, and the conduction losses in the machine.

Graphs of the energy flow for regenerator and heat exchangers were presented, and it could be seen that the heat flow rate in the regenerator is about three times as great as that for the other components, emphasising the importance of effective regeneration.

Kirkley, [62], used a simplified form of this method of analysis and derived equations for the mass distribution in a Stirling engine which he had divided into only four volumes for the purpose of the analysis, the expansion space, the compression space, and two 'equivalent flow' volumes which contained the dead volume in the heat exchangers and regenerator. Numerical results were presented showing the effect on the theoretical thermal efficiency of the engine of adiabatic processes, non-ideal regeneration and pressure drop in the heat exchangers and regenerator. Experimental data were also presented. It was found that the friction factor, f, a function of the pressure drop in the regenerator, given by

$$f = 2g\Delta P \; P/[RT(\frac{dm}{dt})^n]$$

(where the value of n was found to be 2) which had been measured under steady-flow conditions and used in the theoretical model, was lower than that found in pulsating flow conditions. It was suggested that a factor of 1.8 should be used to multiply the steady-flow friction factor for use in the pulsating-flow conditions of the engine, in order to obtain better agreement between the model and the experimental data. No justification for such an arbitrary choice of factor was given.

This analysis, in common with several others, described by Walker, [2], [54], requires substantial programming effort, a large scale computer and much computer time.

The second approach to the problem is illustrated by Rios et al, [58], and Harris et al, [63]. The overall steady-state performance of a Stirling refrigerator with adiabatic cylinders and perfect heat exchange components was first derived. The resulting performance was then corrected for the effects of axial conduction, pressure drop, and gas-to-wall temperature differences. The model ignored the extra load on the regenerator caused by imperfect heat transfer in the heat exchangers and just considered the effect that this had on the temperature ratio of the refrigerator. However it did consider the effect of pressure drop, regenerator inefficiency and axial conduction.

The advantage that these treatments have over the more rigourous method of Finkelstein is their simplicity. However, the various losses are assumed to be independent and are treated in isolation, which may not be the case in a working refrigerator. Neither method of analysis includes the shuttle heat loss, probably because they were based on early double piston machines. Low temperature effects on gas and regenerator specific heats and non-perfect gas behaviour were also not considered.

Both of the approaches described above require a detailed knowledge of the heat transfer processes which occur in a cryocooler. They will only be rewarding if the physical models on which they are based are accurate, and if the heat transfer correlations assumed are valid under the conditions encountered in a working miniature refrigerator.

Very little data have been found in the literature comparing actual machine performance with that predicted by these models.

The effects of imperfect heat transfer can govern the performance of a refrigerator, as shown in the analyses discussed above. For this reason a great deal of practical experimentation on the heat transfer properties of regenerator materials, and theoretical modelling, have been applied to regenerator behaviour and, to a lesser extent, to some of the other problems involved.

3.4 REGENERATOR ANALYSIS

3.4.1 Steady-flow Regenerator Analysis

Regenerator analysis is extremely complex and, in order to obtain solutions, simplifying assumptions must be made. Most of the analysis performed has been on large scale steady-flow regenerators, such as those used in glass furnaces. By steady-flow it is meant that, (a) the mass flow rate and pressure within the regenerator are constant during a blow period (the time between flow reversals), and (b) that the time required for an element of gas to pass through the regenerator is short compared to the blow period.

The assumptions made in the analyses were,

(1) The thermal conductivity of the matrix is zero in the gas flow direction and infinite in the direction normal to the flow.

(2) The specific heats of the gas and matrix material are constant with temperature.

(3) No mixing of the gas occurs during the switch from hot to cold flows.

(4) The convective heat transfer coefficient between the gas and the matrix is constant with temperature.

(5) Entering gas temperatures are uniform over the flow cross section, and are constant with time.

(6) Regular periodic conditions were established.

On the basis of these idealisations the following differential equations were derived.

For the hot gas flow, an energy balance for an element dx of the regenerator, [64],

$$\frac{dq_g}{dx} = \frac{M_m c_m}{L} \frac{\delta T_m}{\delta t}$$

$$= -\left[\dot{m}_g c_g \frac{\delta T_g}{\delta x} + \rho_g A_{fl} c_g \frac{\delta T_g}{\delta t}\right] \qquad (3-2)$$

The convective heat transfer rate equation is,

$$dq_g = \frac{hA_s}{L}(T_g - T_m)\, dx \qquad (3-3)$$

Elimination of dq yields,

$$\dot{m}_g c_g \frac{\delta T_g}{\delta x} + \rho_g A_{fl} c_g \frac{\delta T_g}{\delta t} = - \frac{M_m c_m \delta T_m}{L \quad \delta t} \qquad (3-4)$$

$$= -\frac{hA_s}{L} (T_g - T_m) \qquad (3-5)$$

A similar pair of equations results for the cold gas flow.

The overall performance of a regenerator is most conveniently expressed in terms of its efficiency ϵ, which compares the actual heat transfer rate to the maximum possible heat transfer rate. Separate efficiencies are defined for the cooling and heating periods.

For the cooling period,

$$\epsilon_c = \frac{(T_{hgin} - T_{cgout})}{(T_{hgin} - T_{cm})} \qquad (3-6)$$

For the heating period,

$$\epsilon_h = \frac{(T_{cgin} - T_{hgout})}{(T_{cgin} - T_{hm})} \qquad (3-7)$$

where the subscripts h and c refer to the hot and cold end temperatures respectively.

Regenerators are said to be in equilibrium when the enthalpy transfers to and from the matrix during the heating and cooling periods are equal.

The efficiency is a function of the capacity ratio of the regenerator, given by,

$$\frac{c_m m_m}{c_g \dot{m}_g \tau_h}$$

and the number of heat transfer units (NTU) of the matrix, where,

$$NTU = \frac{hA_s}{m_m c_m}$$

In this equation h is the overall heat transfer coefficient from the gas to the matrix, and is defined as,

$$\frac{1}{h} = \frac{1}{h_g} + \frac{1}{h_m} \qquad (3\text{-}8)$$

where h_g is the convective coefficient in the gas and h_m is the conductive coefficient in the matrix, [6]. Generally the matrix coefficient is much larger than the convective coefficient, so that the overall coefficient is determined principally by the convection.

Coppage and London, [64], and Jakob, [30], discuss the solutions derived by Hausen, [65], Nusselt, [66], Illiffe, [67], and Saunders and Smoleniec, [68]. These solutions are presented in tabular or graphical form, although closed form solutions were obtained for two cases, that of a matrix with

infinite heat capacity, and that where the convective heat transfer coefficient is infinite. Neither of these cases has practical relevance for regenerators in miniature refrigerators. Coppage and London introduced severe approximations to obtain a general closed form solution. They admitted that these approximations render the solution obtained insufficiently accurate to be of direct practical applicability.

Granville et al, [69], have shown that the differences between the various regenerator solutions are negligible in comparison to the differences between experimental and predicted efficiencies.

In steady-flow operation the heat capacity of the gas flowing through the regenerator during a blow period, typically several minutes, [69], is of the same order as that of the matrix (the capacity ratio equals one). Steady-flow theory is concerned primarily with the prediction of the temperature swing of the matrix at each position during a blow period, and the effects of flow reversal are ignored. Regenerator efficiencies in steady-flow applications are of the order of 60% to 90%, [64], where an uncertainty of 1% or 2% in the predicted efficiency may be acceptable. Regenerators in miniature refrigerators however, have efficiencies of over 98%, so that uncertainties of the size mentioned render the theory of no practical use. For these reasons steady-flow analysis is not adequate to explain the behaviour of regenerators in cryocoolers.

3.4.2 Rapidly Cycled Regenerator Analysis

The analysis of rapidly cycled regenerators, such as those used in miniature refrigerators, involves a completely different set of assumptions to that used in steady-flow theory. The heat capacity of the gas during one blow period is much smaller than that of the matrix (unless the temperature is very low, discussed above). The mass flow is always accompanied by large pressure variations and the time required for an element of gas to pass through the matrix is of the same order as, or smaller than, the blow time. Some gas will therefore always remain within the regenerator and will flow back and forth with the pressure variation. The effect of this 'hold up' of gas was modelled by Harness and Neumann, [71], who, using a digital computer simulation, predicted higher regenerator efficiencies than those expected from steady-flow models. However, the solutions obtained did not take into account the temperature dependence of the physical properties of the gas and matrix, and are therefore of limited use for regenerators with large temperature gradients such as those experienced in miniature refrigerators.

Rea and Smith, [72], developed a theory for regenerators in which flow cycling is accompanied by large pressure variations, and presented their results in a series of curves describing axial temperature distributions. The assumptions made in this analysis were of constant gas and matrix properties, no pressure drop, and a negligible temperature difference between the gas and matrix. The pressure and mass

flow variations in the theory and in the experimental verification presented were square-wave and saw-tooth respectively, whereas in a Stirling refrigerator both pressure and mass velocity vary approximately sinusoidally. A heat transfer correlation of the form,

$$StPr^{0.667} = 0.71\ Re^{-0.41} \qquad (3\text{-}9)$$

for a regenerator made of steel spheres was obtained from experimental data.

The analysis of Rea and Smith was extended to the operating conditions of a Stirling cycle refrigerator by Qvale and Smith, [73]. A series of differential equations for the processes involved in the regenerator were derived and a correlation for the steady-flow heat transfer coefficient,

$$h = K|\dot{m}|^{n}$$

was used, where K is a function of temperature and thus also of position along the regenerator.

Rios and Smith, [74], investigated the effect of the variation of the specific heat of the matrix at low temperatures on the performance of regenerators, using the Debye model of specific heats. As expected, the results showed a decrease in effectiveness as the temperature of the cold end of the regenerator was lowered.

The performance of regenerators for low temperature refrigeration was also analysed by Daney and Radebaugh, [75], who included the effect of the heat capacity of the gas in the void spaces of the regenerator. Using a time dependent, one-dimensional, incompressible flow, numerical model the void volume fluid heat capacity was shown to strongly influence regenerator behaviour. Inclusion of the void volume term gave significant improvements in the predicted efficiencies when the void volume and matrix heat capacities were of the same order. This effect had earlier been suggested by Stuart et al, [47], as an explanation for the performance of lead shot regenerators in their three-stage Gifford-McMahon refrigerator which reached 6.5K. The regenerator efficiency was estimated from experimental data to be around 60%, although regenerator theories which did not include the heat capacity of the void volume gas predicted efficiencies of between 0%, [30], and 30%, [74].

Eder, [76], extended regenerator analysis to include longitudinal conduction losses and presented data for a novel matrix consisting of polycrystalline iron whiskers. The data presented showed an improvement in performance for a regenerative refrigerator when an iron whisker matrix was used instead of a bronze screen matrix (made from 160 mesh gauze). The heat transfer areas and porosities (the proportion of the total regenerator volume which is void) of the two matrices were not the same, so that the improvement in performance cannot be attributed to any one particular cause.

Imperfect heat transfer, conduction losses, and pressure drop losses in regenerators were considered independently in the work of Harris et al, [63]. A computer program was used to find the optimum value of the parameter L/D_h, the ratio of the length of the regenerator to the hydraulic diameter, for a regenerator operating between room temperature and liquid nitrogen temperature. It was found that the conduction loss did not notably effect the optimum L/D_h, particularly at the relatively high speeds used in refrigerators, so that more generally applicable results could be obtained by considering only the losses due to pressure drop and imperfect heat transfer. No allowance for the effect of variable matrix specific heat, temperature swing of the matrix, or hold-up of gas in the regenerator was made, but some data for the loss due to imperfect heat transfer were presented and found to be in reasonable agreement with steady state data.

3.4.3 Experimental Studies Of Regenerator Efficiency

In addition to the mostly theoretical studies discussed above, many workers have measured regenerator efficiencies and heat transfer performance of regenerator matrices. A search of the literature produces very little work on regenerators inside actual working refrigerators, most measurements have been performed in apparatus which attempted to simulate the conditions encountered inside a refrigerator.

The effect of different regenerators on the performance of a Stirling machine has been measured, but, because the regenerator loss could not be separated from other losses,

only a qualitative assessment could be made. The results of Walker, [77], show that an increase in regenerator surface area (with the porosity and weight of the matrix held approximately constant) gave an increase in the machine performance, but at a diminishing rate. The sensitivity of performance to change in surface area was decreased at high and low values of both speed and pressure level, possibly because other effects were becoming increasingly important.

Gifford et al, [78], measured total regenerator thermal losses using apparatus consisting of two equivalent regenerators connected at their cold ends through a heat exchanger in thermal contact with a liquid nitrogen reservoir. As gas flowed from one regenerator to the other it was cooled to near liquid nitrogen temperature. The regenerator loss was derived from the resulting boil-off. The regenerators used consisted of bronze mesh screens of different mesh, and lead spheres. The results indicated that, in general, the efficiency increased with an increase in regenerator length and remained approximately constant for flow rates above 5000cm^3/s (11 scfm) of helium.

Similar apparatus was used by Ackermann and Gifford, [79], to investigate the effect of regenerator diameter and longitudinal conduction on performance. The regenerator wall undergoes a smaller temperature swing than the matrix material during a blow period and a large irreversibility is introduced into the system by heat exchange between the wall and matrix. Ackermann and Gifford measured the efficiencies of regenerators with different wall materials and concluded that

this 'wall effect' could strongly influence performance.

These experiments were extended by Gifford and Acharya, [80], to a lower temperature range. The efficiencies of regenerators working with their hot ends at 78K and their cold ends at 10K were measured using the boil-off from a reservoir of liquid hydrogen to calculate the thermal loss. Efficiencies measured in this range were found to be almost identical to those measured by Gifford et al for regenerators working between 300K and 78K. This result was unexpected as all theory predicts lower efficiencies at lower temperatures. Gifford and Acharya suggest that the conduction loss through the wall of the cylinder containing the matrix is considerbly smaller in the lower temperature range, concealing any decrease in the efficiency of the regenerator.

Bretherton et al, [81], performed experiments on regenerators operating with the hot end at 300K and with the cold end temperature controlled by a refrigerator in the range 35K to 65K. Regenerator efficiencies were meaured by monitoring the inlet and outlet gas temperatures with fast-responding thermocouples. The operating pressure was varied between 5.23 atm and 28.5 atm. Correlations for the apparent heat transfer coefficient were developed for the experimental results and included a hold-up group,

$$\frac{L}{v_g \tau}$$

and a pressure dependent group, in addition to the more usual Reynolds number dependence. The correlations given were specific to the experimental work presented and should not be considered as general equations for other systems. However they do illustrate the importance of hold-up and suggest that the operating pressure may be a significant factor, which had not been considered by other workers.

The experiments described above were all performed at low operating frequencies (in the range 0.3Hz to 3.0Hz). Individual factors such as the wall effect and hold-up, which strongly influence regenerator performance at these frequencies, may be of different relative importance at the higher frequencies (25Hz to 60Hz) at which most miniature refrigerators operate.

3.4.4 Experimental Studies Of Matrix Heat Transfer

Much data on heat transfer characteristics of various matrices have been obtained by a number of workers using a variety of experimental techniques. The results of many workers have been presented by Kays and London, [82], and Gutfinger and Abauf, [83], among others, [84,85,31].

Experiments have also been performed to determine properties of regenerator matrices at low temperatures. Walker and Wan, [86], have measured heat transfer coefficients for matrices of bronze mesh screens at liquid nitrogen temperatures. The properties of packed-particle beds and regenerators have been tested at these temperatures and also

in the range 4K to 20K by Barclay et al, [87], who did not observe any systematic behaviour in their results.

Qvale and Smith, [88], present a simple correlation for data derived by various experimental methods using both transient and steady-state unidirectional flow through packed beds of spheres, which have been replotted, correlated and compared with the data derived from an experiment on reversing flow in regenerators. It was found that the total scatter for all investigations was of the same order as the experimental scatter within any one particular investigation (±40%). Qvale and Smith concluded that the uncertainties between the instantaneous local heat transfer coefficients for the particular flow configurations discussed were no greater than the uncertainties in experimental data derived by any one experimental method, and that steady state heat transfer data could be applied to transient or cyclically steady problems. The correlation obtained for the sphere matrices was,

$$StPr^{0.667} = 1.1\ \sigma\ Re^{-0.41} \qquad (3\text{-}10)$$

where σ is the matrix porosity defined by,

$$\sigma = \frac{\text{matrix total volume - volume of metal}}{\text{matrix total volume}}$$

The data are presented in Figure (3.4)

3.5 SHUTTLE HEAT TRANSFER ANALYSIS

More than a quarter of the total refrigeration produced

by a miniature refrigerator may be required to overcome the shuttle heat loss.

This loss has been analysed by Zimmerman and Longsworth, [89]. A greatly simplified solution is presented in which it is assumed that all gas and material properties are constant with temperature and that the thermal capacity of the displacer and wall are infinite. The rate that heat is transferred from the hot to the cold end of the cylinder wall depends on,

(1) the size of the clearance gap between the wall and displacer
(2) the length of the stroke of the displacer
(3) the cycle rate
(4) the temperature gradient in the wall and displacer.

Zimmerman and Longsworth show that by using this simplified theory, an expression for the heat flow due to the shuttle loss can be derived, given by

$$Q_s = \frac{k_g \pi D_d S^2}{5.66t} \frac{(T_h - T_c)}{L_d} \qquad (3\text{-}11)$$

for sinusoidal displacer motion, and considering only the conduction across the clearance gap. The derivation of this expression is shown in Appendix 2.

It can be seen that this method gives a shuttle heat transfer that is independent of frequency. The effect of the limited heat capacity and thermal conductivity of displacer and wall materials would decrease the shuttle heat transfer. The rate of heat transfer across the clearance gap between the displacer and the wall is proportional to the temperature difference between them. If the heat capacity of the displacer material is not infinite its temperature will change as heat is transferred to it, or from it, and the temperature difference between it and the wall would be reduced. Thus the rate of heat conduction between them, and therefore the shuttle heat loss, would also be reduced. At higher frequencies there is less time for this process to take place so that the shuttle heat transfer rate would increase with frequency up to a limiting value, given by the expression derived from the simplified theory.

Zimmerman and Longsworth also present a computer solution, which includes the effect of variations in specific heat and thermal conductivity of the displacer and wall materials, and also of the interaction of shuttle heat transfer with longitudinal conduction. The computer solution predicts smaller values for the shuttle heat loss than those predicted from the simplified theory and are frequency dependent.

This solution, together with that of Harness and Newmann, [90], requires considerable computer time. A compromise has been suggested by Radebaugh and Zimmerman, [91], who present the only experimental data of shuttle heat transfer that has

been found in the literature.

Radebaugh and Zimmerman suggest that the problem can be split into two parts, the transfer of heat across the clearance gap between the wall and the displacer (gas conduction), and conduction into the displacer material. The latter problem is one of sinusoidal temperature fluctuations on the surface of a semi-infinite solid and is treated by Schneider, [92], who derives an expression for the total heat tranferred in this case, which is frequency dependent. The gas conduction problem is that treated by Zimmerman and Longsworth in their earlier simplified theory. Radebaugh and Zimmerman consider these effects as thermal resistances in series and give the total shuttle heat transfer rate as,

$$\frac{1}{Q_s} = \frac{1}{Q_g} + \frac{1}{Q_d} \qquad (3\text{-}12)$$

where Qg and Qd are the shuttle heat transfers limited by the gas gap and solid material respectively. The derivation of the component due to conduction into the displacer is also described in Appendix B.

The experimental data presented gave good agreement with the calculated values for short displacer strokes and at high temperatures. For longer strokes and at low temperatures the agreement worsens, and it is suggested that this could be due the interaction between shuttle heat transfer and longitudinal conduction, and that the temperature gradient may not be constant over the stroke length for longer strokes. The data presented were for operating frequencies in the range 0.5Hz to

2Hz.

3.6 THE PRESENT EXPERIMENTAL STUDY

The heat transfer and pressure drop losses in miniature refrigerators have been shown to govern the machine performance, [43], [61]. Detailed knowledge of these processes is vital in order to obtain an adequate basis for a model of the system. Heat transfer measurements have been made for some regenerator matrices but there are many possible geometries for which no data have been found. There is also scope for an investigation of heat transfer in the hot and cold end heat exchangers, which normally constrain the gas to pass through annular passages.

The literature suggests that it is possible to obtain heat transfer results, valid for transient flow, using steady flow techniques, [88].

Systematic measurement of the losses encountered in a cryocooler has not been documented. Clearly there is scope for such a study, both to enable improvements in performance to be made, and also to investigate the validity of the assumptions on which Stirling-cycle models are based.

The experimental work presented here is in two parts.

The first part, described in Chapter Four, is a study of the heat transfer and pressure drop characteristics of a set of regenerator matrices and annular flow passages, using a steady flow technique.

The second part of the study, described in Chapters Five and Six, involves an investigation of the losses experienced in a working Stirling cycle refrigerator, with the instrumentation and experimental techniques required to measure pressure drop, regenerator, shuttle heat transfer and conduction losses, and those due to irreversible processes during compression. An energy balance is performed on the machine.

Figure 3.1 Sinusoidal Piston and Displacer Motion

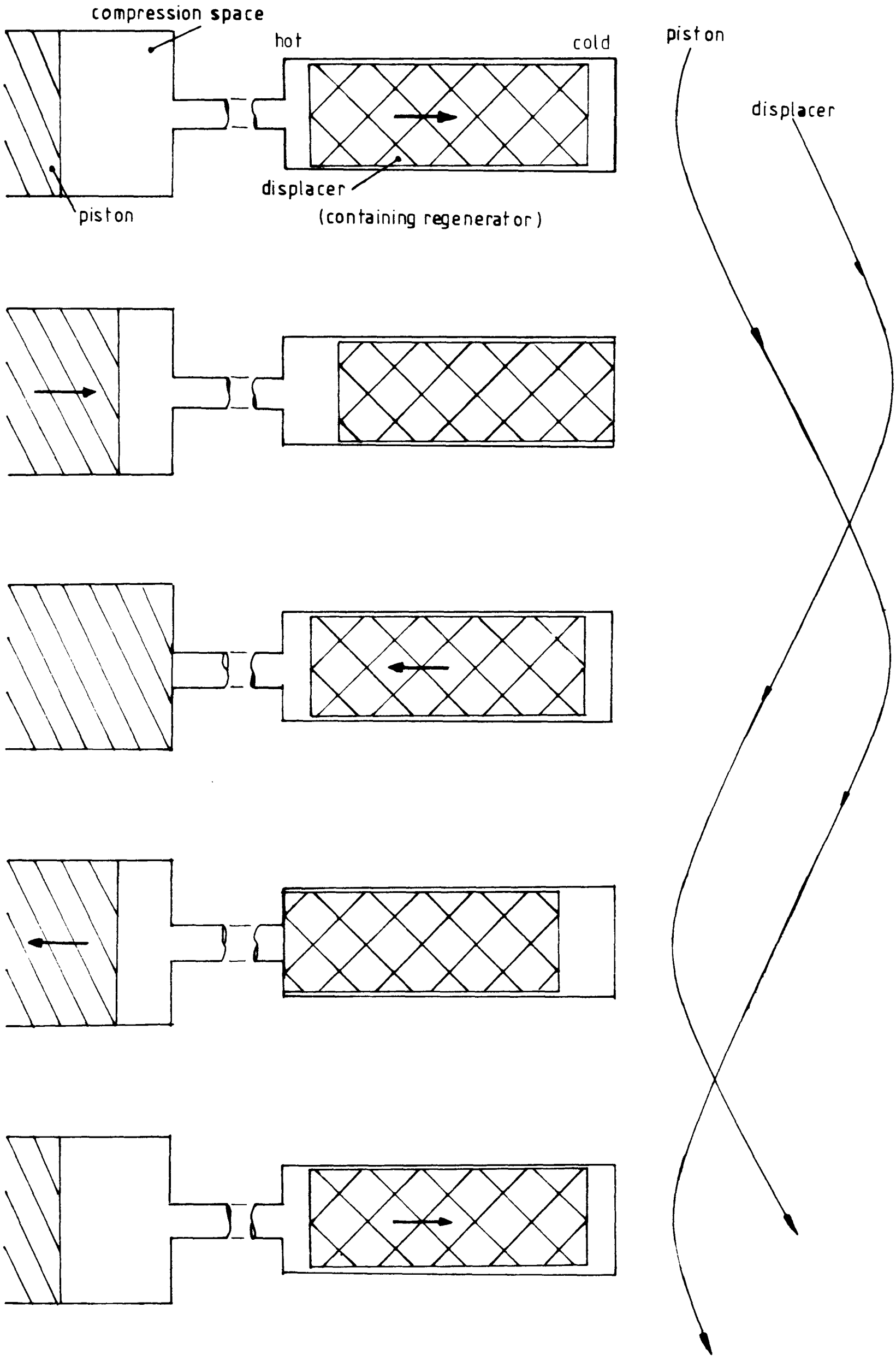

Figure 3.2 The Effect of Sinusoidal Motion on Indicator Diagrams

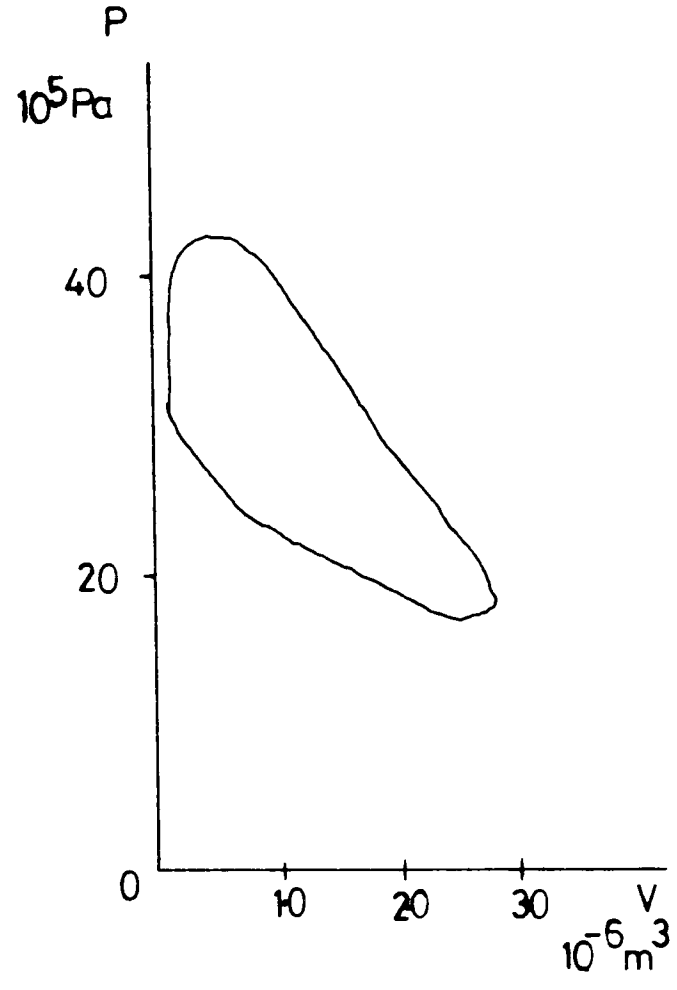

Expansion space

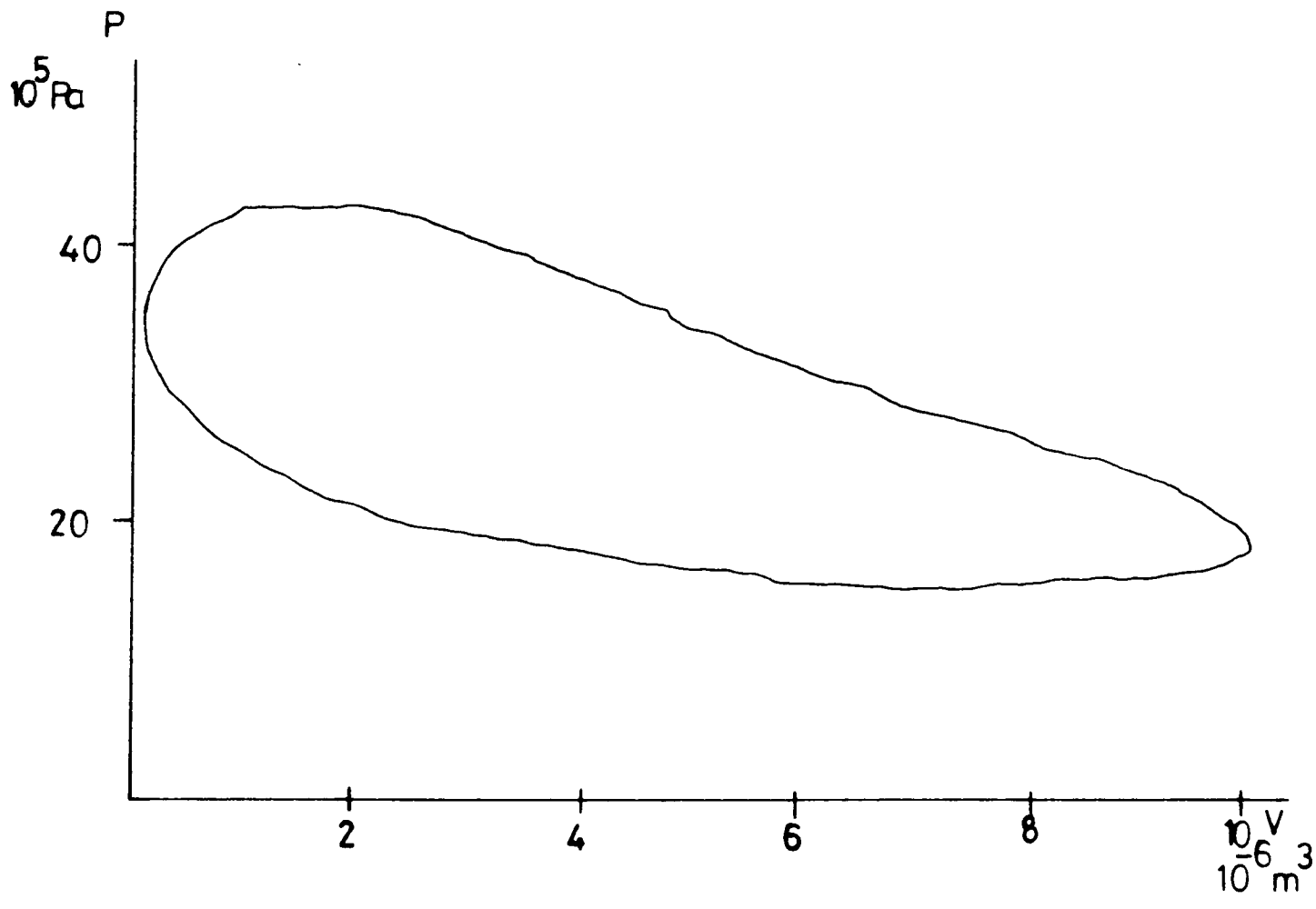

Compression space

TABLE 3.1 Effect of the Regenerator Efficiency on Overall Efficiency [43]

REGENERATOR EFFICIENCY	HOT END TEMPERTURE K	COLD END TEMPERATURE K	REFRIGERATION REMAINING (% OF TOTAL)
0.98	300	200	0.95
0.98	300	100	0.86
0.98	300	50	0.67
0.98	300	20	0.06
0.95	300	200	0.88
0.95	300	100	0.66
0.95	300	50	0.30

Figure 3.3 Shuttle Heat Transfer

(3.3a)

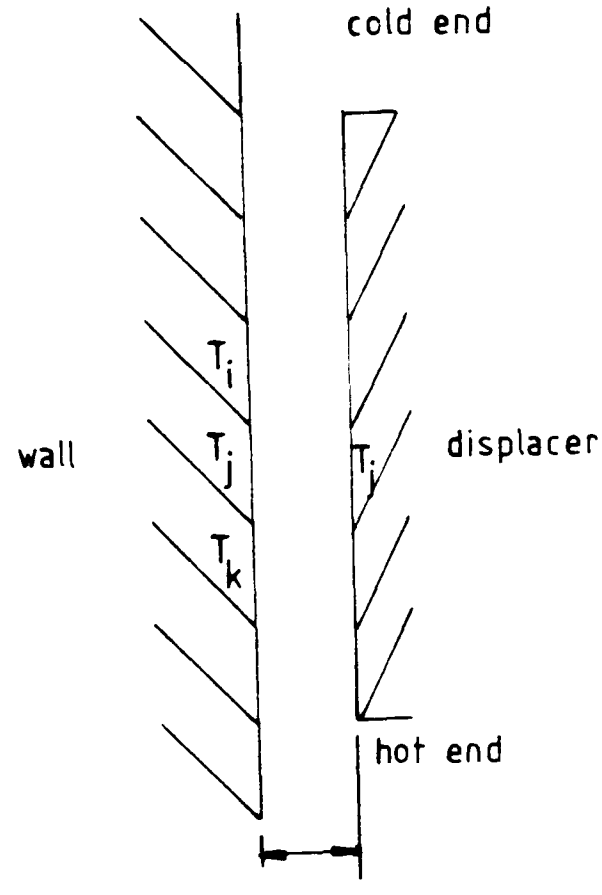

(3.3b)

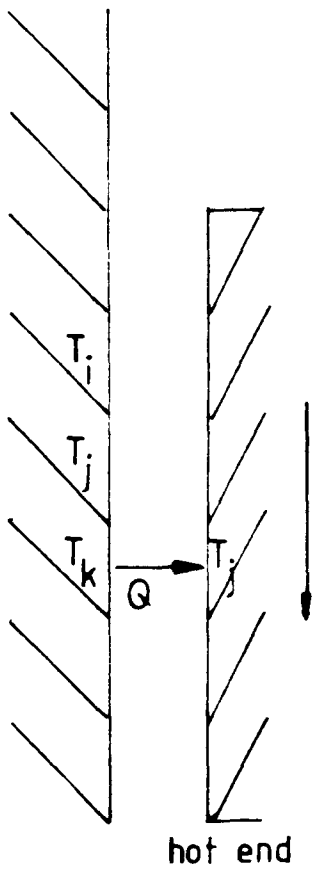

(3.3c)

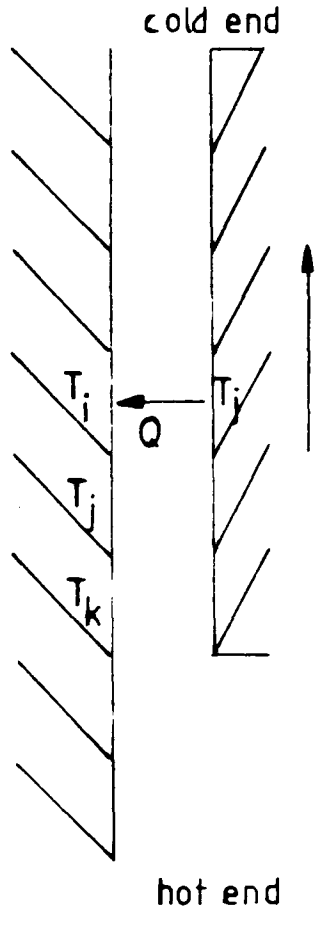

Figure 3.4 Heat Transfer Data for Sphere Matrices, [88]

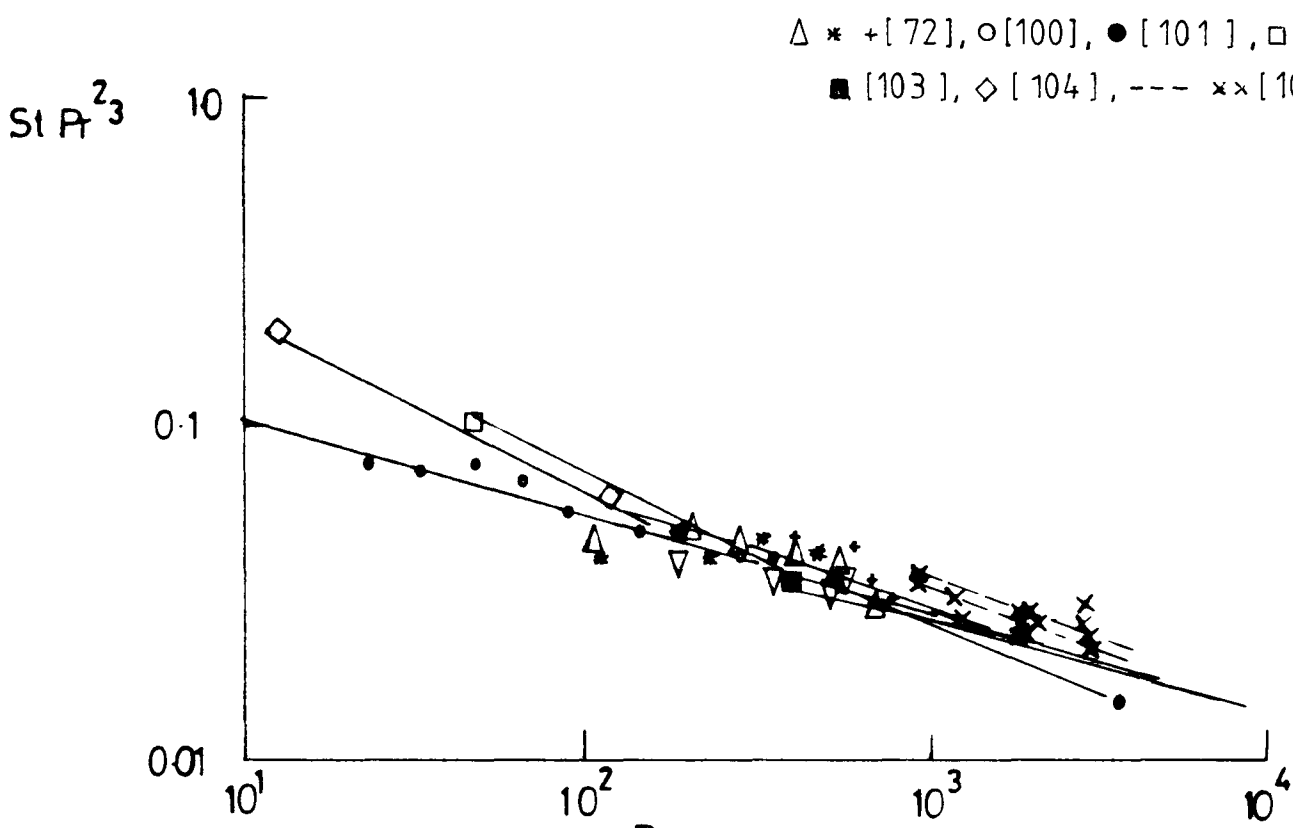

CHAPTER 4

EXPERIMENTAL INVESTIGATION OF HEAT TRANSFER

Experiments to compare the heat transfer from helium gas to various regenerator matrices and in annular gaps, at temperatures in the range 90K to 140K, have been performed. The pressure drop across the matrices has been measured.

It is very difficult to accurately measure changing gas temperatures because of the thermal inertia of the temperature measuring device, and poor heat transfer between the gas and the instrument. Because of these factors the temperature indicated will be between the actual temperature of the gas and that of its surroundings.

The steady-flow technique used here avoids the necessity of measuring changing gas temperatures. Although even the measurement of steady gas temperatures is likely to include an error due to the conduction and radiation of heat from the surroundings to the thermometer (in this case a thermocouple), this will be a constant offset, which can be minimised, when equilibrium is reached and the temperatures of both gas and surroundings are constant. Most transient flow methods involve measurement of rapidly changing gas temperatures, requiring much more sophisticated equipment to gain the same

accuracy in temperature measurement.

4.1 EXPERIMENTAL APPARATUS

The experimental apparatus is shown in Figures (4.3) and (4.2), and a schematic diagram is shown in Figure (4.1).

The matrix to be tested was packed in a 12.7mm inner diameter copper tube, 100mm long, the "test section". A copper cooling jacket, consisting of two parts, containing narrow passages through which liquid nitrogen flowed, was clamped around the test section. Helium gas, which had passed through a long coil immersed in liuid nitrogen to remove condensable impurities, continued through a liquid nitrogen cooled pipe and then flowed vertically downwards through the matrix. Pressure tappings were set into flanges immediately above and below the test section. The helium inlet and outlet tubes, and those for the pressure tappings were constructed from thin walled stainless steel to minimise heat conduction from the surroundings to the test section.

The test section and cooling jacket, wrapped in alternate layers of 'superinsulating' foil (aluminised Mylar*†) and nylon mesh to reduce heat transfer by radiation from the surroundings, were enclosed in a Dural* vacuum jacket which was maintained at a pressure of less than 10^{-4} torr. The cold helium gas and the liquid nitrogen supply for the cooling jacket were brought in and out of the vacuum jacket through evacuated transfer lines in order to keep the top plate of the vacuum jacket at room temperature (this allows O-ring seals to

† * denotes a tradename

be used and so eliminates some of the problems involved in achieving vacuum, and also ensures that the electrical 'lead throughs' on the top plate are uniformly at ambient temperature).

Liquid nitrogen was supplied to the cooling jacket from a pressurised dewar in which the pressure could be varied, thus controlling the flow through the jacket. Two electrical heaters (100 ohm resistors) were bolted to the jacket, allowing the temperature of the test section to be maintained at a desired level.

A heating coil of resistance wire was wrapped around a section of the helium inlet tube in order that the temperature of the gas entering the test section could also be controlled. A needle valve was inserted in the outlet helium line to throttle the flow and raise the pressure in the test section if required.

Indium and Silastic* seals were used between flanges in the cold part of the apparatus in order to maintain vacuum. As much of the construction as possible was welded or hard soldered in an endeavour to minimise leaks.

4.2 INSTRUMENTATION

4.2.1 Flow Rate Measurement

The helium flow rate was measured by monitoring the pressure drop across a small orifice upstream from the test section, using a Druck* differential pressure transducer powered by dry cell batteries, (an excessive amount of

electrical noise was experienced when a mains fed power supply was used). The orifice plate and pressure transducer were calibrated using a Parkinson Cowan* wet gas meter for flow rates up to 200cm^3/s and a Parkinson Cowan dry gas meter for higher flow rates. The agreement between the two flow meters was within ±2% for flow rates up to 200cm^3/s (the highest flow rate for which the wet gas meter could be used).

The orifice plate calibration is shown in Figure (4.4).

4.2.2 Pressure Measurement

The pressure drop across the test section was measured using a second Druck differential pressure transducer, which was positioned outside the vacuum jacket, so as to be at ambient temperature.

System pressure was monitored with a Budenberg* Standard Test Gauge, situated upstream from the test section (also at ambient temperature).

4.2.3 Temperature Measurement

Test section temperatures were measured using 0.2mm diameter wire chromel-alumel thermocouples (selected because the conduction of heat along the wires is about 15 times smaller than that of copper/constantan thermocouples, [35]) soldered on to Micromeasurements* Bondable Terminals which had been attached to the outer wall of the test section using a thin layer of Loctite* Superfast Cyanoacrylate Adhesive IS415. The bondable terminals serve to electrically insulate the

thermocouple beads from the test section wall (and thus from each other), but are extremely thin, so that good thermal contact is maintained. Once affixed, the terminals, the soldered thermocouple bead, together with approximately 2cm of the thermocouple wires which had been coiled and laid flat around the terminals, were coated with Rapid Araldite*. This served two purposes, to strengthen the mechanical bond, and to thermally anchor the wires to the test section wall (reducing heat transfer by conduction along the wires).

The thermocouples were spaced at 2cm intervals along the test section and some were placed at opposite positions on the tube wall, to check that there was a symmetrical temperature distribution.

For tests involving matrix geometries other than the annular gaps, additional thermocouples were inserted into the matrix material, at evenly spaced intervals.

Gas temperatures were also measured using chromel-alumel thermocouples. For these measurements the thermocouple beads were filed down and flattened, to increase the surface area to volume ratio, and thus improve the transfer of heat from the gas to the bead. The thermal conduction path from the flanges, through which the thermocouple wires passed (immediately above and below the test section), was increased by coiling approximately 20cm of the wires in the gas stream above the bead, thus reducing the temperature gradient and decreasing the heat transferred along the wire.

The thermocouple wires, interwoven between the layers of superinsulation, to reduce temperature gradients and thus conduction along the wires, were taken to terminal blocks inside the vacuum jacket from which copper wires led to the electrical lead throughs in the top plate of the vacuum jacket. The terminal blocks were also wrapped in superinsulation to ensure that they were at a uniform temperature.

The thermocouples were calibrated at liquid nitrogen temperature (77.3K) and showed agreement to within ±0.5K with the international standard (BS.4937 part 4).

Pressure transducer and thermocouple signals were amplified and the data were collected by a Research Machines 380Z computer, using the data logging system described by Richardson, [35].

The computer contains an analogue to digital converter which accepts inputs in the range 0-5V and yields an output between 0 and 1023 'bits'. The resolution of this conversion is ±1 bit, which corresponds to approximately ±5mV at the amplifier output. In the case of the thermocouple signals the amplification factor is 1000, so that the error introduced by the computer is equivalent to ±5μV at the amplifier input. This is approximately ±0.25K for a thermocouple at liquid nitrogen temperature.

4.3 TEST GEOMETRIES

The regenerator geometries tested were,

100 mesh† stainless steel gauze discs

200 mesh stainless steel gauze discs

212 - 355μm diameter phosphor bronze spheres

224 - 250μm diameter phosphor bronze spheres

Nickel/chromium metal foam

Compressed nickel/chromium metal foam

The nickel/chromium expanded metal foam (which can be machined to fit the test section) was first tested in one cylindrical piece, then divided into five plugs to investigate the effect of longitudinal conduction. The compressed foam matrix was of twice the original density and in ten 1cm slugs (which had been machined 2cm long from the uncompressed foam, and compressed with a constant diameter to half their original length).

Before the matrices were tested, they were baked at about 70°C in a vacuum oven for at least 24 hours. This procedure was followed to eliminate problems of impurities out-gassing from the metal and condensing in the matrix, thereby blocking the narrow flow passages. In practice blockages still occured, only occasionally (for all but the spherical matrices), but could easily be detected by monitoring the pressure drop across the matrix.

† 100 mesh gauze contains 100 wires to the inch

Considerable problems with impurities were only experienced when the spherical matrices were cooled. This was thought to be due to the dense packed geometry which could trap particles small enough to pass through the other matrices. When this was observed to occur (as the pressure drop across the matrix rose) the test was stopped, the matrix heated to above room temperature and flushed with helium, and the cold trap in the helium inlet line was baked and pumped out, before experiments recommenced.

Thermocouple wires were brought out of the matrices in grooves machined along the matrix (between the matrix and the copper tube wall). The grooves were filled with Silastic in order to prevent gas from leaking past the matrix.

Annular passages were constructed with an outer copper tube, of inner diameter 12.5mm (similar to that used for the regenerator matrices), and inner cylinders machined from polyurethane, precision made to tolerances within ±0.01 mm. Several inner pieces of different diameters were made, giving annular gaps of 0.50mm, 0.25mm, and 0.10mm. The inner pieces were held centrally in the outer tube using two sets of three radially spaced tufnol pins (inserted into the surface of the inner pieces), which gave a tight push fit in the outer copper tube. An additional inner piece, of the same diameter as that which gave the 0.25mm gap, was constructed with the tufnol pins of lengths such that the annulus produced was deliberately excentric, with a minimum gap of 0.10mm on one side and a maximum gap of 0.40mm on the opposite side.

4.4 EXPERIMENTAL PROCEDURE

Before each experimental test began the amplifiers were zeroed and calibrated using a millivolt supply. The reference junctions of the thermocouples were held in an oil filled tube which was placed in a vacuum flask containing an ice and water mixture. Each reference thermocouple junction was covered by 'heat shrink' tubing in order to ensure no electrical contact with the others.

The liquid nitrogen dewar was pressurized to between 30 p.s.i. and 80 p.s.i., and the test section was cooled and held at a constant temperature in the range 90K to 140K. The pressure in the dewar, and the voltage applied to the heaters on the cooling jacket, were adjusted in order to maintain the test section temperature. A needle valve in the inlet helium line was opened and a steady flow of helium passed through the test section. The regulator through which the helium passed made it unnecessary to alter the setting on the valve once the original gas flow rate had been set. Pressure differences and temperatures were monitored every 15 seconds by the computer until the readings were steady. For tests at a higher system pressure the outlet helium flow line was throttled.

Tests were performed on each of the regenerator matrices and annular gap geometries using helium flow rates in the range 50 cm^3/s to 700 cm^3/s.

4.5 RESULTS

4.5.1 HEAT TRANSFER IN ANNULAR GAPS

The heat transfer results for the annular gap geometries are shown in Figure (4.5). The results are plotted in the form of Nusselt number against the dimensionless group,

$$\frac{Re\ Pr\ D_h}{L}$$

where the hydraulic diameter, D_h, is given by,

$$D_h = \frac{4 \times \text{flow area}}{\text{perimeter}} \qquad (4\text{-}1)$$

as used by Hasleden, [6], among others.

For the excentric gap the hydraulic diameter was taken to be the same as that for the 0.25mm gap, which had the same diameter inner piece.

Data for the heat transfer from flow in pipes are shown for comparison, [6].

The range of Reynolds number, Re, found in the data is from 50 to 700, implying laminar flow.

The data are correlated to within ±40% by the expression,

$$Nu = 0.97 \left[\frac{RePrD_h}{L}\right] \qquad (4\text{-}2)$$

McAdams, [31], has reported that heat transfer coefficients up to 33% higher than those obtained for water flow in pipes have been observed for water flow in annular gaps. The data obtained for the narrow annular gaps used here give values of the heat transfer coefficient 94% higher than those given by Hasleden, [6], for air flow in pipes with similar length-to-diameter ratios. This discrepancy could be due to the variation of gas properties with temperature.

4.5.1.1 The Effect Of Gas Temperature -

When laminar gas flow in a duct is at a higher temperature than that of the walls of the duct heat transfer from the gas to the wall is enhanced, [84], [31]. The contribution to the overall heat transfer of this effect will depend on the temperature difference between gas and wall.

The correlation was modified by the inclusion of a term,

$$\frac{T_{gin}}{T_w}$$

to take account of this effect, Figure (4.6). The data agreed with the new correlation,

$$Nu = 0.70 \frac{T_{gin}}{T_w} \left[\frac{RePrD_h}{L}\right] \qquad (4\text{-}3)$$

with a scatter of ±20%. The heat transfer coefficients obtained from this correlation are 40% higher than those given by Hasleden.

4.5.1.2 The Mean Gas Temperature -

From conventional forced convection heat transfer theory, discussed in detail by Shah and London, [93], the minimum heat transfer from a laminar flow of gas in a tube to the tube walls is limited by conduction through the gas. In an annular gap this is the conduction of heat across the gap width, from the mean gas temperature, T_{gm}, to the wall temperature, T_w. The Nusselt number obtained from this calculation is a constant (≈5) and is independent of gas flow rate, although at higher flow rates ($RePrD_h/L > \sim 7$) larger Nusselt numbers are expected because of the effects of turbulence in the flow. Data showing this behaviour are presented by Kreith, [84], and Schmidt and Willmott, [85], where the logarithmic mean gas temperature is used, given by,

$$\Delta T_{ln} = (T_{gin} - T_{gout}) / \ln\left[\frac{(T_{gin} - T_w)}{(T_{gout} - T_w)}\right] \qquad (4\text{-}4)$$

If an arithmetic mean, or the initial gas temperature are used then dependence of Nusselt number on Reynolds number is expected even at low gas flow rates, [31]. This behaviour is shown in the data presented in Figure (4.6).

A small inaccuracy in the measurement of the gas temperature has a very large effect on the accuracy of the value of the logarithmic mean gas temperature, as the temperature difference between the outlet gas and the wall governs the equation. For this reason an arithmetic mean gas temperature is used in the data presented here.

4.5.2 HEAT TRANSFER IN REGENERATOR MATRICES

The heat transfer areas, hydraulic diameters, and masses of the regenerator matrices tested are listed in Table (4.1). In these data the hydraulic diameter given by,

$$D_h = \frac{4 \times \text{void volume}}{\text{surface area}} \qquad (4\text{-}5)$$

is the same as that defined by other workers, [84], [2].

The heat lost by the gas as it passes through the matrix can be divided into two parts, that which is transferred directly into the wall, ${}_gQ_w$, and that which is transferred into the matrix, ${}_gQ_m$, so that

$$\dot{m}c_p\Delta T_g = {}_gQ_w + {}_gQ_m \qquad (4\text{-}6)$$

In equlibrium, when the gas, wall and matrix temperatures, and the gas flow rate are constant, the heat that passes from the gas into the matrix must be conducted from the matrix to the wall and thence to the liquid nitrogen cooling the wall.

$$ {}_gQ_m = \frac{k'A'}{x'}(T_m - T_w) \qquad (4\text{-}7)$$

where $\frac{k'A'}{x'}$ is the heat transferred per degree of temperature difference between the matrix and the wall. This contains elements of conduction through both gas and metal. Values for $\frac{k'A'}{x'}$ were measured by monitoring the time for the matrix to reach wall temperature with no gas flow after each test.

Hence,

$$\begin{aligned} \dot{m}c_p\Delta T_g &= h_m A_m (T_g - T_m) + h_w A_w' (T_g - T_w) \\ &= \frac{k'A'}{x'}(T_m - T_w) + h_w A_w' (T_g - T_w) \end{aligned} \qquad (4\text{-}8)$$

where A_w' is the effective wall area (allowing for that part of the wall area in contact with the matrix). Values for the heat transfer coefficient from the gas to the matrix, h_m, are obtained from these equations with substitution of appropriate gas flow and temperature values.

4.5.2.1 Gauze Disc Matrices -

Heat transfer data for 100 and 200 mesh gauze disc matrices are shown in Figure (4.7), and are correlated by the expression,

$$StPr^{0.667} = 0.074\ Re^{-0.31} \qquad (4\text{-}9)$$

to within ±30%. These data represent tests at system pressures ranging from 1 bar to 3 bar absolute. These data give lower heat transfer coefficients than those reported by Kays and London, [82], also shown in Figure (4.7). However the latter data were for heat transfer from air at high temperatures to coarse mesh screens (5 to 60 mesh) and crossed rods using very short matrices consisting of only 5 screens, [94]. It is not surprising that the correlation for these data cannot be extended to the very different conditions encountered in the tests presented here.

Walker and Wan, [86], report that lower heat transfer coefficients are found in matrices consisting of large numbers of gauze discs than are found in short matrices with few discs. Their data for matrices containing 30 to 100 discs at cryogenic temperatures are plotted in Figure (4.8), together with those of Mikulin and Shevich, [95], reported by Walker, [2], who suggest that for gauze disc matrices of more than 200 discs the correlation,

$$Nu = 0.05\ Re^{0.85} \qquad (4\text{-}10)$$

can be applied. It can be seen in Figure (4.8) that the data presented in this study, for 350 and 861 gauze discs of 100 and 200 mesh respectively, agree with this correlation to within ±40%.

4.5.2.2 Sphere Matrices -

Heat transfer data for matrices of phosphor bronze spheres are presented in Figure (4.9), together with those of other workers, [82].The data are correlated by the expression,

$$StPr^{0.667} = 0.38\ Re^{-0.60} \qquad (4\text{-}11)$$

The correlation given by Qvale and Smith, [88], taken from the data on spherical matrices of many workers using a variety of transient flow techniques (reported in Chapter 3),

$$StPr^{0.667} = 1.1\ \sigma\ Re^{-0.41} \qquad (3\text{-}10)$$

and is shown in Figure (4.10), together with the data from this study. It can be seen that the agreement obtained using the steady flow technique presented here (±40%), is as good as that obtained using the transient flow techniques described by Qvale and Smith.

4.5.2.3 Ni/Cr Foam Matrices -

The data for the Ni/Cr foam matrices correlated by the expression,

$$StPr^{0.667} = 0.33\ Re^{-0.61} \qquad (4\text{-}12)$$

to within ±30%, are shown in Figure (4.11). No difference in performance is observed between the matrix consisting of one piece of uncompressed foam 10cm long, and that of five uncompressed pieces, each 2cm long and separated by a very thin ring of Silastic, implying that in this case the longitudinal conduction through the matrix is negligible.

No other data for heat transfer in this matrix geometry has been found in the literature, and it is thought to be a useful addition to the possible regenerator materials because of its high surface area to weight ratio, and the ease with which it can be machined to shape and compressed in order to give a larger surface area to volume ratio.

4.6 PRESSURE DROP IN REGENERATOR MATRICES

Pressure drop data for the regenerator matrices at room temperature are plotted in Figure (4.12).

Kay, [96], shows that the pressure drop for fully developed laminar flow through a packed bed is given by,

$$\Delta P = \frac{K A_s^2 \mu v L}{V^2 \sigma^3} \qquad (4\text{-}13)$$

where K is a constant which has been empirically determined to be 5.

The pressure drop data obtained for the regenerator matrices in these experiments are replotted in Figure (4.13), together with the expression given by equation (4-13), with velocity $v=5ms^{-1}$ for the gauze disc and foam matrices, and $v=0.5ms^{-1}$ for the sphere matrices. The pressure drops measured across the gauze disc and metal foam matrices fit this expression to within ±15%. The spherical matrices, however show pressure drops well below those expected from equation (4-13).

A possible explanation for these data is that in the sphere matrices the gas flow is channelled through the path of least resistance, which would be an annulus at the matrix wall. This can be demonstrated by calculation of the cross-sectional flow areas at the edge of the matrix and at the centre.

Consider the sphere matrix section shown in Figure (4.14). The ratio of the cross-sectional flow area adjoining the wall, A, to that area in the matrix, B, is given by,

$$[(2-\pi/2)r^2]/[(\sqrt{3}-\pi/2)r^2] = 2.66$$

where r is the sphere radius, and the spheres are of identical radii.

If the sphere matrix can be considered to form an annular gap, of length L, outer diameter D, and inner diameter D-2r, the porosity will be,

$$\sigma = \{L\pi Dr - \left[(2/\sqrt{3})L\pi D/4r^2 \times (2/3)\pi r^3\right]\}/L\pi Dr$$

$$= 1-(\pi/3\sqrt{3}) = .395. \qquad (4\text{-}14)$$

The surface area to volume ratio is given by,

$$S/V = [(2/\sqrt{3})L\pi D/4r^2 \times 2\pi r^2]/L\pi Dr$$

$$= \pi/\sqrt{3}r \qquad (4\text{-}15)$$

The radius of curvature of the tube wall has been neglected because of the small diameter of the spheres used in these experiments.

The values for pressure drop across the sphere matrices calculated from equation (4-12), using the values for porosity and surface area to volume ratio given by the expressions in equations (4-14) and (4-15), are plotted in Figure (4.14), and show good agreement with the experimental data.

Some data measuring the flow distribution in large scale packed sphere beds has been found, [97]. Some of these data are reproduced in Figure (4.15) showing the velocity profile expressed as the ratio of the velocity at a given radial position in the bed to the average velocity. It can be seen

that the velocity near the wall of the tube is twice that near the centre of the matrix.

Flow channelling in the sphere matrices may be the reason that these matrices have been found not to perform as well as gauze disc matrices of similar surface area in refrigerators operating at temperatures above about 80K, where the heat capacity of the regenerator is not a limiting factor, [98]. Very little of the the sphere surface area could be used for regeneration, as most of the gas would only see the sphere surfaces adjoining the wall. The pressure drop measured across the sphere matrices is substantially larger than that in the gauze disc matrices and would also limit the performance.

4.7 COMPARISON OF REGENERATOR MATRICES

In Figure (4.16) heat transfer data for the regenerator matrices are plotted in the form of Reynolds number against the group NuA_s/A_{fl}, where A_s is the matrix surface area, and A_{fl} is the flow area in the matrix. This presentation of the data allows a better comparison of the heat transferred to each matrix than do the Nusselt or Stanton numbers alone, since the matrix surface areas for these regenerators differ.

It can be seen that the 200 mesh matrix would be expected to give better performance than the 100 mesh, and that both of these are likely to be more efficient than the foam matrices, although if the compressed foam were to be compressed further, a significant improvement might be made.

It can be seen that the data for the sphere matrices, assuming all the surface area is available for heat transfer, give much higher value of the heat transfered than those for the other matrices. However, if annular flow in the sphere matrices is assumed the data would predict poor performance. It is likely that the true 'effective area' of the sphere matrices is between these two extremes, but since the pressure drop has also to be taken into account when selecting a suitable regenerator matrix, the geometry of a sphere matrix is not ideal for regenerators in miniature refrigerators.

4.8 DISCUSSION

The data reported here provide a comparison between the performance of different regenerator matrices and annular gap heat exchangers.

Although these data, together with those of other workers using different techniques, can be correlated to within ±40%, which in the field of heat transfer correlations is considered reasonable agreement, the scatter found in the data precludes its use to predict the performance of a regenerator in a working refrigerator. Better agreement in the data is difficult to obtain, principally due to the problems involved in the measurement of accurate gas temperatures. In order to have a useful tool for analysis of the performance of a refrigerator it is required to predict the very small difference between perfect regeneration and 99% efficient regeneration under complex flow and temperature conditions. No heat transfer correlation that could be derived from data

taken in experiments on regenerators outside the enviroment of a refrigerator can be expected to do this. Therefore, these data, and those of other workers, do not provide an entirely adequate basis for a model of refrigerator performance, although they do provide a useful comparison between the heat transfer performance of different regenerators. Pressure drop data such as those presented here are vital for the selection of appropriate regenerator geometries.

For this reason experimental techniques have been developed to measure regenerator losses inside a miniature refrigerator without the necessity of measuring gas temperatures. These techniques also allow measurement of other losses such as those due to shuttle heat transfer and irreversible compression, and thus enable an energy balance to be made on the machine.

It is thought that this approach will enable models of performance to be derived, which will prove to be useful tools in the design of miniature refrigerators.

Figure 4.1 Schematic diagram of Heat transfer Apparatus

(Not to Scale)

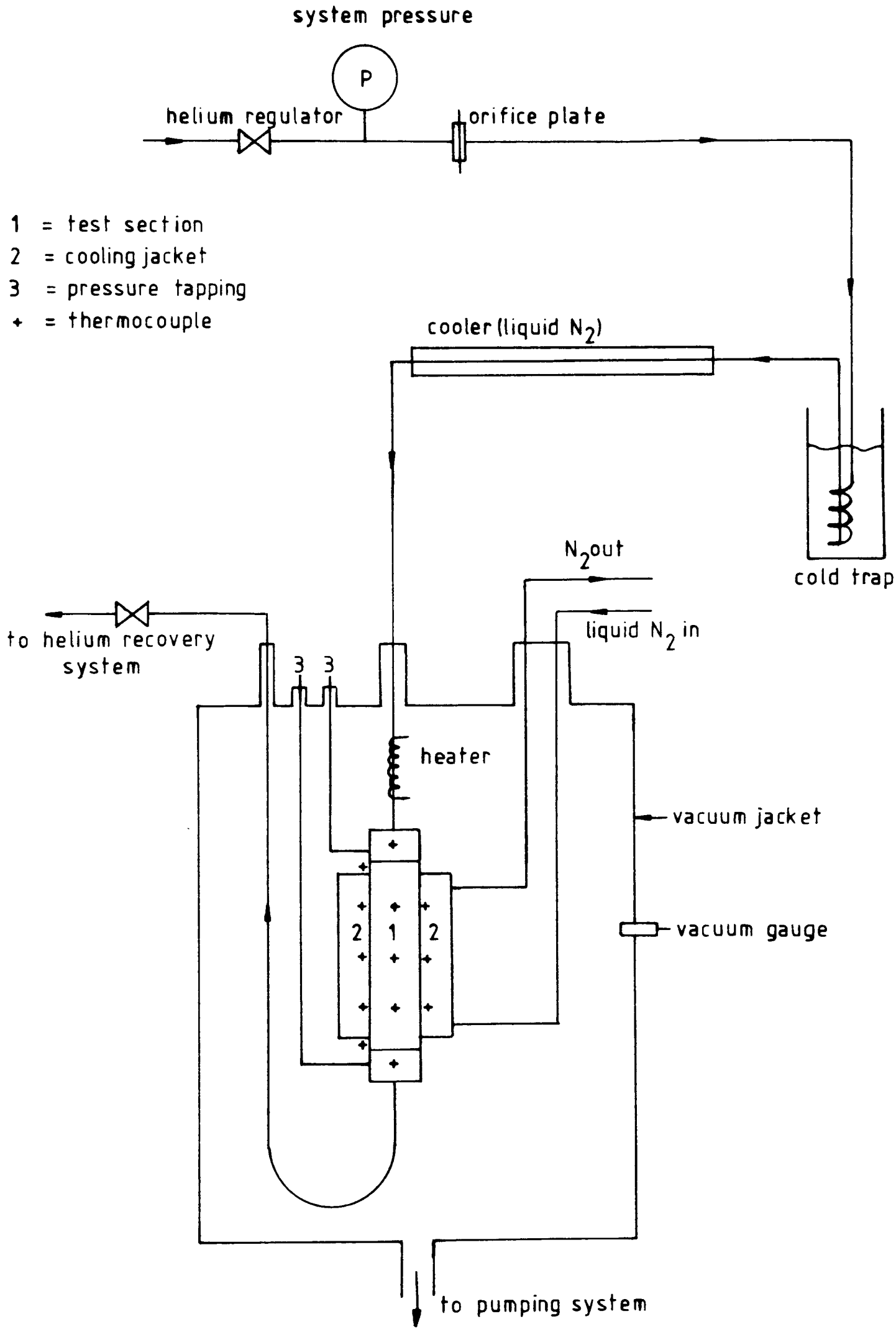

Figure 4.2 Instrumentation of Heat transfer Apparatus

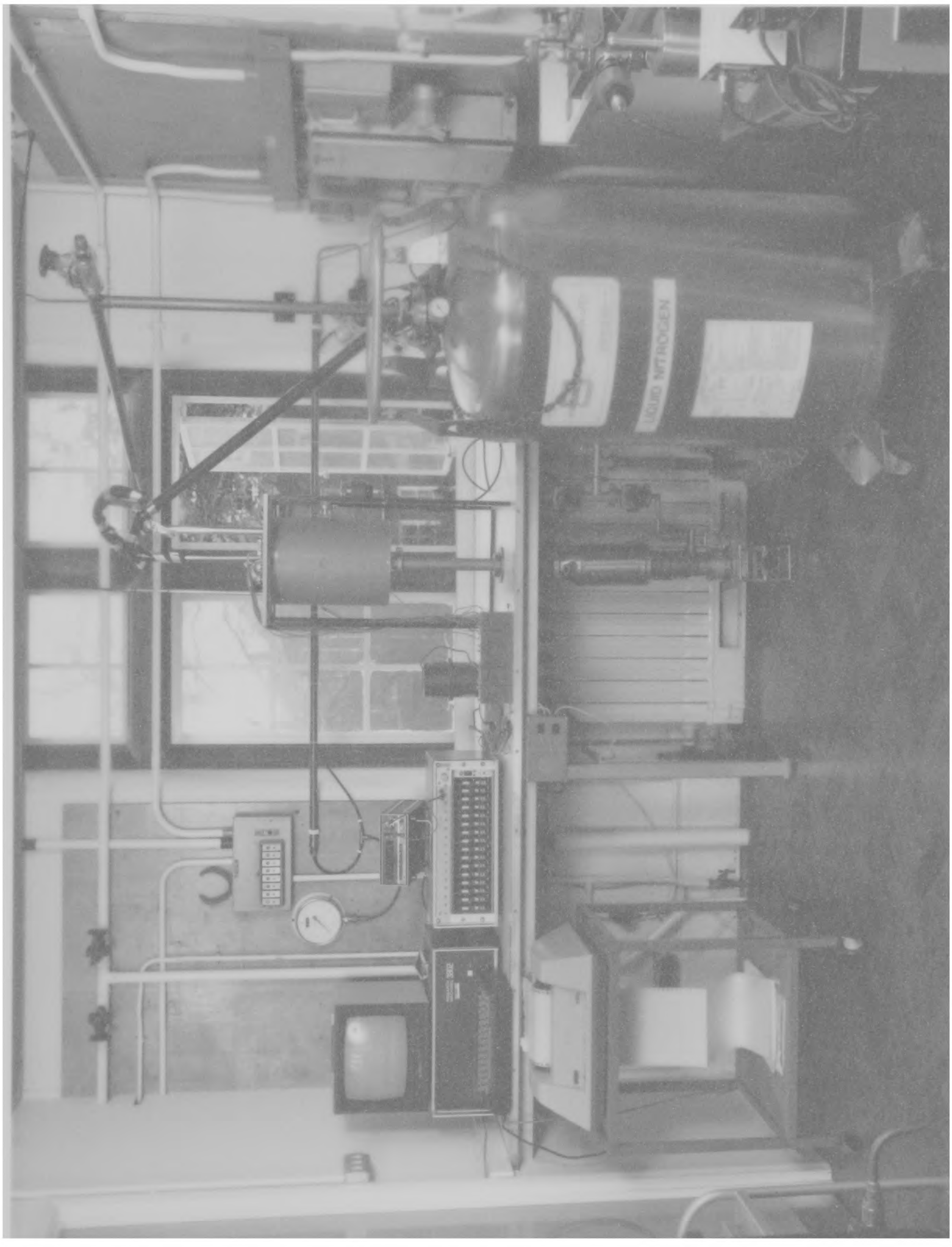

Figure 4.2 Instrumentation of Heat transfer Apparatus

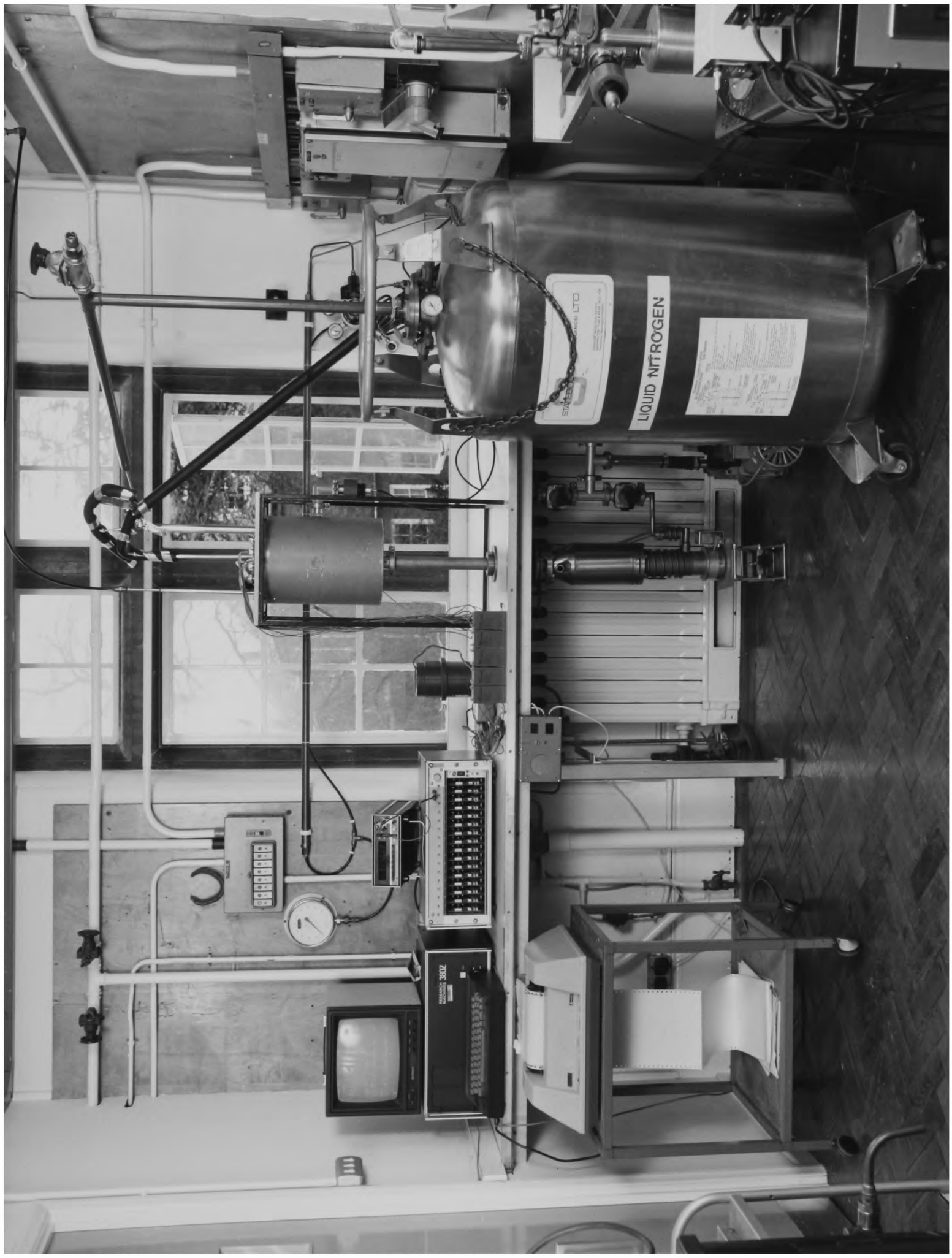

Figure 4.3 Detail of Heat transfer Apparatus

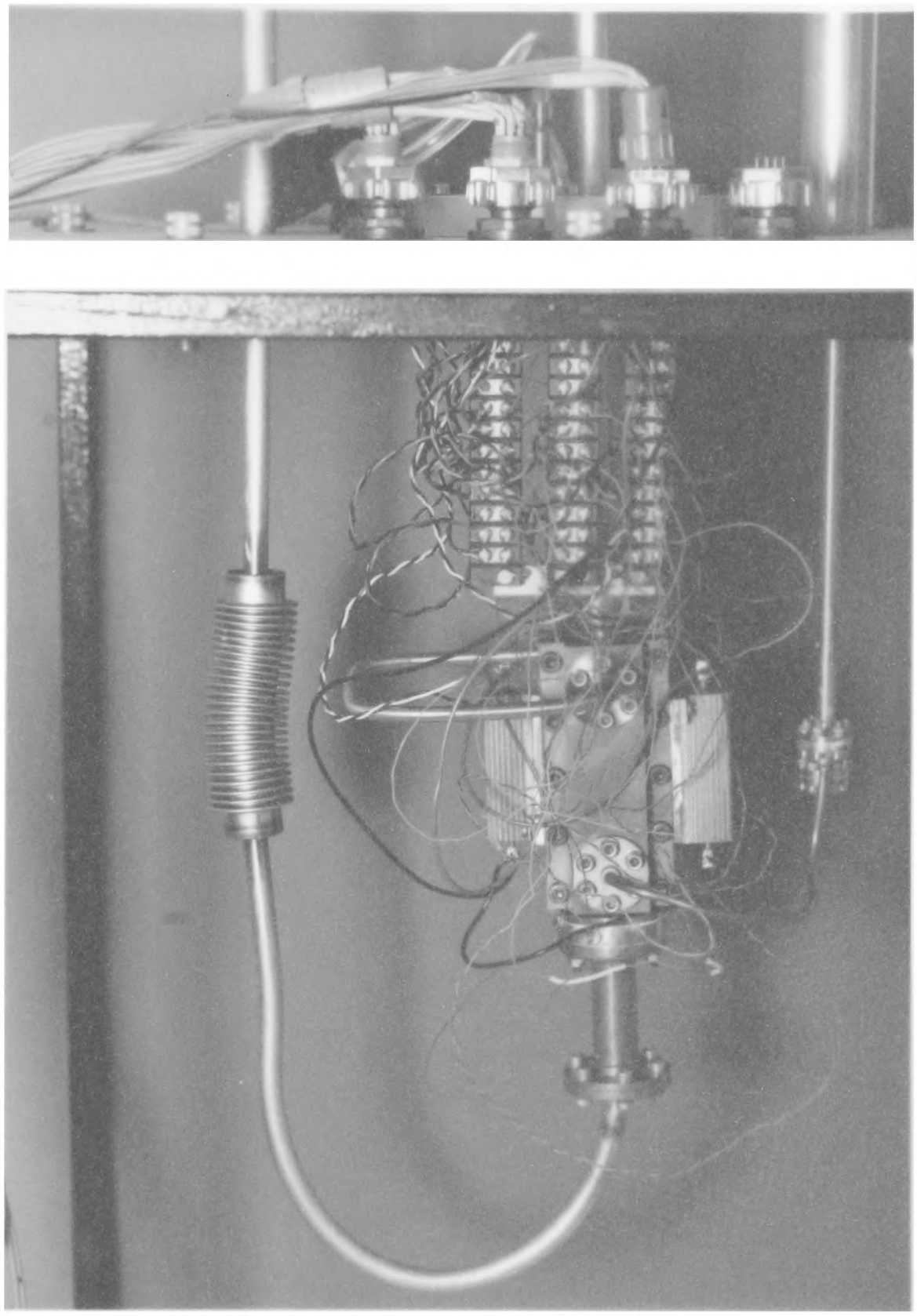

Figure 4.3 Detail of Heat transfer Apparatus

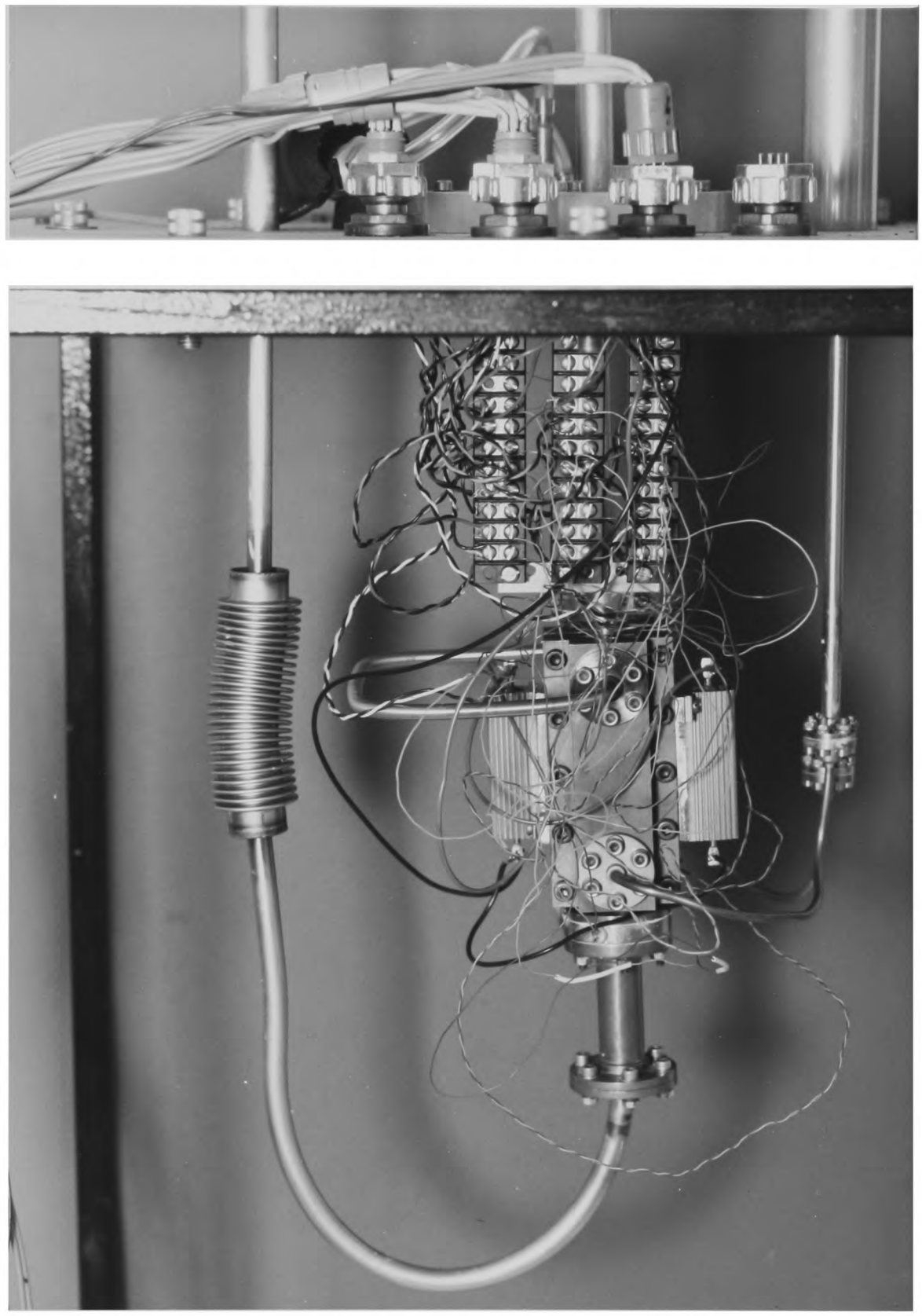

Table 4.1 Matrix Characteristics

Matrix	Heat Transfer Surface Area cm^2	Length cm	D_h cm	Porosity σ	Mass g
Stainless Steel Gauze Discs					
(1)350 ×100 mesh	1020	10.0	0.031	0.78	31.9
(2)861 ×200 mesh	2317	10.0	0.015	0.78	31.9
Bronze Spheres					
(1)212-355μm	1566	7.5	0.009	0.19	66.0
(2)224-250μm	2383	9.5	0.006	0.27	80.0
Ni/Cr foam					
(1)Uncompressed (1 and 5 pieces)	1178	10.0	0.037	0.91	9.1
(2)Compressed (10 pieces)	2356	10.0	0.017	0.82	18.2

Figure 4.4 Calibration of Orifice Plate

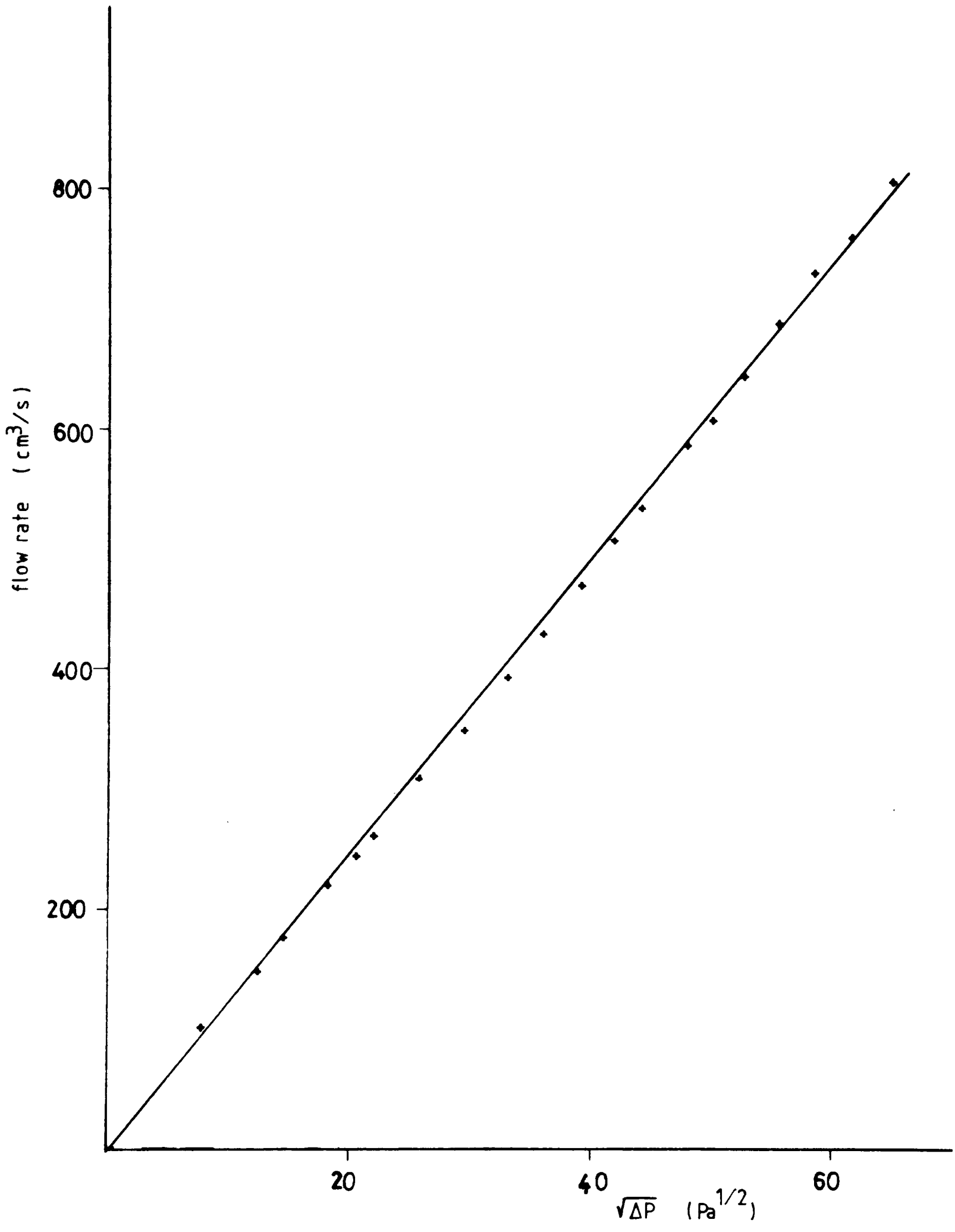

Figure 4.5 Heat Transfer in Annular Gaps

P = 1.0 bar: × 0.1mm gap, • 0.25mm, □ 0.5mm, o excentric
P = 1.6 bar: Δ 0.25mm gap
P = 2.3 bar: ▪ 0.25mm gap
---- data of Hasleden, [6]

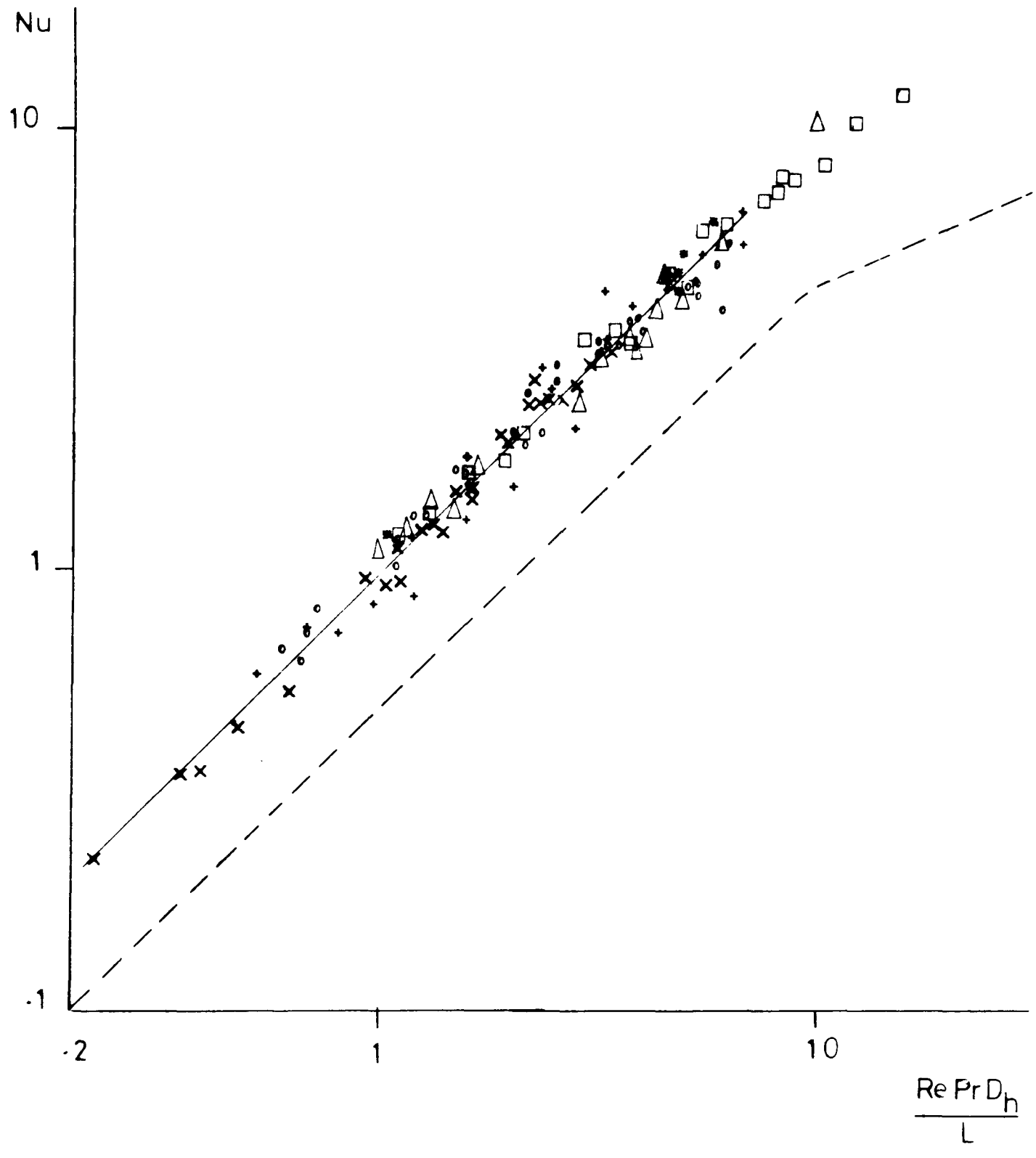

Figure 4.6 Heat Transfer in Annular Gaps

(Temperature Compensated)

P = 1.0 bar: × 0.1mm gap, + 0.25mm, □ 0.5mm, o excentric
P = 1.6 bar: Δ 0.25mm gap
P = 2.3 bar: • 0.25mm gap

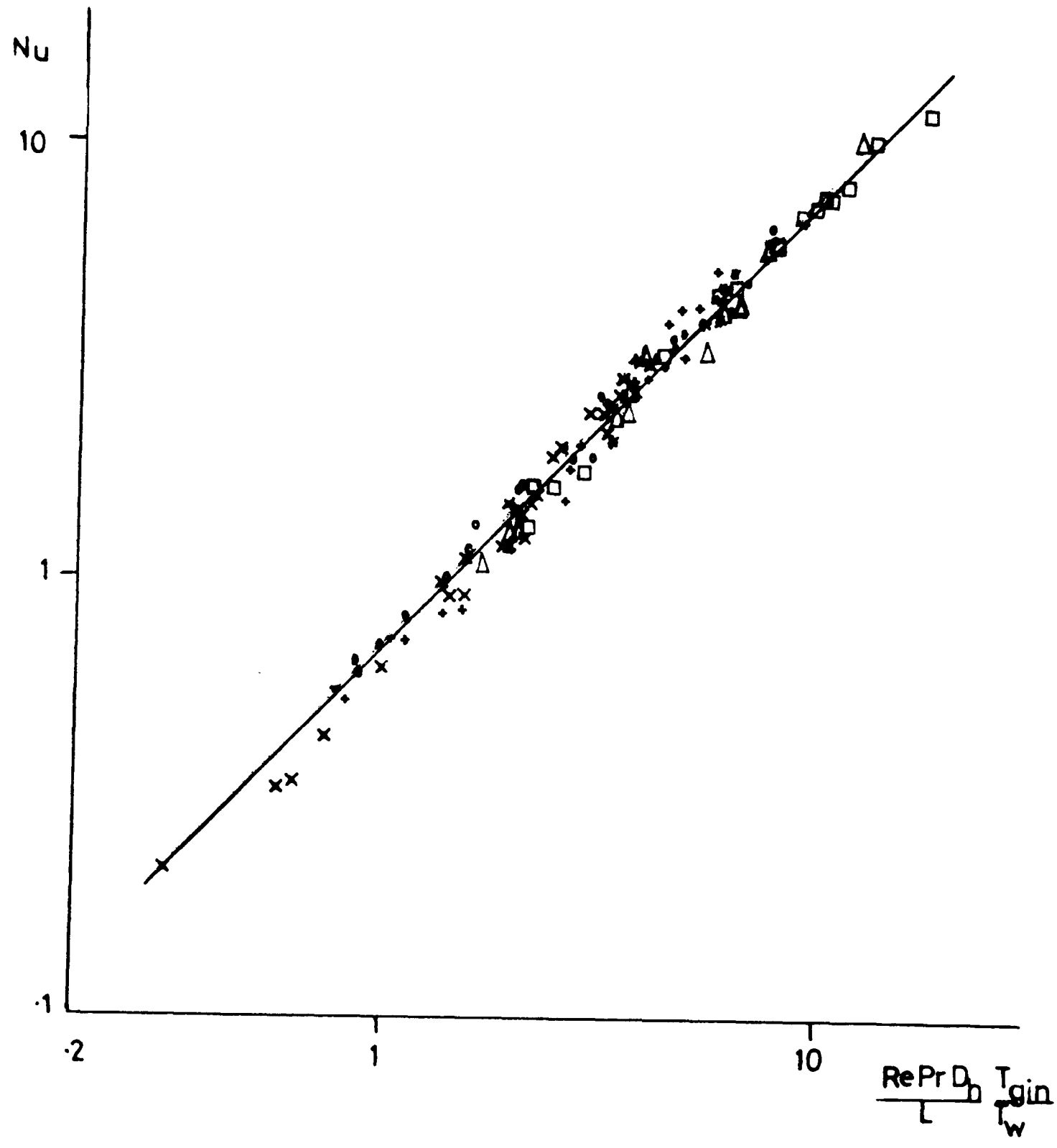

Figure 4.7 Heat Transfer in Gauze Disc Matrices

• 200 mesh, pressure = 1.0 bar:
100 mesh, □ P = 1.0 bar, o 2.0 bar, Δ 3.0 bar
----- data of Kays and London, [82]

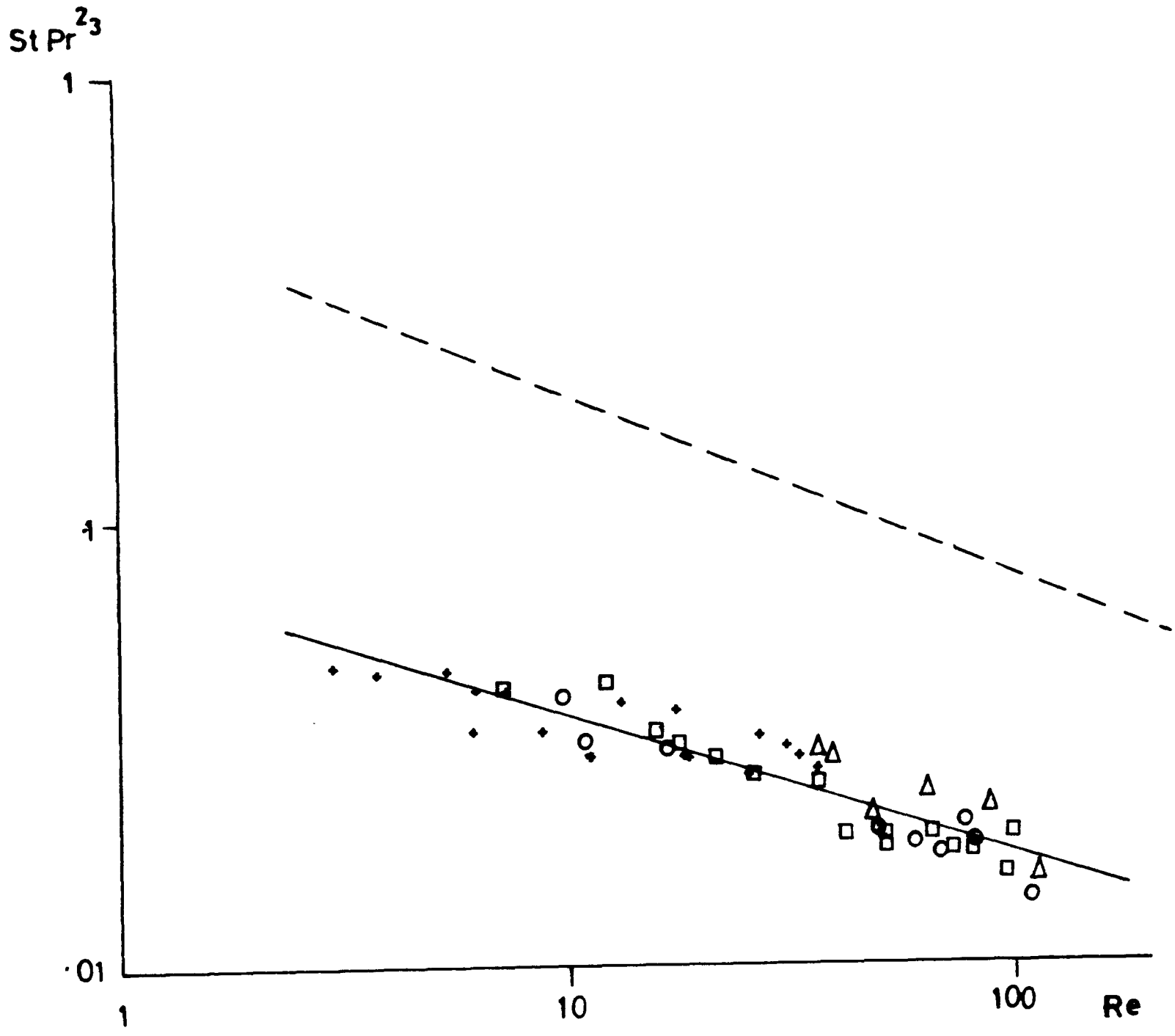

Figure 4.8 Heat Transfer in Gauze Disc Matrices

200 mesh: • 1.0 bar
100 mesh: □ 1.0 bar, ○ 2.0 bar, Δ 3.0 bar
------ data of Walker and Wan, [86]
—·—·—·— equation (4-10)

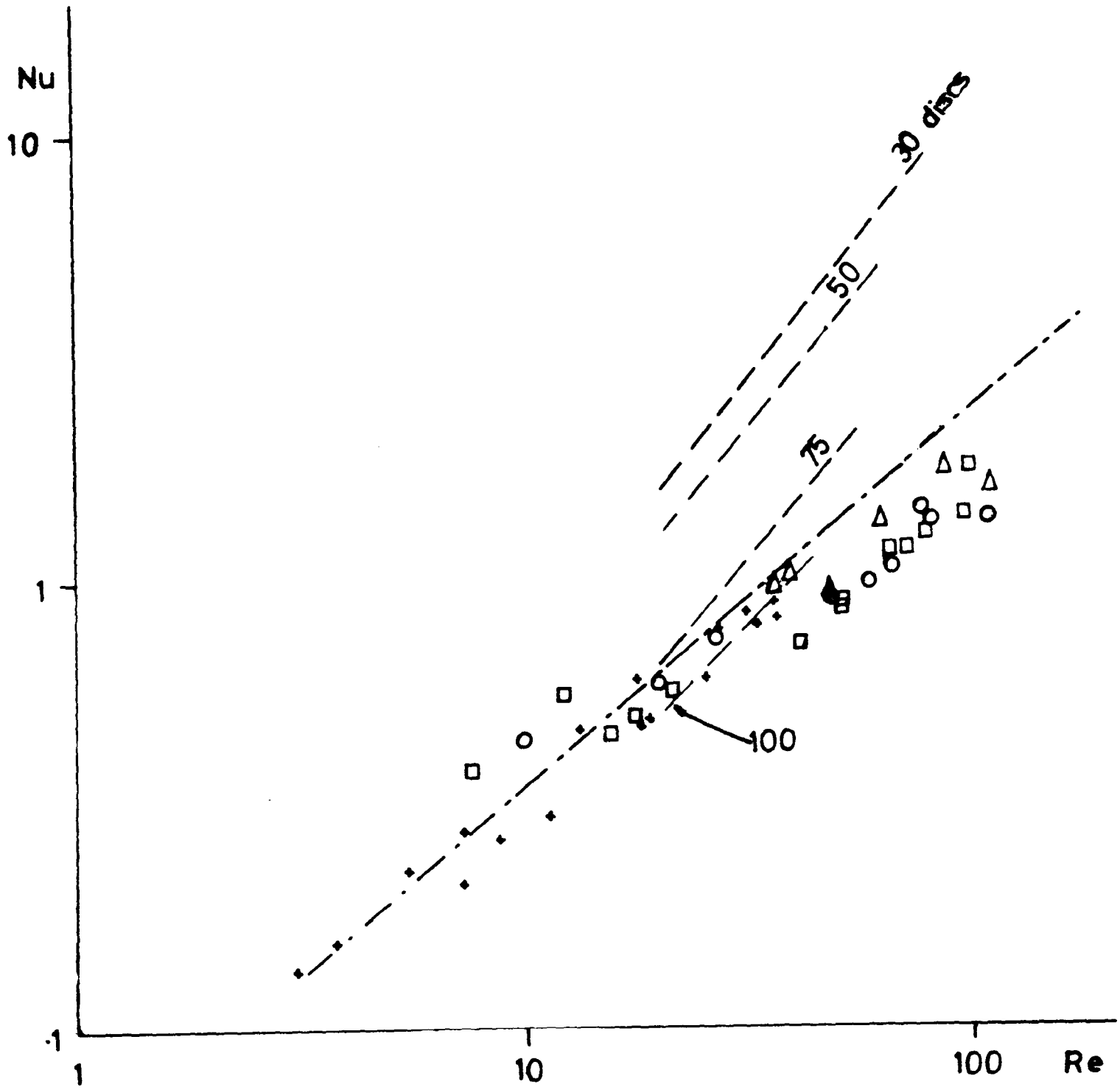

Figure 4.9 Heat Transfer in Sphere Matrices

o 224-250μm spheres, + 212-355μm spheres
--- data of Kays and London, [82]

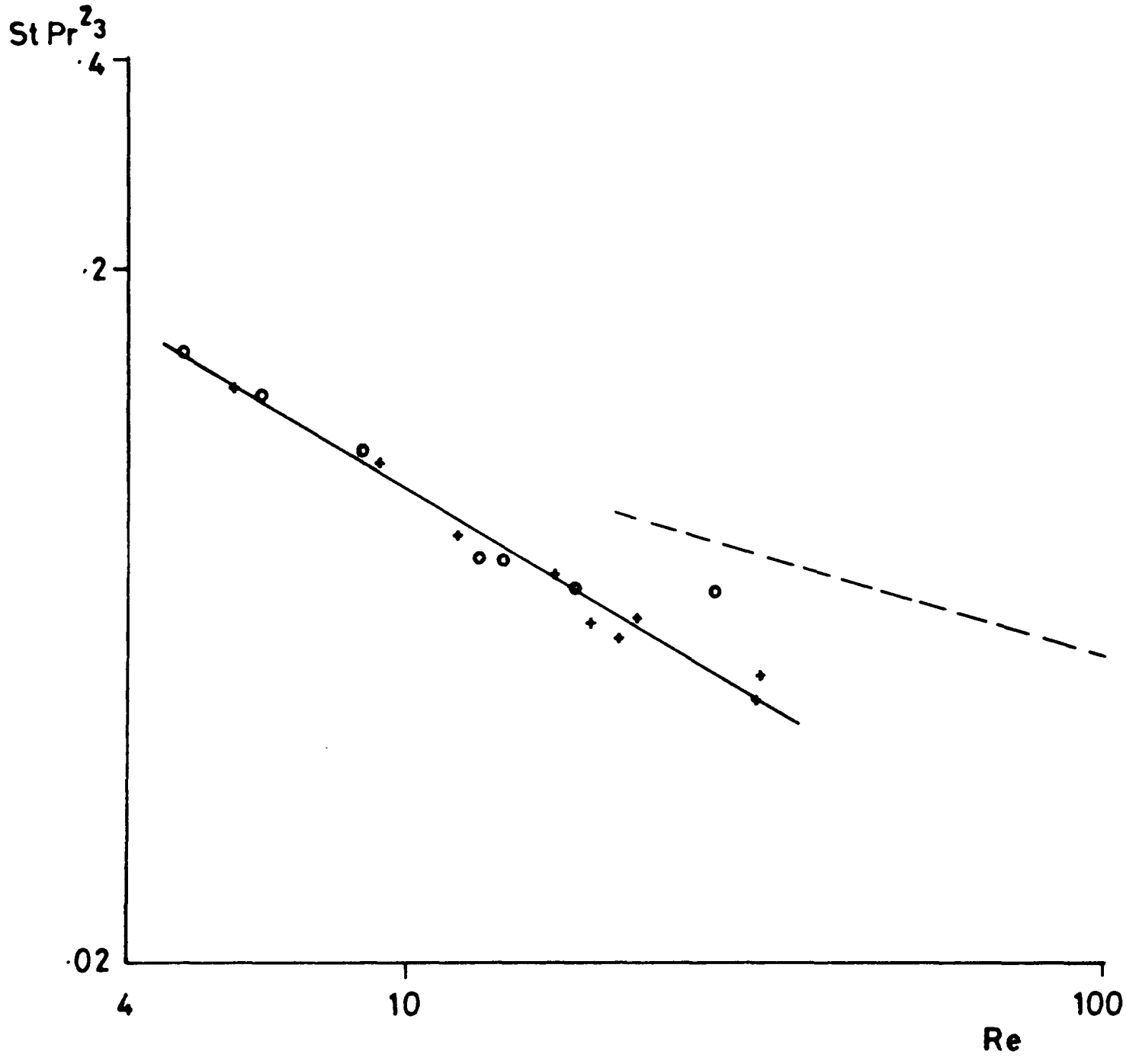

Figure 4.10 Heat Transfer in Sphere Matrices

o 224-240μm spheres, + 212-355μm spheres
---- equation (3-10)

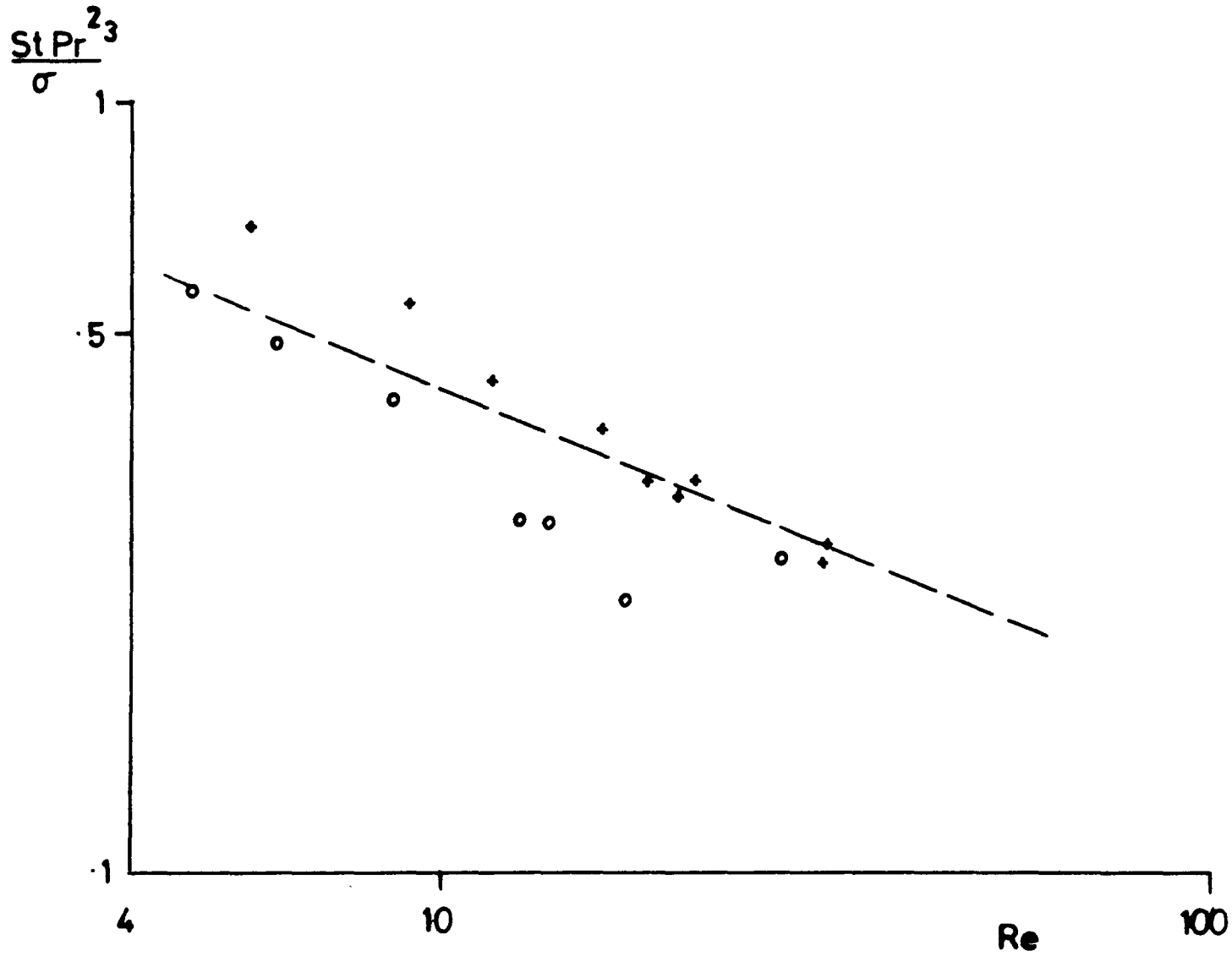

Figure 4.11 Heat transfer in Metal Foam Matrices

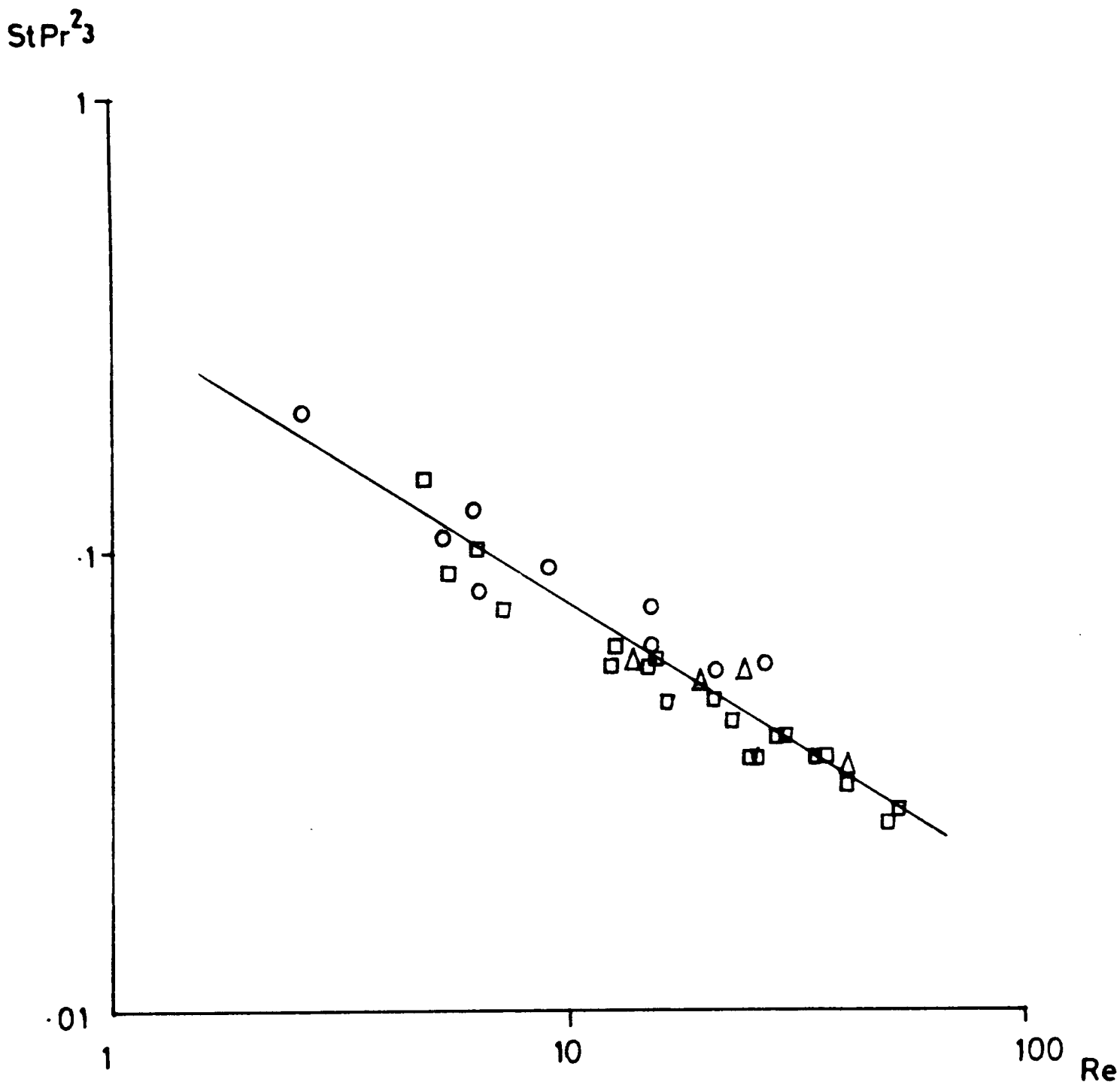

Figure 4.12 Pressure Drop in Regenerator Matrices

o 224-250μm spheres, • 212-355μm spheres,
∇ foam (1 piece), ▫ 200 mesh discs
× foam (5 pieces), Δ compressed foam,

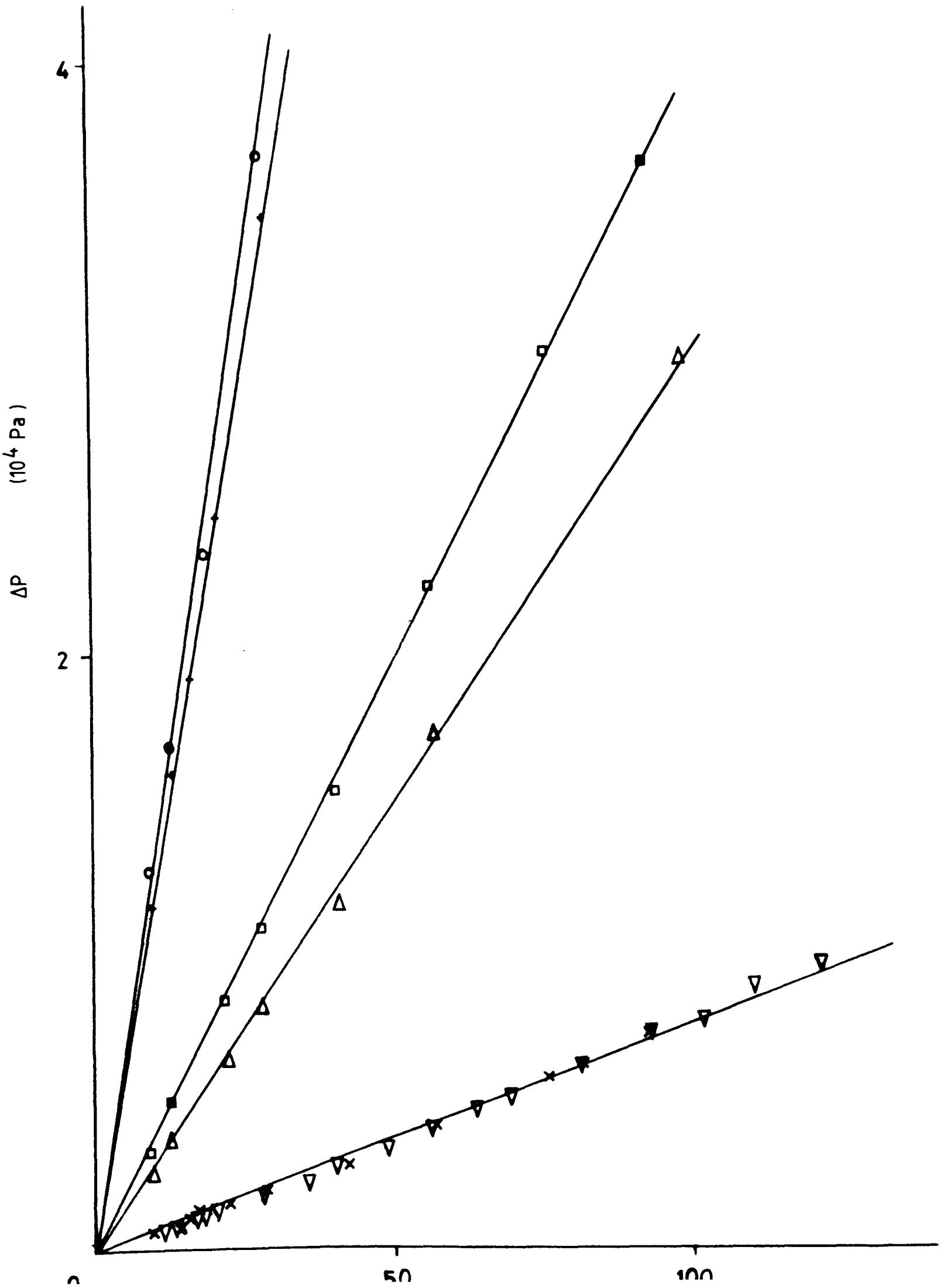

Figure 4.13 Pressure Drop Across Regenerator Matrices

× 200 mesh, o foam, ⋄ compressed foam
Δ 224-250μm spheres, ▫ 212-355μm spheres
● sphere data using equations (4-13) and (4-14)

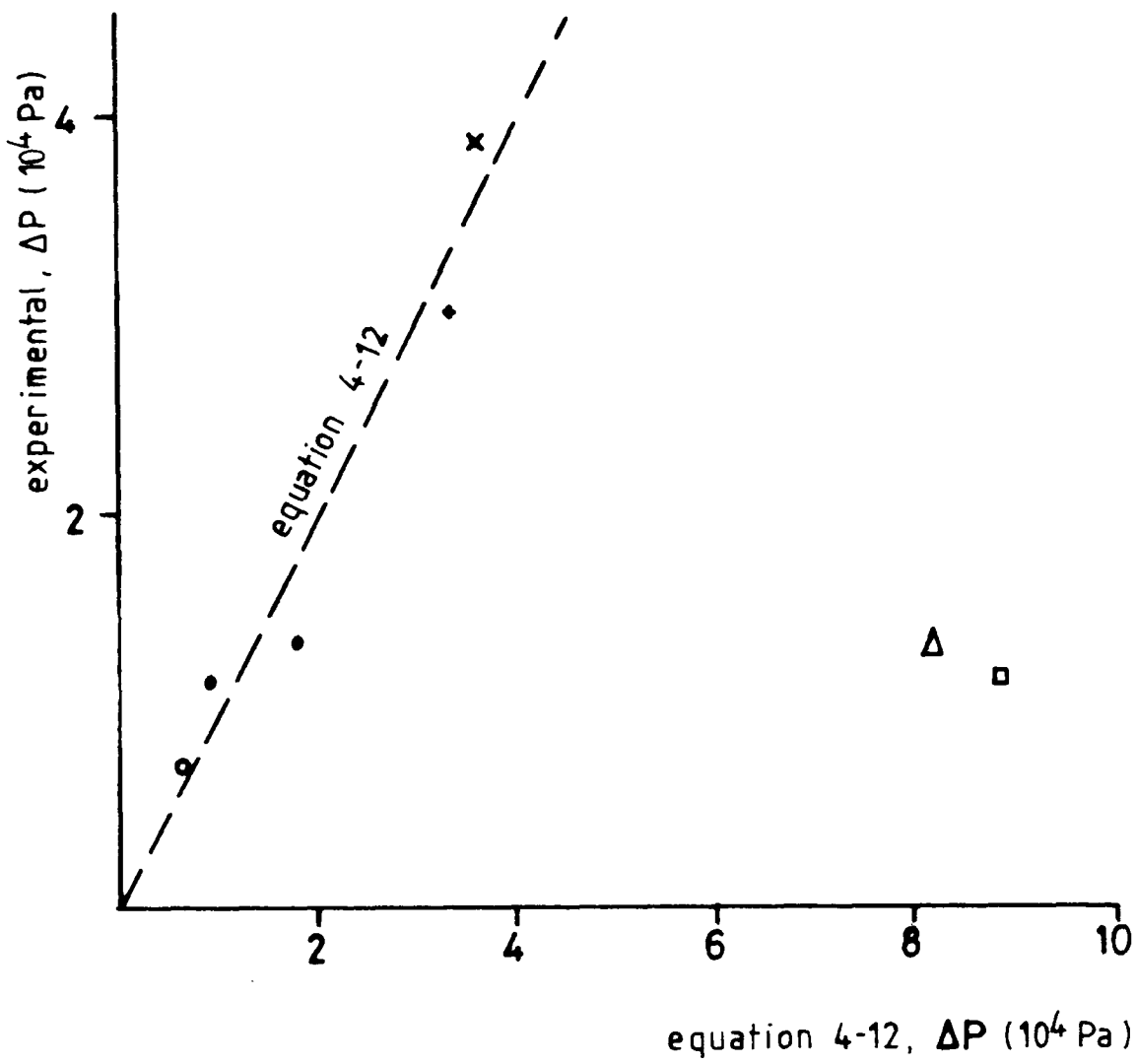

Figure 4.14 Section of Sphere Matrix

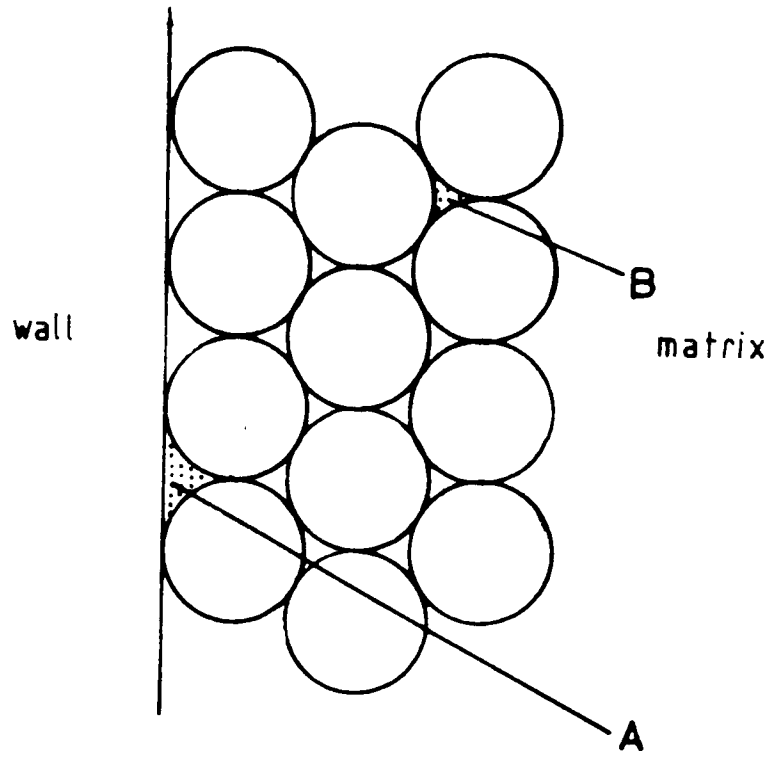

Figure 4.15 Velocity Distribution in Sphere Beds, [97]

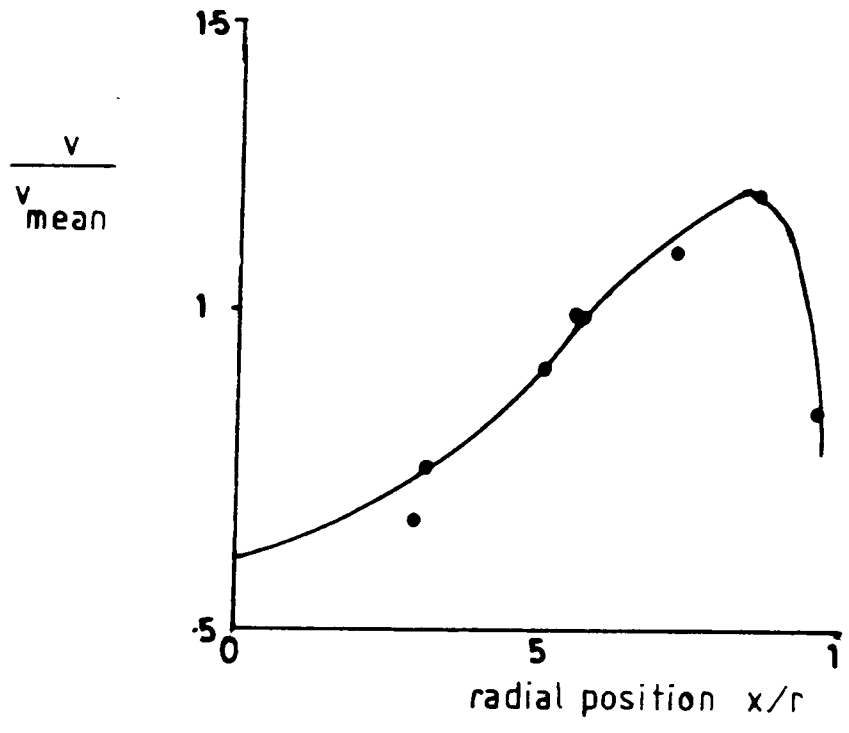

Figure 4.16 Comparison of Heat Transfer
in Regenerator Matrices

o 200 mesh, □ 100 mesh, ◇ foam, ⬩ compressed foam
▽ 224-250μm spheres, △ 212-355μm spheres
▼▲ sphere data assuming annular flow

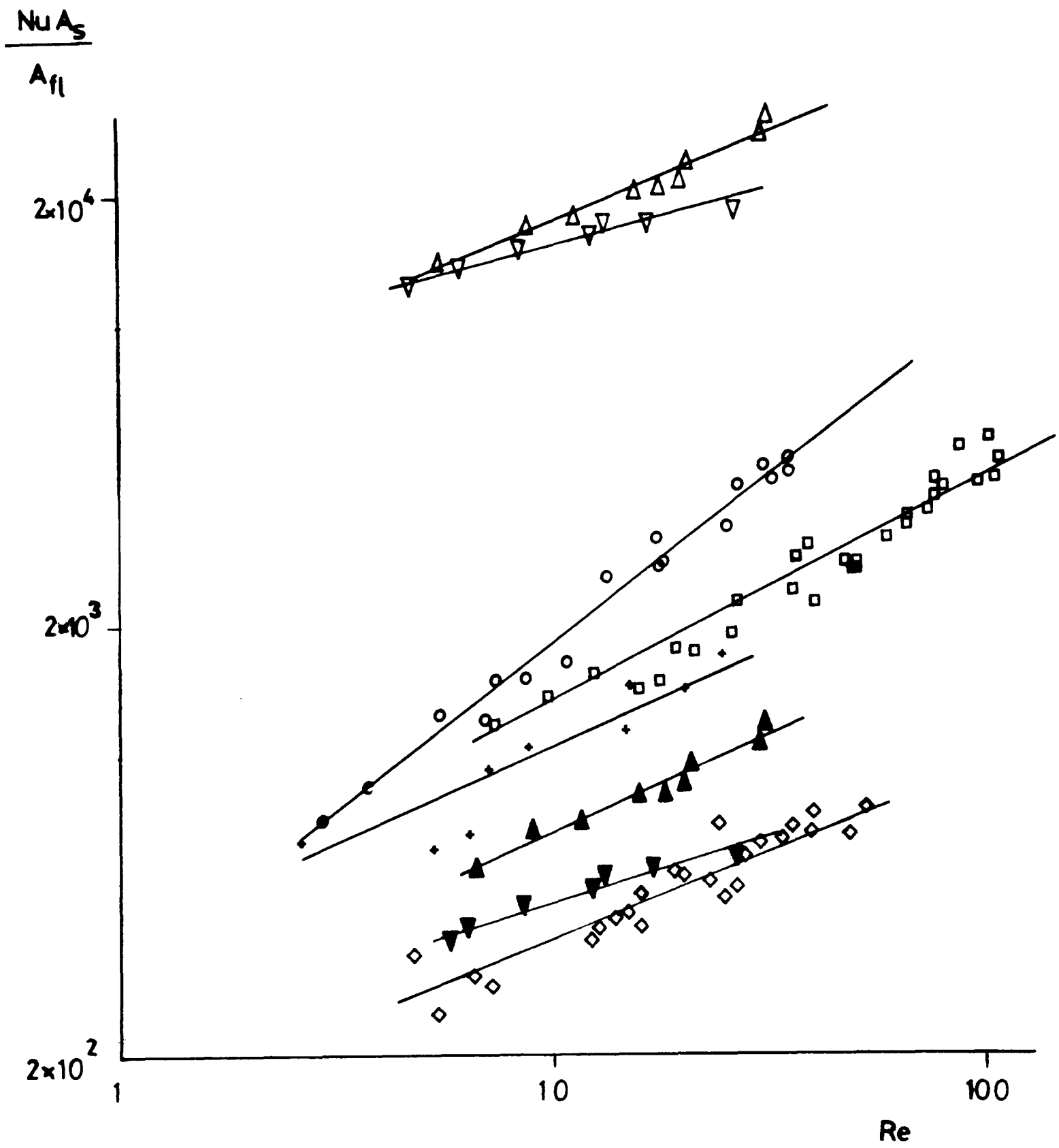

CHAPTER 5

THE STIRLING-CYCLE COOLER: EXPERIMENTAL TECHNIQUES

The work described in this and the following chapter is a study of the losses in a working miniature refrigerator, and their dependence on variables such as frequency and filling pressure, and the development of an energy balance for the machine which could be used as the basis of a future model for refrigerator performance.

The losses that occur can be divided into two categories. Firstly, those that effect the fraction of the input power which is available for refrigeration, for example, Joule heating in the coil windings of the compressor drive system and thermodynamic losses during compression. Secondly, the losses that consume part of the refrigeration produced, i.e. the shuttle heat transfer, regenerator losses (due to imperfect heat transfer and finite heat caspacity of the matrix), pressure drop in the regenerator, and conduction losses. These catagories will be referred to as the 'compressor losses' and the 'refrigeration losses' respectively.

This chapter describes the methods used to isolate and measure these effects, while Chapter Six discusses the data acquired using these techniques.

5.1 DESCRIPTION OF THE REFRIGERATOR

The cooler used in the experiments to measure refrigerator losses in situ was a split-cycle miniature Stirling refrigerator, [40]. This machine is designed to provide 1W of cooling at 80K using about 30W of power, with helium gas at 10.0 bar as the working fluid. Schematic diagrams of both the compressor and the displacer are presented in Figures (5.1) and (5.2), and the gas flow path through the displacer in Figure (5.2(a)).

The linear-motor drive compressor is oil-free and uses a flat spring suspension to provide radial stiffness and to maintain piston alignment. The compressor can be driven at frequencies up to several kilohertz, but because of a combination of heat transfer and resonance considerations the normal operating frequency is in the range 30Hz to 50Hz. The maximum compressor swept volume is 3.15cm^3, using a stroke of 10mm.

The regenerator is contained within the displacer (which also has linear drive) and consists of a stack of phosphor bronze gauze discs, 0.71 cm in diameter. Under normal operating conditions the displacer has a stroke of 3mm, with a possible maximum of 4mm. Two different regenerator matrices were used in the experiments, one of 250 mesh, and the other of 150 mesh. The physical characteristics of the two matrices

are presented in Table (5.1).

The displacer is designed to be pneumatically driven at approximately the optimum phase angle and stroke, the linear motor allows the phase angle and amplitude to be controlled.

A variable frequency sine wave generator is used with two variable gain power amplifiers to run the compressor and displacer at the desired frequency and amplitude. A phase control circuit in the displacer drive allows the phase between the piston and displacer to be controlled.

The cooler is filled to the operating pressure with helium gas which has been passed through a liquid nitrogen cooled trap to remove condensible impurities.

The complete assembly is shown in Figure (5.3), with the necessary instrumentation shown in Figure (5.4). In Figure (5.5) the cold finger of the refrigerator with the vacuum jacket removed can be seen, showing the demountable copper flange at the cold end, which contains the thermometer diode and the heater coil.

5.1.1 Instrumentation

Piston and displacer positions were monitored using Linear Voltage Displacement Transducers (L.V.D.T.'s), mounted at the bases of the compressor and displacer units, which measured the displacement of soft iron slugs attached to the piston and displacer shafts. These were calibrated under static conditions using a vernier gauge and reading the output from a digital voltmeter.

The alternating pressure in the system was measured using a Kulite* pressure transducer mounted in the gas cooler at the top of the compressor, and a similar transducer at the base of the displacer unit. These were calibrated at static pressures. It is assumed that the pressure in all parts of the refrigerator is uniform. This assumption is justified by the fact that the pressure measured in the displacer was within 5% of that measured in the compressor, and showed a phase difference of less than 3°, and also by the graph of Figure (5.6), which shows that the power required to drive the piston with a given stroke is proportional to frequency. Pressure drop losses would be proportional to higher powers of frequency. These losses are discussed in more detail in Chapter 6.

Filling pressure was measured using a Budenberg Standard Test Gauge.

P-V diagrams for the compression space and the expansion space could be displayed on an oscilloscope using the output from the piston L.V.D.T. (in the case of the compression space P-V loop), or the displacer L.V.D.T. (in the case of the expansion space P-V loop), on the x-axis and the pressure transducer output on the y-axis. The traces obtained were photographed, and the areas of the loops measured. The errors involved in this procedure are estimated to be ±10%, due to electrical noise on the pressure transducer output, and limits on the scale of the diagrams imposed by the size of the oscilloscope screen.

The temperature at the cold end was monitored using a calibrated ITT* diode (type 4148) mounted in the copper flange at the end of the cold finger. The diode was calibrated at liquid nitrogen temperature (77.3K) and at room temperature, and the temperature response was assumed to be linear, as shown in previous experiments, [98]. The diode monitors temperatures of the cold end in the range 70K to 130K where the error in this assumption is small (±1.5K). It was not considered necessary to calibrate the diode more rigourously for the experiments described below because the reproducibility of temperature measurements is of greater importance than the exact value of temperature. The diode was recalibrated at intervals and always found to give consistant values, ($\pm 5\times10^{-4}$V, which corresponds to ±0.2K).

The cold finger assembly was surrounded by alternate layers of superinsulation and nylon mesh, and enclosed in a vacuum jacket which was evacuated to less than 5×10^{-5} torr prior to running the refrigerator.

Piston and displacer were separately driven and the phase between the two displacements could be altered by the imposition of electrical drive onto the displacer, which is already pneumatically driven by the gas pressure pulse provided by the compressor, [35]. The position of the piston in the cylinder could be adjusted by applying a d.c. offset to the drive voltage. Power input was measured using a Feedback Electronic Wattmeter EW604*, which measures true watts regardless of the current and voltage waveforms. The errors involved in power measurements were approximately 5% of

the input power. However, when very low powers (<200mW) were monitored, for example, in the pressure drop tests described below, the accuracy was typically ±15%. Drive current was measured using a Fluke* multimeter which measures true r.m.s. values (to an accuracy of typically ±2%).

A heater coil wound around the cold end flange provided the means of applying an external load, in order to measure the useful refrigeration produced by the machine. This load was also measured using a Feedback EW604 wattmeter.

5.2 EXPERIMENTAL METHODS

5.2.1 Compressor Losses

The gas seals in the machine, those around the piston and displacer, are clearance seals (the clearances maintained are up to 0.05mm between the displacer and cylinder wall, and 0.01mm around the piston and the displacer drive shaft), thus eliminating frictional losses. Leakage of gas past the piston could be a problem with such a system. However, this can be monitored by measuring the pressure pulse produced by a given piston stroke at different frequencies. It was found that at low frequencies (0-20Hz) the pressure pulse increased as the frequency increased, implying that the gas was leaking past the piston, but above 25Hz the pressure pulse was independent of frequency. The operating range for this cooler, 30Hz to 50Hz, is in the latter region.

5.2.1.1 Joule Heating -

The current required to drive the piston to produce a given pressure pulse depends strongly on the resonant frequency of the system (as this affects the position of the coil in the air gap of the magnetic circuit, and hence the lines of magnetic flux cut, when the current through the coil windings is a maximum). The resonant frequency is governed by the piston area, the mass of the reciprocating parts, and depends on the filling pressure (as the gas provides the main 'spring' in this system), and the volume of the system. The precise variation of compressor efficiency with these parameters is beyond the scope of this investigation. Here the drive current (both the a.c. and the d.c. components), and the resistance of the coil, when already hot, were measured. Joule heating losses could then be subtracted from the total power input to derive the actual power provided to the gas.

Typical compressor efficiencies are in the range 50-55% when running at 30Hz, 65-75% at 40Hz, and 75-80% at 50Hz, depending on the filling pressure and the cold end temperature.

5.2.1.2 Windage -

To estimate the windage of the spring suspension and coil of the compressor, and any hysteresis loss in the magnet, the piston was driven in air at atmospheric pressure and room temperature as in these conditions it has comparable density and viscosity to helium at 10 bar, and there is no effect of

irreversible compression or expansion. The power needed to drive the piston was measured and the I^2R losses were subtracted. It was found that the remaining power, that required to overcome windage and friction losses, was very small (<100mW) when compared to a typical input power of 28W.

The assumption that joule heating is the only significant loss in the compressor is justified by the P-V diagrams obtained for the compression space, the area of which are equal to the total input power minus the joule heating losses (to within 1W).

$$W_{tot} - I^2R \approx \int PdV \qquad (5\text{-}1)$$

5.2.2 The Effect Of Irreversible Compression

As described above, a P-V diagram for the compression space could be displayed on the oscilloscope while the refrigerator was running. If the displacer is held still (by reversing the drive terminals and adjusting the phase and power controls until a stationary trace is obtained), another P-V diagram for the compressor is obtained. As no refrigeration is being produced by the cooler, this loop represents the effect of irreversible processes during compression in the system. The amount of power going into these processes, W_{ir}, was measured from the area of this P-V diagram.

The nature of these losses was investigated by measuring the variation of power (minus I^2R losses), required to drive the compressor with a fixed stroke, with frequency, while holding the displacer still. The data for two stroke lengths are shown in Figure (5.6). The loss measured is seen to be proportional to frequency, and the graph obtained is a straight line through the origin. This suggests that the cause is thermodynamic, involving a loss per cycle, such as the loss due to irreversible compression. Losses due to gas velocity, such as pressure drop, would involve a higher power dependence on frequency. The probable cause of these losses is discussed in Chapter 6.

5.2.3 Refrigeration Losses

5.2.3.1 Static Heat Losses -

The static heat losses are the conduction to the cold end through regenerator, displacer, cylinder wall, and helium, and radiation heat transfer from the vacuum jacket to the cold finger together with residual gas conduction. These were obtained by timing the warm up between two selected temperatures with a heat load applied to the cold end. A graph of the reciprocal of the warm up time against the heat applied gives the static heat losses as the intercept on the heat load axis. These measurements were performed around three temperatures, 120K, 90K, and 72K, and are shown in Figure (5.7). This method of measurement eliminates the need for accurate knowledge of the heat capacity of the cold end. If thermal time constants had a significant effect the graphs

of Figure (5.7) would be expected to curve, their linearity over a wide range of applied heat loads indicates that this is not the case.

This graph was used as the calibration for the shuttle and regenerator loss measurements. The warm up time measured while the displacer is running can be compared to that of a known heat load, from Figure (5.7), so that the heat load imposed by the movement of the displacer can be found. This technique relies on the measurement of time intervals (typically 15-50 seconds) in which high accuracy can be achieved.

5.2.3.2 Displacer Losses -

The sum of losses due to regenerator inefficiency, shuttle heat transfer, and pressure drop through the regenerator will be termed the 'displacer losses' as all are apparent when the displacer moves.

Measurements of displacer losses were made by timing the warm up when the displacer was allowed to move at a given stroke. To prevent the working gas from doing work against the piston a d.c. offset was applied to the compressor drive to hold the piston stationary against the compression cylinder head. In order to separate the three contributory causes of heat loss, the pressure drop and shuttle heat transfer had to be measured independently of the regenerator loss.

5.2.3.2.1 Pressure Drop Losses -

The displacer losses described above contain the energy used to overcome pressure drop across the displacer. This was separately measured by comparing the power (minus any I^2R losses) needed to drive the displacer in vacuum, and in helium at atmospheric pressure and at the normal operating pressure of 10.2 bar. These measurements were made while varying the frequency and cold end temperature.

5.2.3.2.2 Shuttle Heat Transfer -

Shuttle heat transfer was measured in a similar way to the displacer loss, but the working fluid in the cooler was reduced to atmospheric pressure in order to make any regenerator losses negligible. The value of heat loss obtained in this way includes the effect of pressure drop, measured above, so this had to be subtracted in order to arrive at the shuttle heat transfer. Measurements were performed while varying the length of displacer stroke, operating frequency and temperature.

5.2.3.2.3 Regenerator Losses -

The remaining displacer loss, after the effects of shuttle heat transfer and pressure drop had been subtracted, is that due to imperfect regeneration.

Regenerator loss data were obtained for both the matrices tested while varying the displacer stroke, the drive frequency and the operating pressure in the refrigerator, and at the

three temperatures used for the static heat losses described above.

5.3 PERFORMANCE DATA

Performance data including measurements of input power and current, piston and displacer stroke, cold end temperature and applied heat load, and losses due to irreversible compresssion, were obtained under a variety of operating conditions. The effects of filling pressure, in the range 8.1 bar to 11.6 bar, frequency, in the range 30Hz to 50Hz, and temperature, in the range 72K to 120K, were investigated.

It was found necessary to limit the possible variables in order to enable their effects to be separated. For this reason the phase angle between the piston and displacer motions was set at 70°, as this was found to give optimum performance. An important factor influencing this decision was that it was almost impossible to alter this phase angle without changing other variables (such as the displacer stroke length and total power input). The input power for all the tests was chosen so that the power into the gas was approximately 20W. This allows the effect of compressor efficiency to be divorced from the heat transfer and thermodynamic losses in the system.

5.4 THE ENERGY BALANCE

As the power into the cooler, W_{tot}, is known and the Joule heating was measured, the compressor efficiency can be calculated. This provides the power input to the gas. Losses

due to irreversible effects in the compressor, W_{ir}, were measured as described above. Equation (5-1) holds both when the displacer is moving (as the power delivered by the compressor to the gas is measured), and when the displacer is stationary (as the losses due to irreversible compression are measured).

When these losses are subtracted from the power input to the gas, the remaining power, W_g, is that which is available to provide refrigeration. The theoretical maximum amount of that refrigeration can be calculated, at a given temperature, from Carnot's expression for refrigerator efficiency, [32].

$$\text{Maximum refrigeration} = (W_g T_c)/(T_h - T_c)$$

The sum of the static loss at a given operating temperature, and the regenerator, pressure drop, and shuttle heat transfer losses (for the appropriate displacer stroke, frequency, temperature, and operating pressure) and the applied heat load, make up the total refrigeration produced by the working gas. Total refrigeration is also measured by the area of the indicator diagram in the expansion space. If no significant losses have been neglected the two values should be equal.

In addition to the sources of inefficiency mentioned above, there may be others which have not been measured, for example, work done by the gas in pneumatically driving the displacer, and the effect of a temperature difference between the gas in the cold end and the temperature measured by the diode on the cold end flange. These losses can be estimated from the data obtained using the methods outlined above.

The following chapter describes the data obtained from this refrigerator and suggests a simple model of performance which will be useful in the design of future coolers.

Figure 5.1 Schematic diagram of Compressor Unit

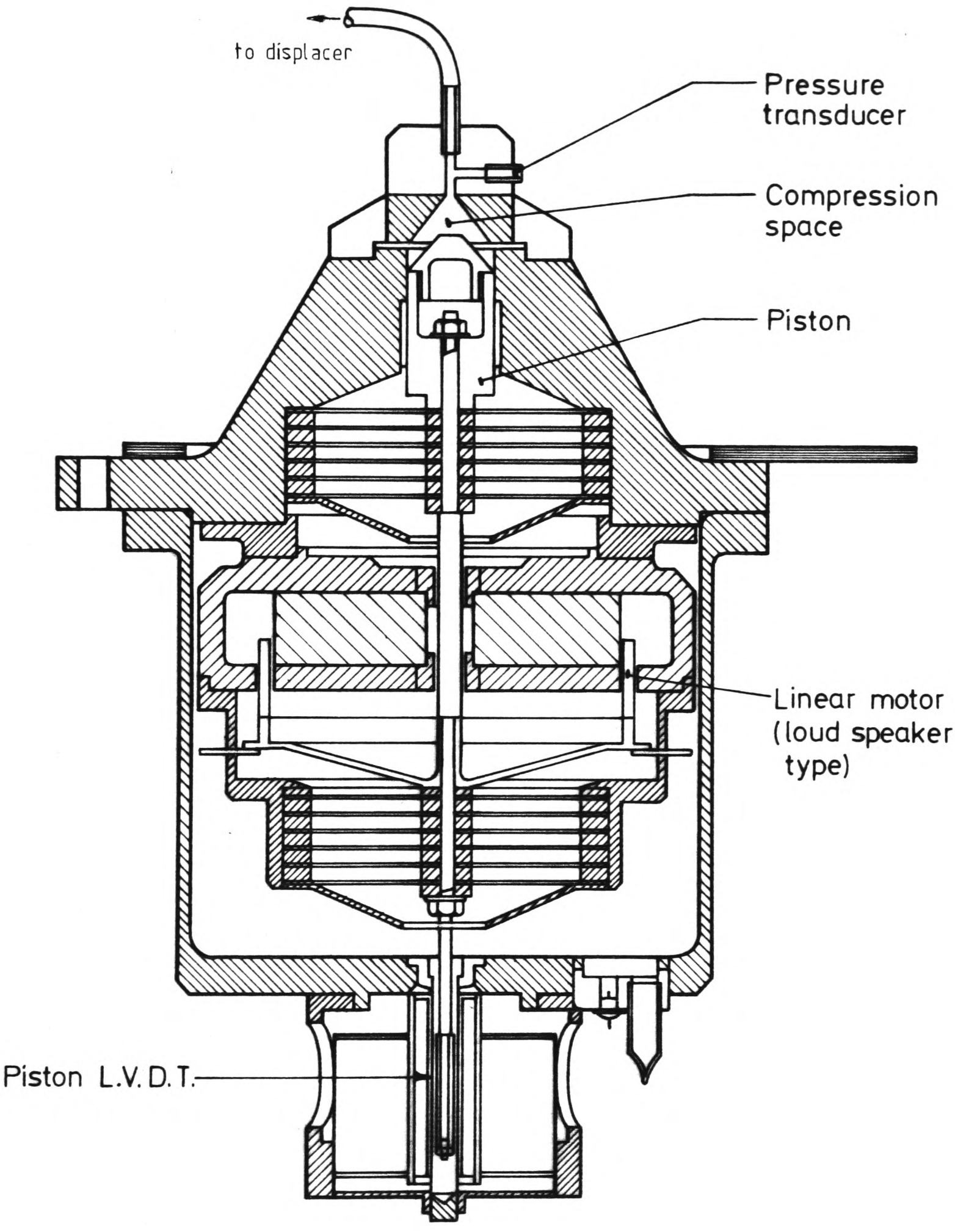

Figure 5.2 Schematic Diagram of Displacer Unit

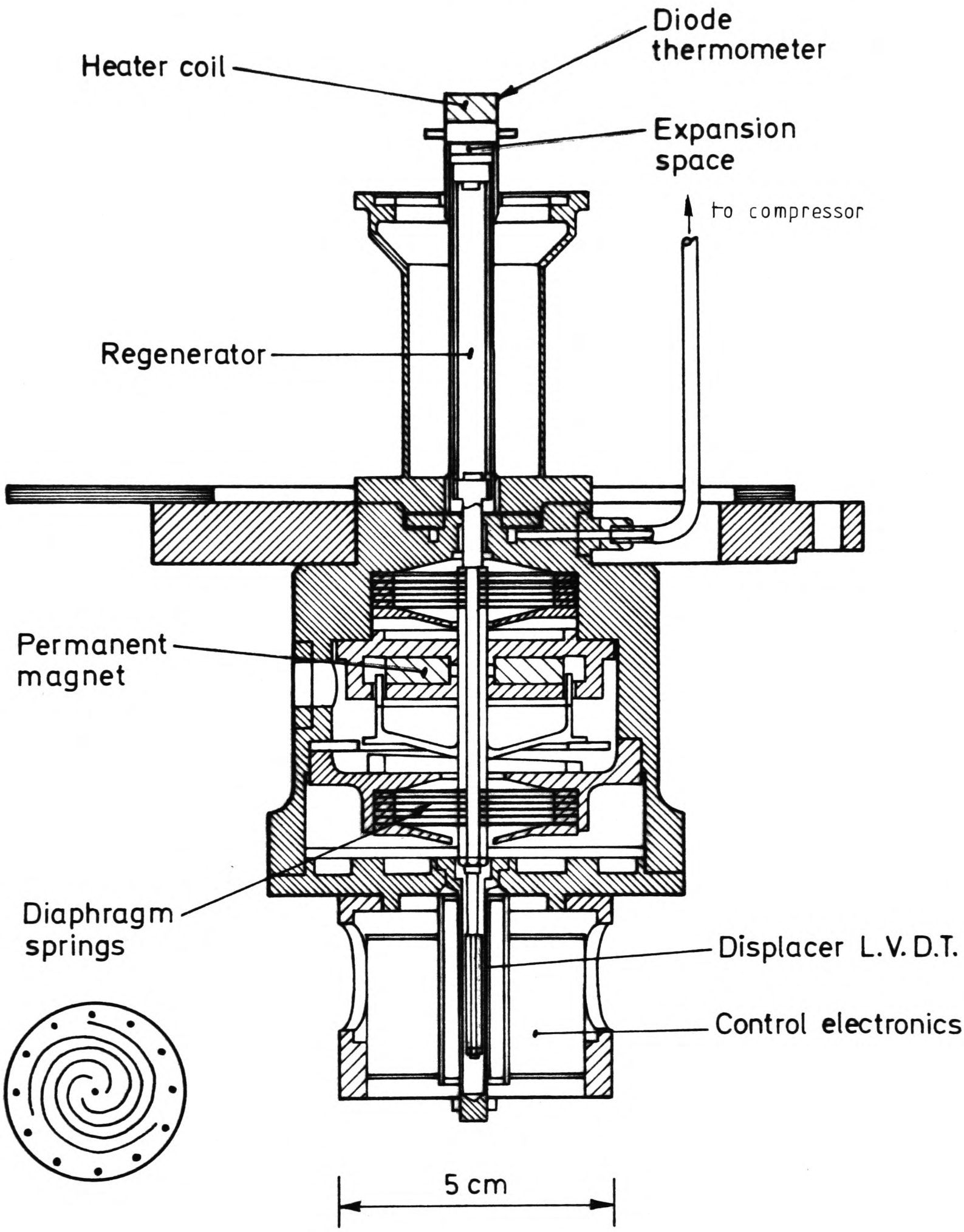

Figure 5.2(a) Detail of Gas Flow through Displacer
(not to scale)

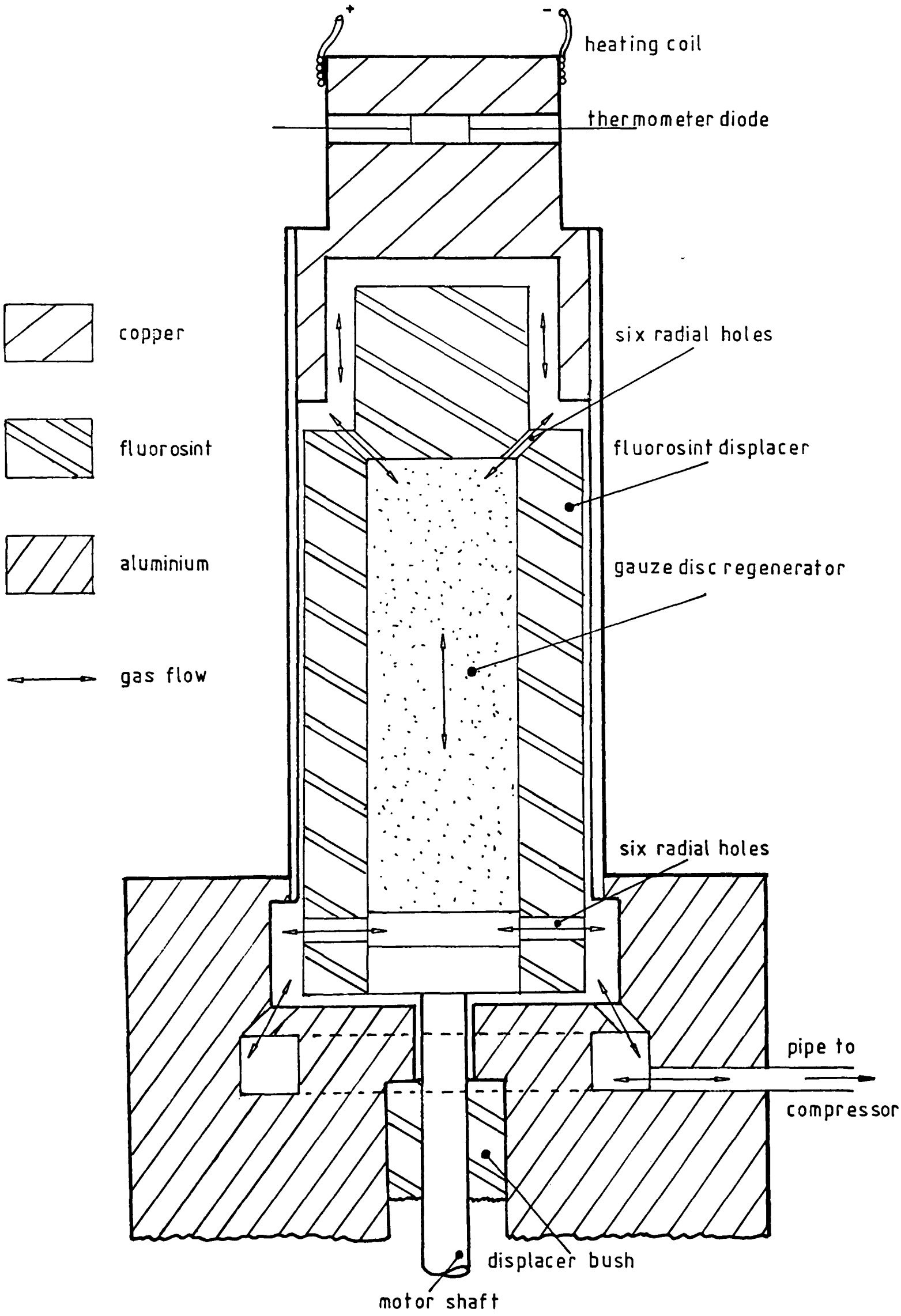

Figure 5.3 Stirling Cycle Refrigerator

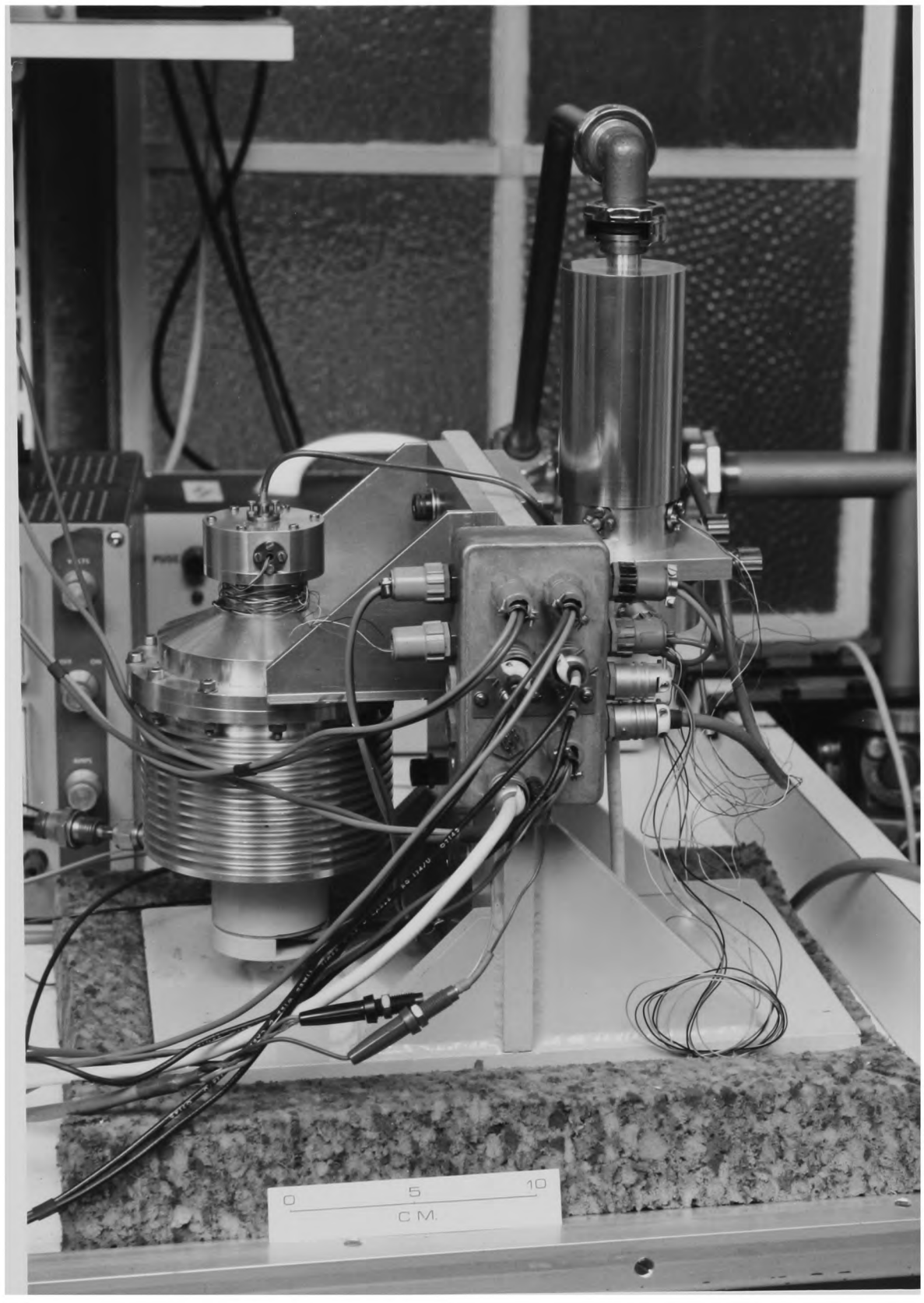

Figure 5.4 Refrigerator Assembly and Instrumentation

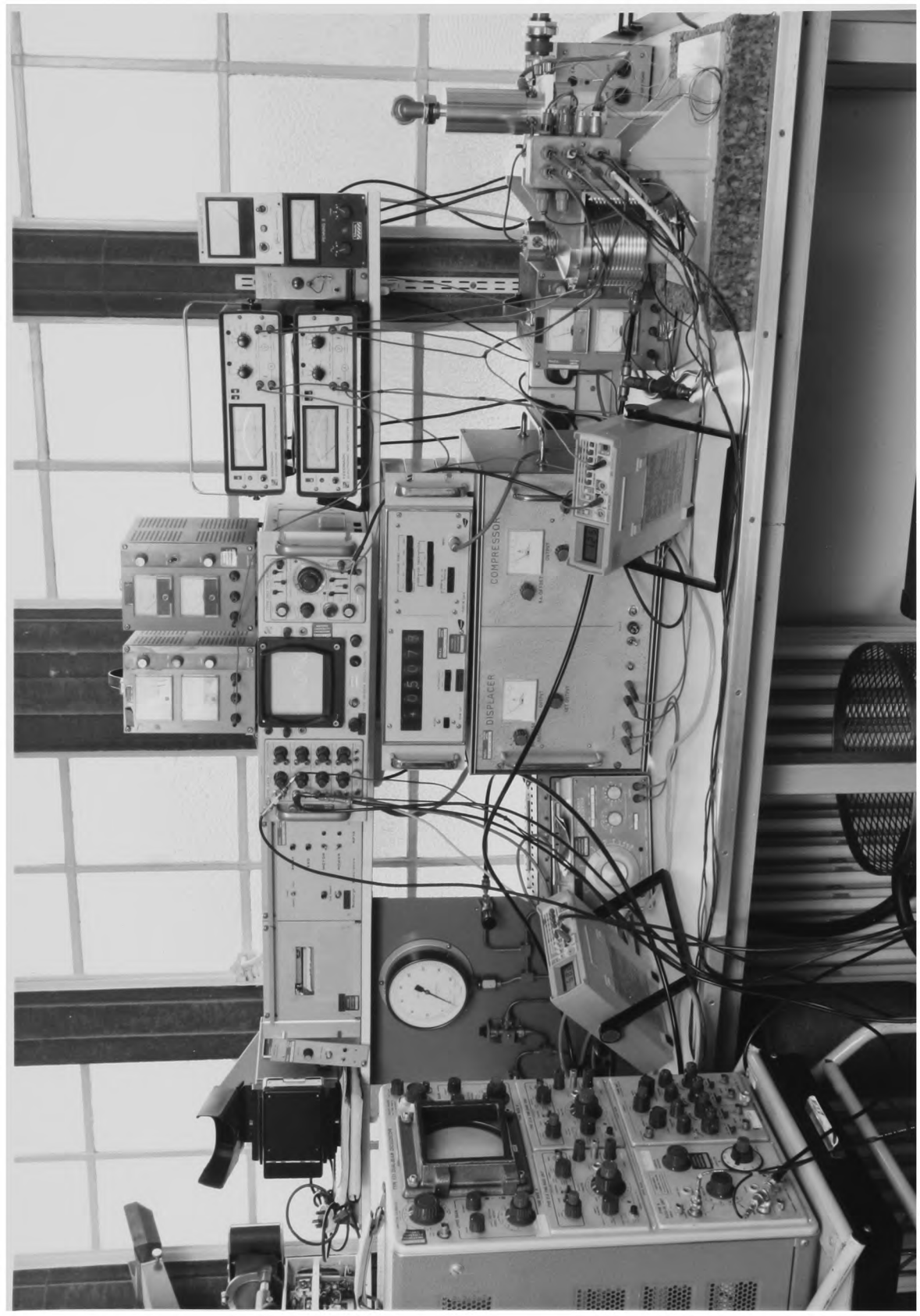

Figure 5.5 Cold Finger

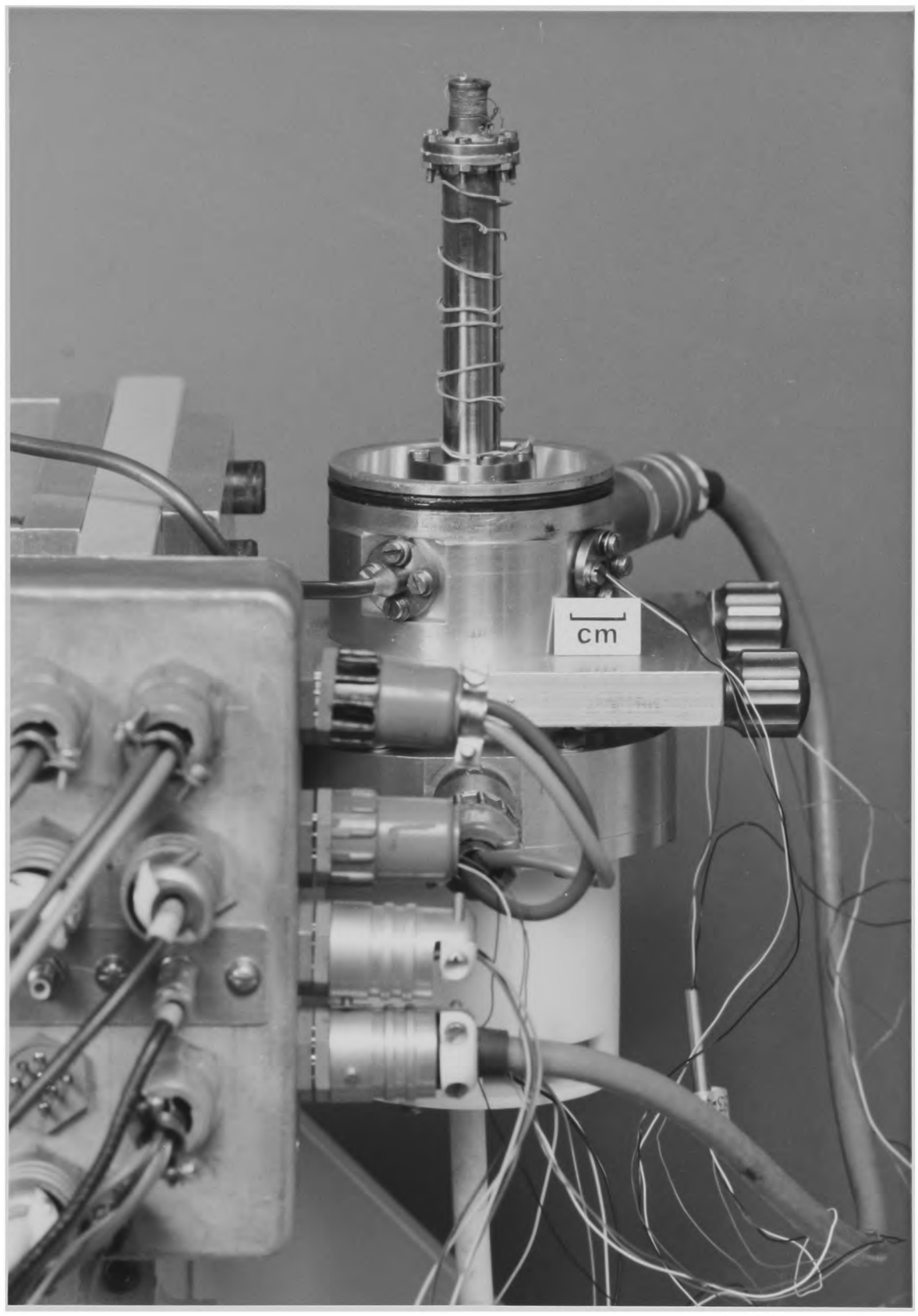

Table 5.1 Regenerator Characteristics

Mesh Size	Number of Discs	Surface Area cm^2	Mass g	D_h cm
250	455	395.1	4.09	0.0133
150	292	295.9	4.83	0.0168

Figure 5.6 Variation of Power Supplied to Gas with Frequency

o piston stroke = 7.1mm, □ piston stroke = 4.8mm

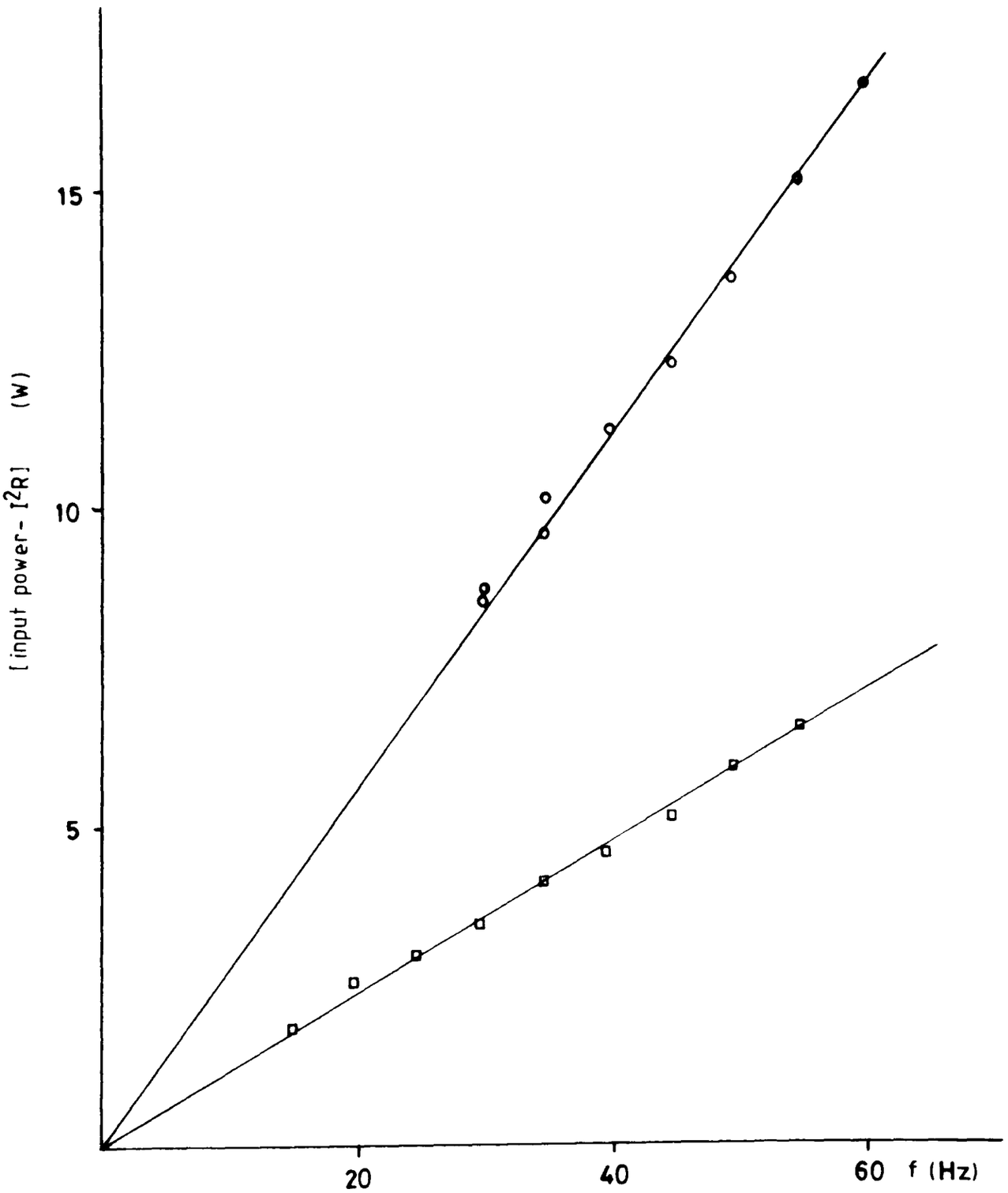

Figure 5.7 Conduction Losses and Calibration of Cold End

• 72K, ▫ 90K, o 120K

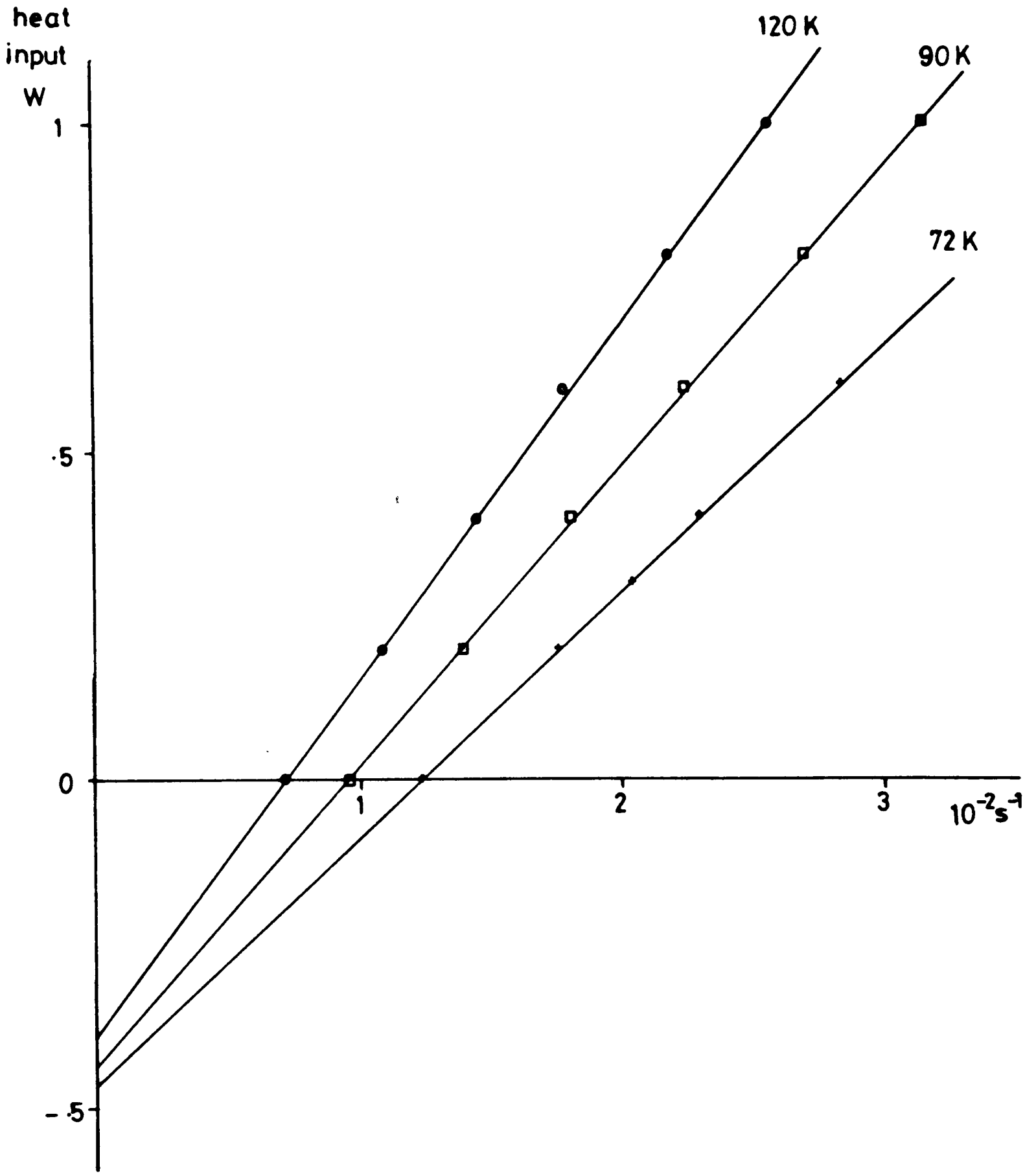

CHAPTER 6

EXPERIMENTAL DATA AND ANALYSIS

6.1 REFRIGERATION LOSSES

The variation of displacer losses with displacer stroke (S), filling pressure, cold end temperature and frequency is shown in Figures (6.1) to (6.3).

It can be seen that the losses increase rapidly with increasing displacer stroke and frequency, and decreasing cold end temperature. Change in filling pressure has a less pronounced effect.

The displacer losses are caused by the combined effect of pressure drop across the displacer, shuttle heat transfer, and regenerator inefficiency. The dependence of each of these components on the variables (frequency, filling pressure and cold end temperature) is examined below.

6.1.1 PRESSURE DROP

The work done during one half cycle by the gas due to a pressure drop, ΔP, across the displacer moving with a stroke S, and at a frequency f, will be

work done = $\Delta P\ A_f\ S$

The power lost by the gas experiencing this pressure drop will be

$$\text{power} = \Delta P A_f S 2f \qquad (6\text{-}1)$$

The power loss measured due to pressure drop is shown in Figure (6.4), showing the effects of filling pressure and frequency, and Figure (6.5), showing the effect of displacer stroke and cold end temperature.

The pressure drop across the displacer will have two components, that due to the regenerator gauzes, and that due to the structure of the displacer casing. The pressure drop across the gauze discs can be calculated from equation (4-13), and the power loss resulting from this pressure drop will be (from equation (6-1)),

$$\text{power} = \frac{10\ A_s^{\,2} \mu A_f f^2 S^2}{V^2\ \sigma^3} \qquad (6\text{-}2)$$

It can be seen that the power lost due to pressure drop across the gauze discs is proportional to the square of the displacer stroke, and the square of the frequency, but is independent of filling pressure. Equation (6-2) is also plotted in Figure (6.4), and gives good agreement with the data at 1 bar, but does not account for the variation of

pressure drop with filling pressure and frequency that has been observed, nor for the variation with displacer stroke, as shown in Figure (6.5). The errors in these measurements are large (±50%), due to the small currents and powers used (<0.2A, <0.2W). However, the data show a clear trend away from the straight line predicted by equation (6-2).

This behaviour could be explained if there is a pressure drop due to the geometry of the displacer, in addition to that due to the matrix it contains, which shows the same dependence on gas density and velocity as does the pressure drop across an orifice plate, [95]. The gas enters and leaves the displacer in this refrigerator through 6 radially spaced holes at both the hot and cold ends, each of about 0.4mm diameter. It is possible that these holes, especially if they were to be partially blocked by contaminants, could provide such a pressure drop.

The pressure drop across an orifice is proportional to the density of the gas, and to the square of the gas velocity. When the displacer is moving with a stroke S, the gas velocity through any part of the displacer will be proportional to 2fS (the constant of proportionality will depend on the flow area involved). The power used to overcome such a pressure drop will therefore be proportional to the third power of both the frequency and the stroke.

$$\text{power} \propto \rho\, f^3\, S^3 \qquad (6\text{-}3)$$

The 'additional loss', that not accounted for by the pressure drop due to the matrix, is plotted against $\rho(fS)^3$ in Figure (6.6) and is seen to be proportional to this group of variables, indicating that it could be due to an 'orifice type' pressure drop.

To find the average gas velocity through the matrix (and hence the pressure drop) when one end is cold, consider the mass distribution in the machine. If it considered as three spaces, the warm space at temperature T=300K, the regenerator dead space where T=195K, and the cold space where T=90K, then, with the displacer at the top (cold end) of its stroke, the mass in the engine is given by,

$$m = P_1/R \times [(V_h/300) + (V_d/195)]$$

and with the displacer at the bottom of its stroke (for a 4mm stroke)

$$m = P_2/R \times [(V_h'/300) + (V_d/195) + (V_c/90)]$$

where, for this machine with the piston held against the cylinder head, $V_h=1.41cm^3$, $V_d=1.35cm^3$, $V_c=0.312cm^3$, and $V_h'=1.178cm^3=V_h-V_c$.

Since mass is conserved, these equations give

$$P_1 = 1.20\ P_2$$

and $\dot{m}_c = 1.72\ \dot{m}_h$

where $\dot{m}_c = P_2 V_c/90$, is the mass flow at the cold end of the displacer, and $\dot{m}_h = 1/300(P_1 V_h - P_2 V_h')$, is the mass flow at the hot end of the displacer.

By the conservation of momentum, as the displacer moves up,

$$\dot{m}_c\ v_c = \dot{m}_h\ v_h$$

$$v_h = 1.72\ v_c$$

and the arithmetical average velocity is given by $(v_h+v_c)/2=1.36v$, where v is the gas velocity when the displacer is at a uniform temperature.

In addition to the dependence on gas velocity, the pressure drop is proportional to the viscosity, which decreases as the temperature decreases. The gas viscosity at 195K (the mean matrix temperature when the cold end is at 90K) is 147.5g/cms, compared with 200g/cms at 300K, a decrease of 36%. Since $\Delta P \propto v\mu$, the pressure drop is virtually unchanged at 90K. This result can be shown to hold for other stroke lengths and cold end temperatures.

The data in Figure (6.5) for cold end temperatures of 72K, 90K, and 120K, appear to be slightly lower than those at 300K, this could be due to errors in taking an arithmetical average velocity, but the discrepancy is within the bounds of

experimental accuracy.

6.1.2 Shuttle Heat Transfer

Shuttle heat transfer data, as a function of the square of the displacer stroke, are shown in Figures (6.7) and (6.8). The variation of this loss with frequency and temperature is indicated.

From the theory outlined in Chapter 3 and Appendix B, the shuttle heat transfer, Q_s, depends on gas conduction across the gap between displacer and wall, and the transient conduction into the displacer material, Q_d. Both are proportional to the square of the displacer stroke and to the temperature gradient along the displacer. However, the gas conduction component, Q_g, is independent of frequency, equation (3-11), while the displacer material component, Q_m, varies as the square root of the frequency, [91], so that

$$Q_m = D_d S^2 \frac{(T_h - T_c)}{l_d} \times \sqrt{(0.5 f \pi k_d c_d \rho_d)} \qquad (6\text{-}4)$$

and the shuttle heat transfer is given by,

$$\frac{1}{Q_s} = \frac{1}{Q_g} + \frac{1}{Q_d} \qquad (6\text{-}5)$$

The thermal properties of the displacer material, Fluorosint* (a mica filled P.T.F.E.), and their dependence on temperature are not well documented, so those of P.T.F.E. were used in the calculation, [99].

It can be seen that, for this refrigerator, the governing factor in shuttle heat transfer is the gas conduction. For example, at 40Hz, with a 3mm displacer stroke and the cold end at 90K, Q_g, given by equation (3-11), is 0.543W, while Q_s, given by equation (6-4), is 2.69W.

The agreement between this theoretical expression and the experimental data is very good (±8%), Figure (6.9). Some deviation might be expected because of the uncertainty in the Fluorosint properties, tolerances in the size of the gas gap between displacer and cylinder wall (≈0.051mm), and the effect of longitudinal conduction on the temperature gradient in the cylinder wall.

6.1.3 Regenerator Losses

The variation of regenerator loss (for both the 150 mesh and the 250 mesh gauze) with displacer stroke, indicating the effect of different frequencies, filling pressures, and cold end temperatures, is shown in Figures (6.10), (6.11), and (6.12).

From these graphs it can be seen that losses increase with higher frequency and longer stroke (showing dependence on gas velocity and/or heat load on the regenerator), while the variation of regenerator loss with filling pressure is much

less pronounced.

The 150 mesh matrix has a smaller surface area for heat transfer but a larger mass (and hence thermal capacity) than the 250 mesh matrix (Table (5.1)). In Figures (6.10) to (6.12), regenerator losses for the 150 mesh matrix are clearly larger than those for the 250 mesh, especially at low temperatures and high frequencies, while showing similar behaviour with respect to these variables. This implies that, under the operating conditions encountered in this refrigerator, the regenerator performance is governed by limited heat transfer rather than finite heat capacity.

Regenerator efficiency, given by

$$\epsilon_r = \frac{\text{regenerator load - measured losses}}{\text{regenerator load}} \qquad (6\text{-}6)$$

is plotted as a function of mass flow rate, in Figures (6.13) to (6.15) for both the 250 and 150 mesh matrices, where $\dot{m}$, the mass flow into the cold end, is given by

$$\dot{m} = fS\rho_c A_f$$

It can be seen that the efficiency decreases as velocity increases, but that higher efficiencies are obtained as the gas density increases. This effect is observed both as the filling pressure is increased, Figure (6.13), and as the cold

end temperature is decreased, Figure (6.14), although the difference in efficiency between the 90K and the 72K data is small. Since both the regenerators exhibit this behaviour to approximately the same extent, it is not thought to be due to decreasing matrix heat capacity, but to poor heat transfer at low temperatures. The operating frequency does not appear to have a governing effect on efficiency, Figure (6.15).

The data are presented in the form of a conventional Nu-Re heat transfer correlation in Figure (6.16). The data obtained in the steady flow experiments described in Chapter 4, and those of Mikulin and Shevich, [95], are shown for comparison. The values of Nusselt number found for the longer regenerators described in Chapter 4 are on average 40% below those for the regenerators used in this refrigerator. The latter agree with the correlation given by equation (4-10) to within ±40%.

Measurement of the heat transferred from the gas to the matrix is thought to be less relevant to the problem of regenerator efficiency in miniature refrigerators than the discussion of the losses (i.e. the heat **not** transferred). An additional disadvantage of the correlations usually used in heat transfer is that they involve the Reynolds number as a variable, which will disguise any separate dependence of the losses on gas density and gas velocity (such as that encountered here). For this reason it is considered that presentation of the losses measured, as in Figures (6.10) to (6.12), or of the efficiency of the regenerator, as in Figures (6.13) to (6.15), is of more value in this context than the

more generally used heat transfer correlations.

In Figure (6.17) the regenerator inefficiency, I_e=(1-efficiency), is plotted against $\rho_c^{-0.41} v_c^{0.38}$, for both regenerators, and it can be seen that

$$I_e \propto \rho_c^{-0.41} v_c^{0.38} \qquad (6\text{-}7)$$

This result could be used as the basis of an empirical model of regenerator performance. The scatter in the data is ±25%, which compares very well with heat transfer correlations such as that presented in Figure (6.16), since an uncertainty of ±10% in the heat transferred to the matrix leads to uncertainty of several hundred per cent in the regenerator inefficiency.

6.1.4 Additional Displacer Losses

During operation of the cooler, the regenerator will be under load from two sources, the displacement of gas into and out of the cold end expansion space (caused by displacer motion), and the compression of the gas in the entire refrigerator (caused by movement of the piston). This effect could also cause an additional pressure drop loss.

Attempts were made to measure the additional regenerator loss by holding the displacer still, running the compressor, and timing the warm up (as described for the measurement of displacer losses). However, it proved impossible to obtain consistant data, mainly because the piston could not always be

made to oscillate about the same mid-position, and because it was not always possible to hold the displacer completely stationary for the time required for such tests (the power and phase required to do so varied with the cold end temperature). Although the errors introduced by these factors were small enough (±0.5W) to allow measurement of losses due to irreversible compression (10W to 14W), obtained using a similar technique, to be performed to within ±5%, they were of the order of 100% to 200% of the regenerator losses due to compression of the system, and so prevented assessment of the latter.

Although both components of the load on the regenerator will cause losses, the resultant regenerator efficiency will not be due to the simple sum of the two contributory factors because the sources of load are not in phase. For the purpose of the energy balance described below, only the regenerator loss due to displacer motion is included, as this is the largest load on the regenerator.

6.2 COMPRESSOR LOSSES

Typical oscilloscope traces showing the P-V loop obtained for the compression space (with the displacer moving and refrigeration taking place), the loss due to irreversible processes in the compression space, and the P-V loop in the expansion space, are shown in Figures (6.18), (6.19), and (6.20) showing data at 30Hz, 40Hz and 50Hz, respectively.

If compression was purely isothermal, the pressure pulse would be in phase with the piston movement and the P-V diagrams with the displacer held still would be diagonal lines with no area and hence no losses (this would also occur with purely adiabatic compression but the refrigerator could not function under such a condition).

From the shape of the P-V loops in the compression space, it appears that during the main part of the upward piston stroke the compression is adiabatic, but as the piston approaches the end of the cylinder heat is transferred from the gas to the walls and the temperature of the gas falls, causing the pressure to fall while the piston is still moving upwards (a large part of the pressure change occurs during a very small part of the stroke). As the piston moves downwards, the expansion in the cylinder appears to follow a second adiabatic process until the piston is close to the end of the stroke, where heat is transferred to the gas from the walls, the gas temperature rises, and the pressure rises. The heat transfer takes place when the gas is moving slowly, at both ends of the stroke, and is most pronounced at the end of the upward stroke when the distance through which heat is transferred is smallest.

Figures (6.18) to (6.20) also show the displacer L.V.D.T. and piston L.V.D.T. output waveforms, and it can be seen that the displacer motion leads the piston motion by about 70°. The 30Hz data, Figure (6.18), display a distorted displacer stroke. This was caused by the imposition of electrical drive far out of phase with the pneumatic drive in order to maintain

the phase difference between piston and displacer.

6.3 THE ENERGY BALANCE

6.3.1 Input Power

Performance data for the refrigerator with both 250 and 150 mesh regenerators are shown in Tables [6.1] and [6.2].

Values for the input power to the gas, measured from the area of the compression space P-V loop (with the displacer running) are presented. The P-V loop (indicated) power is typically 0.5W to 1W lower than that measured electrically (from total input power minus I^2R losses), and is probably due to the effects of windage and pneumatic driving of the displacer. Evidence for this can be found in the corresponding measurements for the loss due to irreversible compression, where the displacer is not moving, and the discrepancy between electrically measured power and indicated power is much smaller (from 0 to 300mW).

6.3.2 Total Refrigeration

The total refrigeration is measured both as the indicated power in the expansion space, and as the sum of the refrigeration losses (taken from the data presented above for the appropriate conditions) and the useful refrigeration (measured using the heater at the cold end). There is a shortfall of between 0-300mW between these values (the indicated power is larger), which is greatest at low temperatures. This shortfall is not due to any uncertainty in

the distribution of the displacer losses between shuttle heat transfer, regenerator losses and pressure drop, as it is the sum of these components that has been measured.

A small part of this discrepancy occurs because the pressure transducer used is not at the cold end. However the pressure drop through the regenerator, equation (4-13), is of the order of 1 p.s.i., which is less than 2% of the peak-to-peak pressure pulse. Of more importance are the additional regenerator and pressure drop losses due to compression of the gas in the entire system. As discussed above, these losses cannot be added directly to those which occur when just the displacer moves, and the precise effect of an additional load out of phase with the main load on the regenerator is not known, but it might be expected to be more pronounced when demands on the regenerator are greatest, for example, at low temperature. This effect can be seen in the data in Tables (6.1) and (6.2). It is noticable that the shortfall is greater for the 150 mesh regenerator, possibly because this regenerator is already inefficient.

The effect, on the temperature gradient in the cylinder wall, of power supplied to the cold end heater has not been previously considered. This may cause the shuttle heat transfer to differ from that measured when no heat is applied. This might also contribute to the deficit recorded above.

The greatest difference between indicated refrigeration and that measured from the sum of losses and useful refrigeration occurs in the data taken at 30Hz. This is thought to be primarily due to the distorted shape of the

displacer waveform, which will affect regenerator losses.

6.3.3 Refrigerator Efficiency

Using the indicated refrigeration as the total produced by the gas receiving power W_g, where,

$$W_g = W_{tot} - I^2R - W_{ir} \qquad (6\text{-}8)$$

the efficiency obtained is over 80% of that expected from Carnot's expression for a refrigerator working between 300K and T_c (the temperature measured at the cold end). This percentage is greatest at lowest temperatures and highest frequencies.

Since the indicated refrigeration includes all refrigeration losses (even if not all have been included in the discussion above), and compressor losses have been accounted for, Carnot efficiency should be attainable.

A likely explanation for the discrepancy in efficiency described, is that the apparently 'missing' refrigeration is not in fact missing, but that the Carnot expression has been incorrectly applied, as it refers to the temperature of the gas at the cold end, not to that of the flange. If the temperature of the gas in the expansion space is lower than that of the flange, Carnot's expression would predict less refrigeration. It is likely that such a temperature difference, ΔT_c, does exist as a large amount of heat (>1W) must be transferred across a small surface area ($\approx 1cm^2$).

It is extremely difficult to measure gas temperatures accurately, especially when there is so little gas in the cold end, and it has not been attempted here. However, there is indirect evidence supporting the hypothesis of a significant ΔT_C, in that the measured discrepancy in efficiency is greatest for highest applied heat loads (where the temperature gradient needed to transfer the load will be greatest), and at lowest frequencies. At higher frequencies the convective heat transfer from the inside of the cold end flange to the gas should be greater than at lower frequencies (and hence lower gas velocities).

The effect of such a temperature difference would also contribute to the discrepancy between indicated and measured refrigeration, as regenerator losses and shuttle heat transfer would both increase with the additional load furnished by the greater temperature gradient in the gas.

In order to give 100% of Carnot efficiency it is found that ΔT_C must be about 10K per watt of applied heat.

NOTE

It must be remembered that this is the efficiency defined in the first sentence of this section, and that conventionally the efficiency of a refrigerator is defined as the ratio of useful refrigeration produced to total input power. Typically, this refrigerator has a conventionally defined efficiency of only about 10% of the value predicted by Carnot.

6.4 A SIMPLE EMPIRICAL MODEL OF PERFORMANCE

From the data presented above, it appears that the energy balance for this refrigerator can be expressed,

$$W_{tot} - I^2R - W_{ir} = Q_T \times \left[\frac{T_h - T_{cg}}{T_{cg}}\right] \qquad (6\text{-}9)$$

where Q_T = useful refrigeration

+

shuttle heat loss

+

regenerator loss

+

pressure drop loss

and T_{cg} is the actual gas temperature at the cold end, which is approximately related to the measured cold end temperature, T_c, by

$$T_c - T_{cg} = \text{(Useful refrigeration)} \times 10\ \text{K}$$

Some of the losses described above have been neglected in this energy balance. However this leads to a simple expression which can be a useful tool in refrigerator design.

Although it is only possible to present theoretical models of the shuttle heat transfer and pressure drop losses here, the losses due to irreversible processes in the compressor should be amenable to a future empirical model, as should the regenerator losses. The compressor efficiency (i.e. the Joule heating losses) is a separate field of study outside the scope of the present work.

This model provides valuable insight into the losses expected in a refrigerator with a given amount of power input to the gas and known displacer stroke. Used in conjunction with a model of the compressor performance, which enables the designer to determine the physical characteristics of the machine (such as the swept volume ratio) required to give the desired input power, this model will predict the useful refrigeration which the cooler will produce.

Figure 6.1 Displacer Loss (150 mesh Regenerator)

Pressure Variation (at 40Hz, 90K)

Δ 11.6 bar, ▫ 10.2 bar, o 8.1 bar

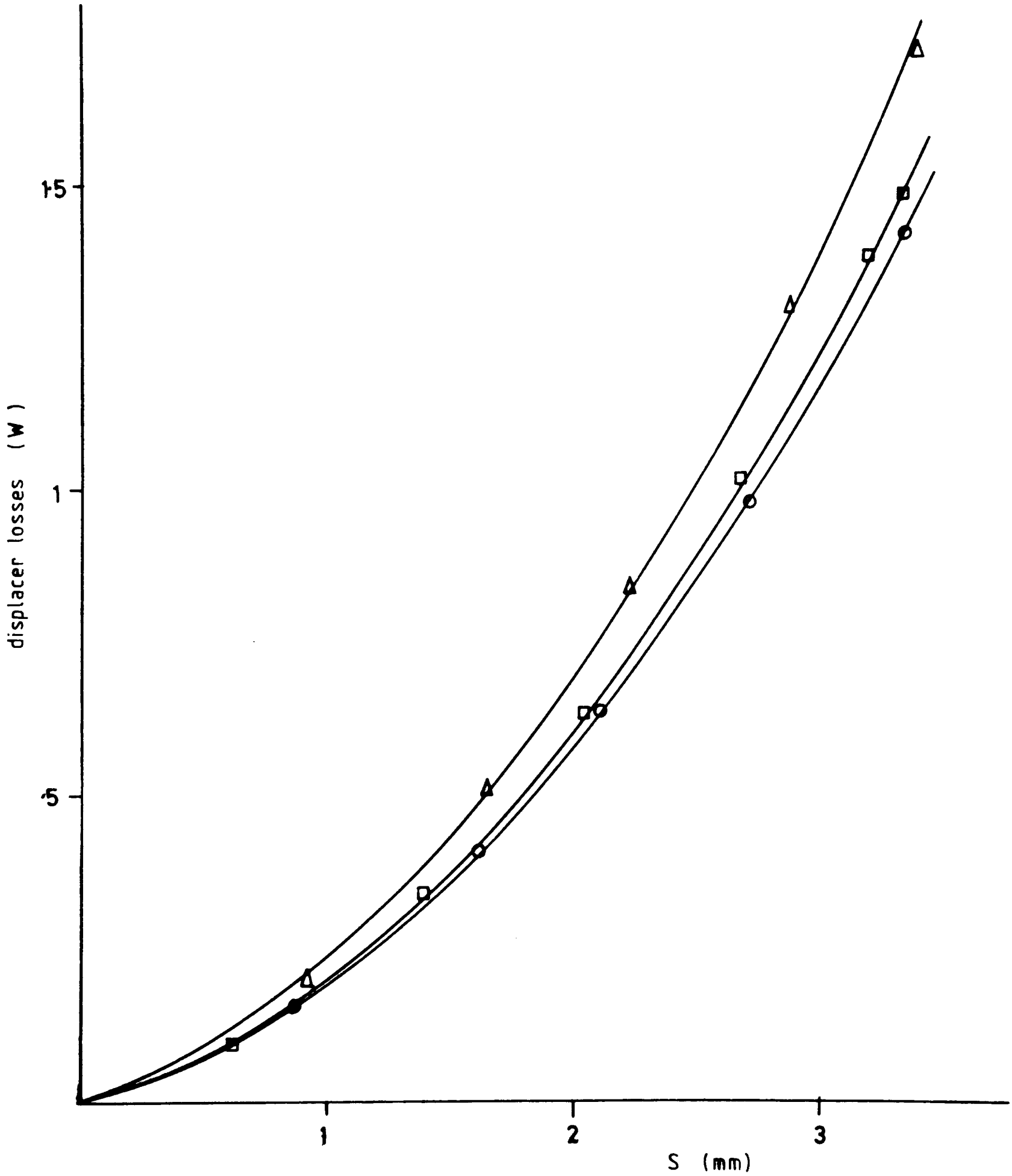

Figure 6.2 Displacer Loss (150 mesh Regenerator)

Temperature Variation (at 40Hz, 10.2 bar)

Δ 72K, ▫ 90K, o 120K

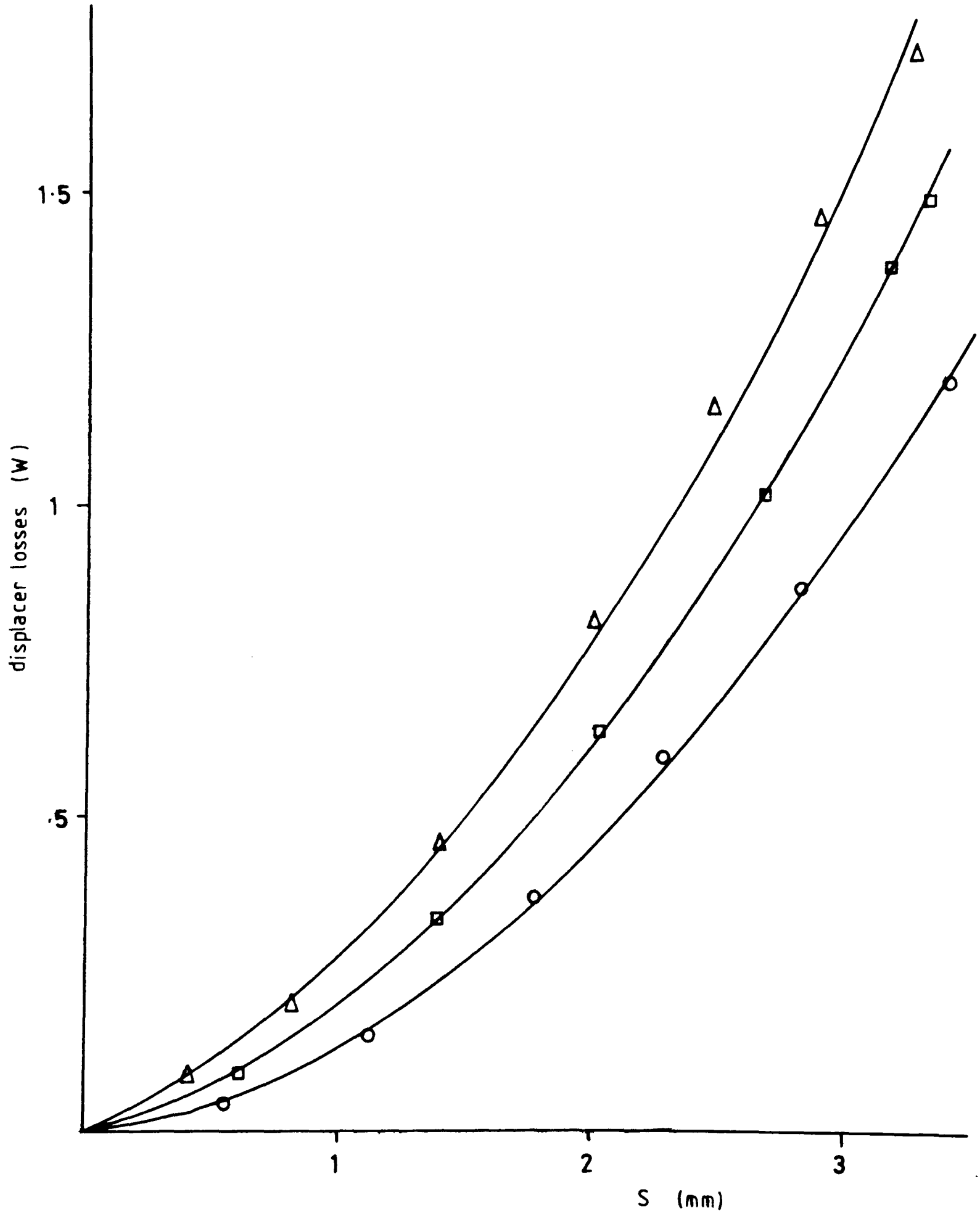

Figure 6.3 Displacer Loss (150 mesh Regenerator)

Frequency Variation (at 90K, 10.2 bar)

Δ 50Hz, ▫ 40Hz, o 30Hz

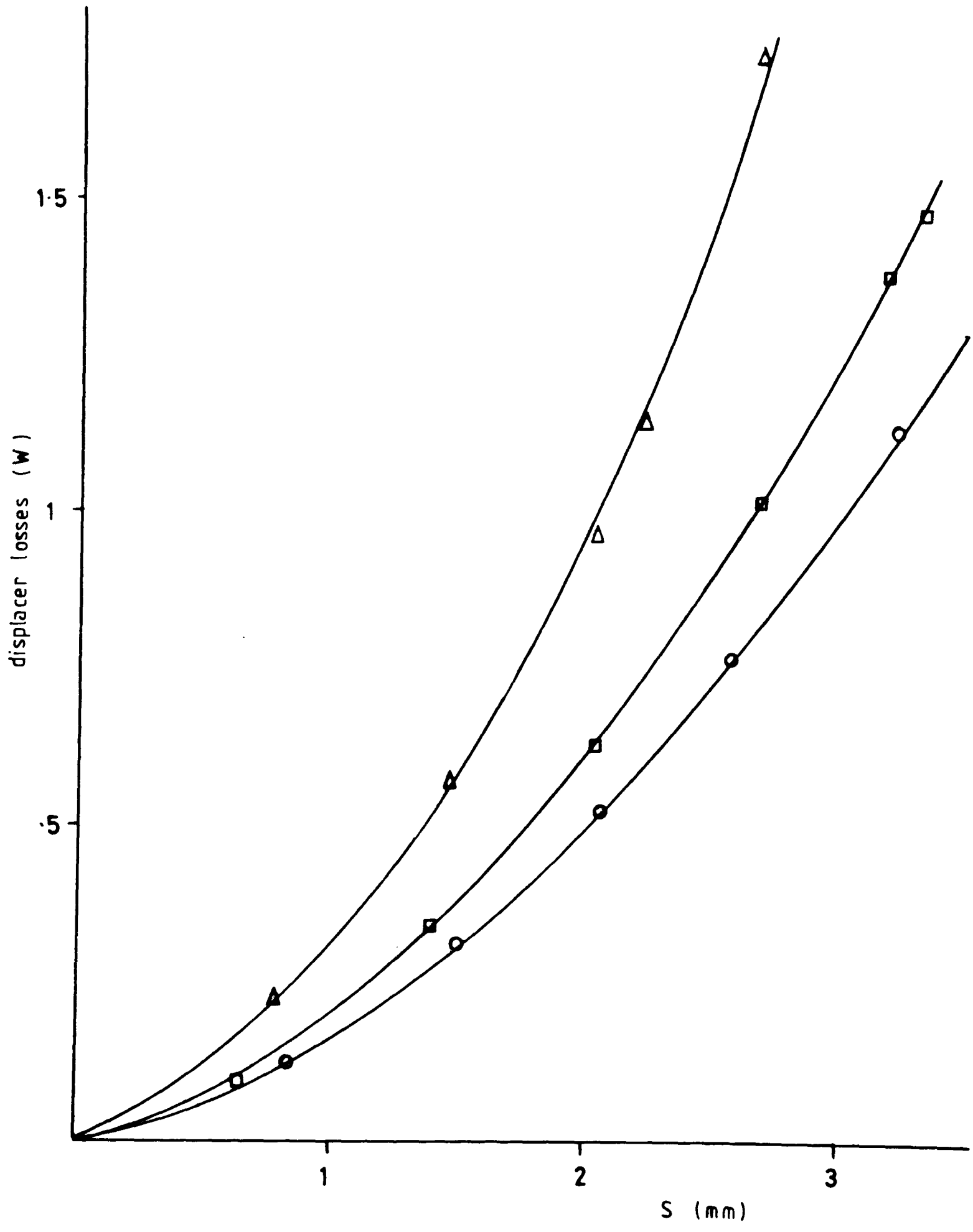

Figure 6.4 Power Dissipated due to Pressure Drop across Displacer (300K)

o 1 bar, • 5.1 bar, Δ 10.2 bar, --- equation (6-2)

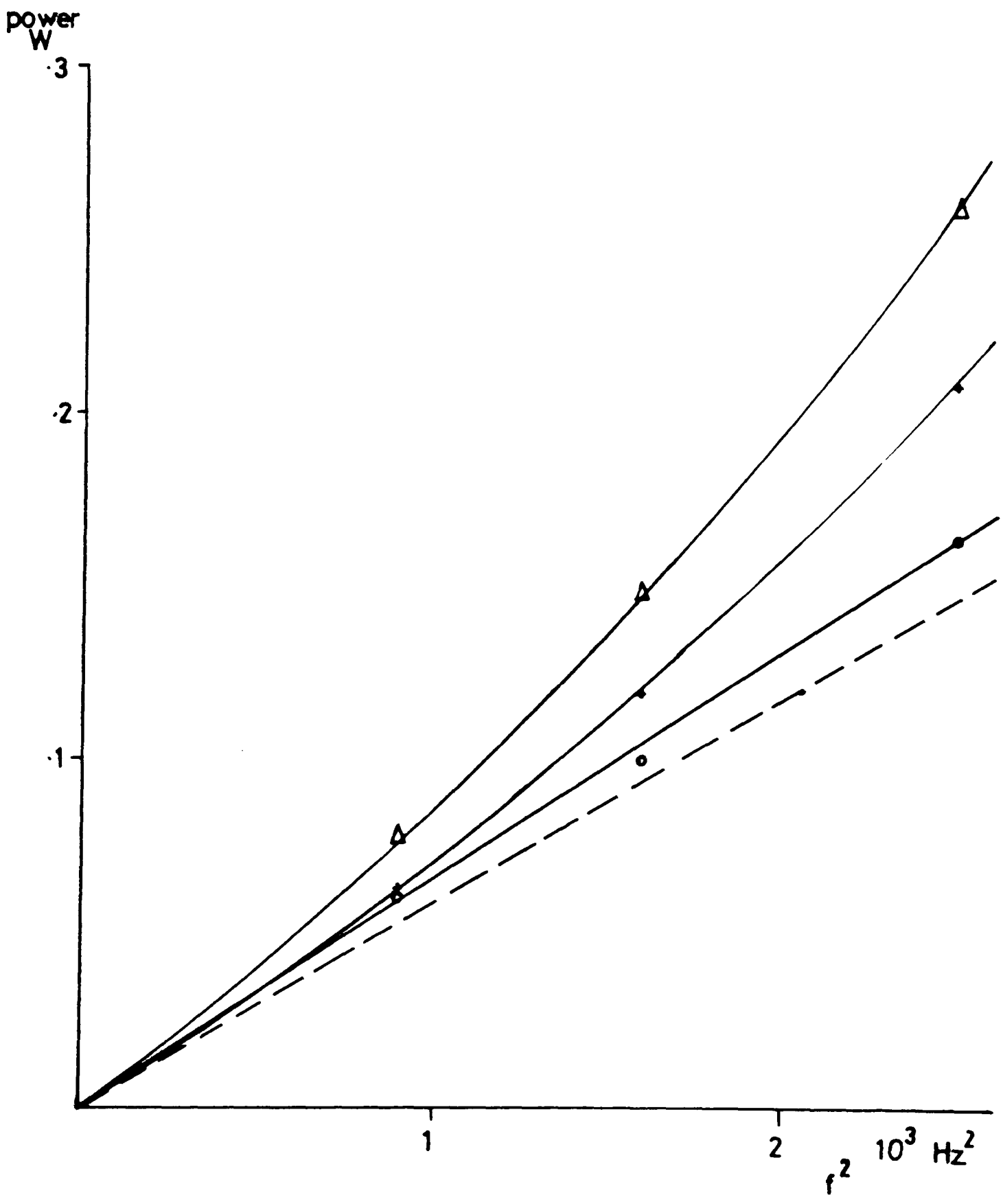

Figure 6.5 Power Dissipated due to Pressure drop across Displacer (40Hz, 10.2 bar)

▫ 72K, + 90K, Δ 120K

— — — — 300K

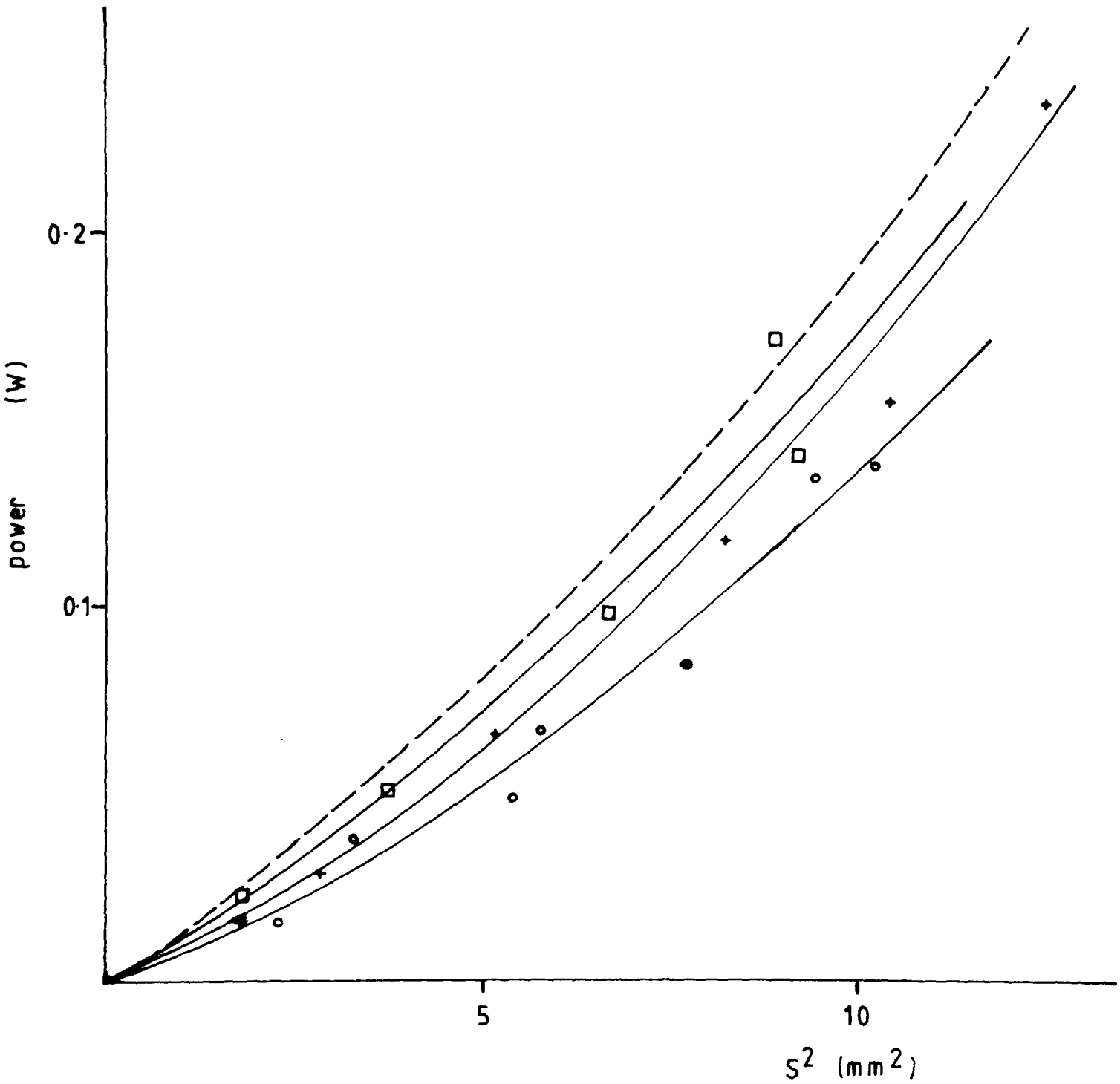

Figure 6.6 'Additional' Power loss due to Pressure drop

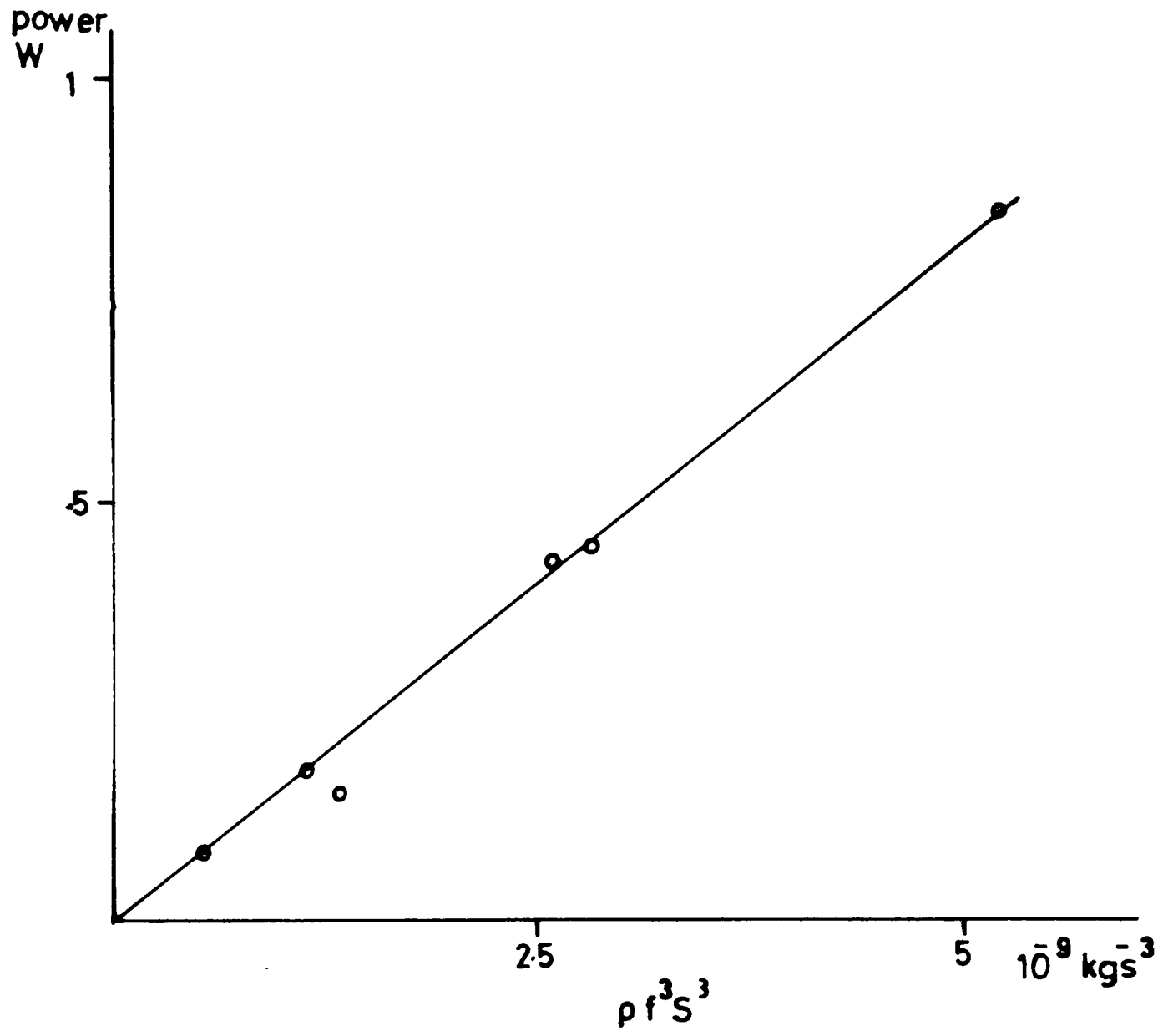

Figure 6.7 Shuttle Heat Loss (Temperature Variation)

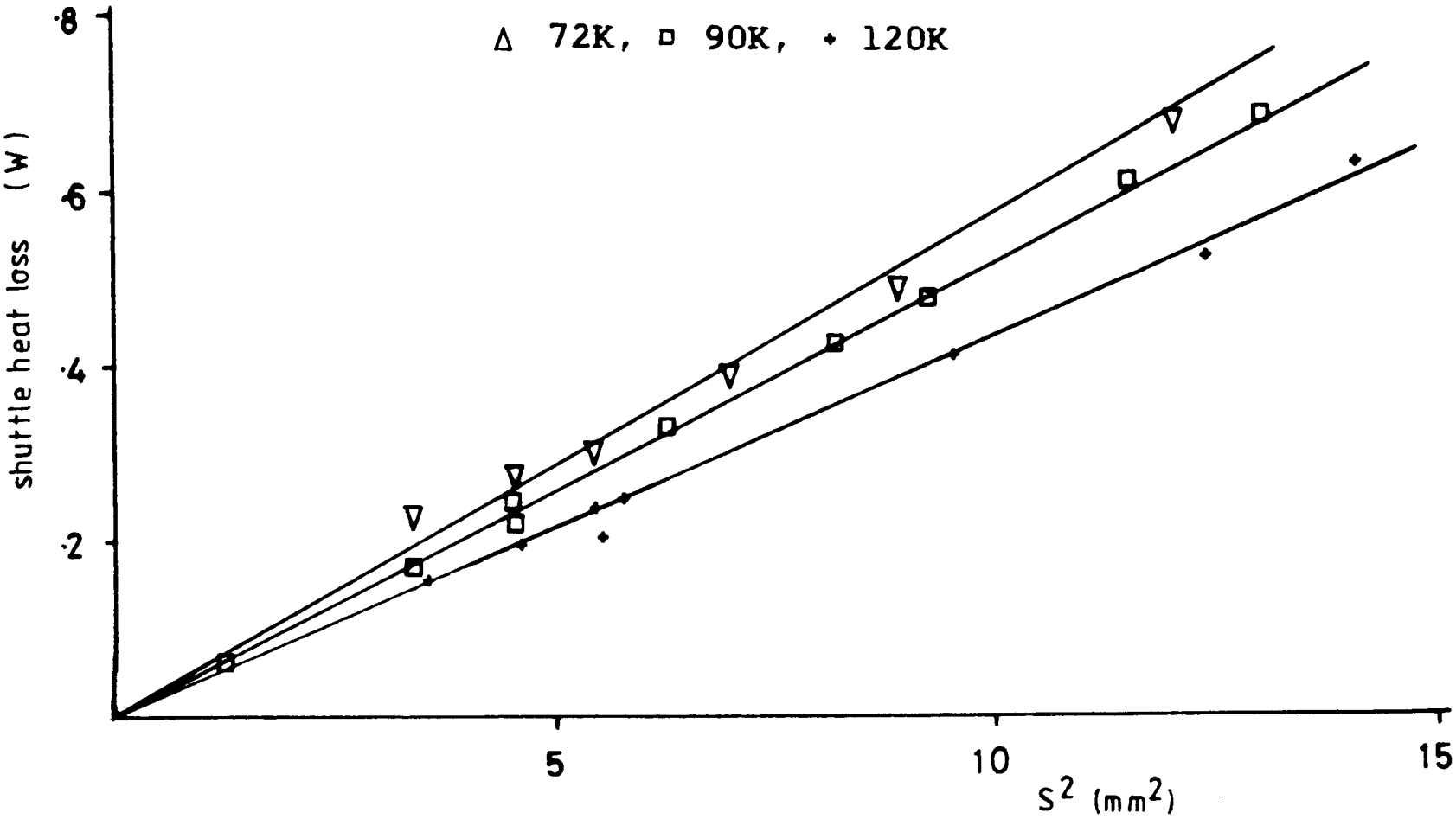

Figure 6.8 Shuttle Heat Loss (Frequency Variation)

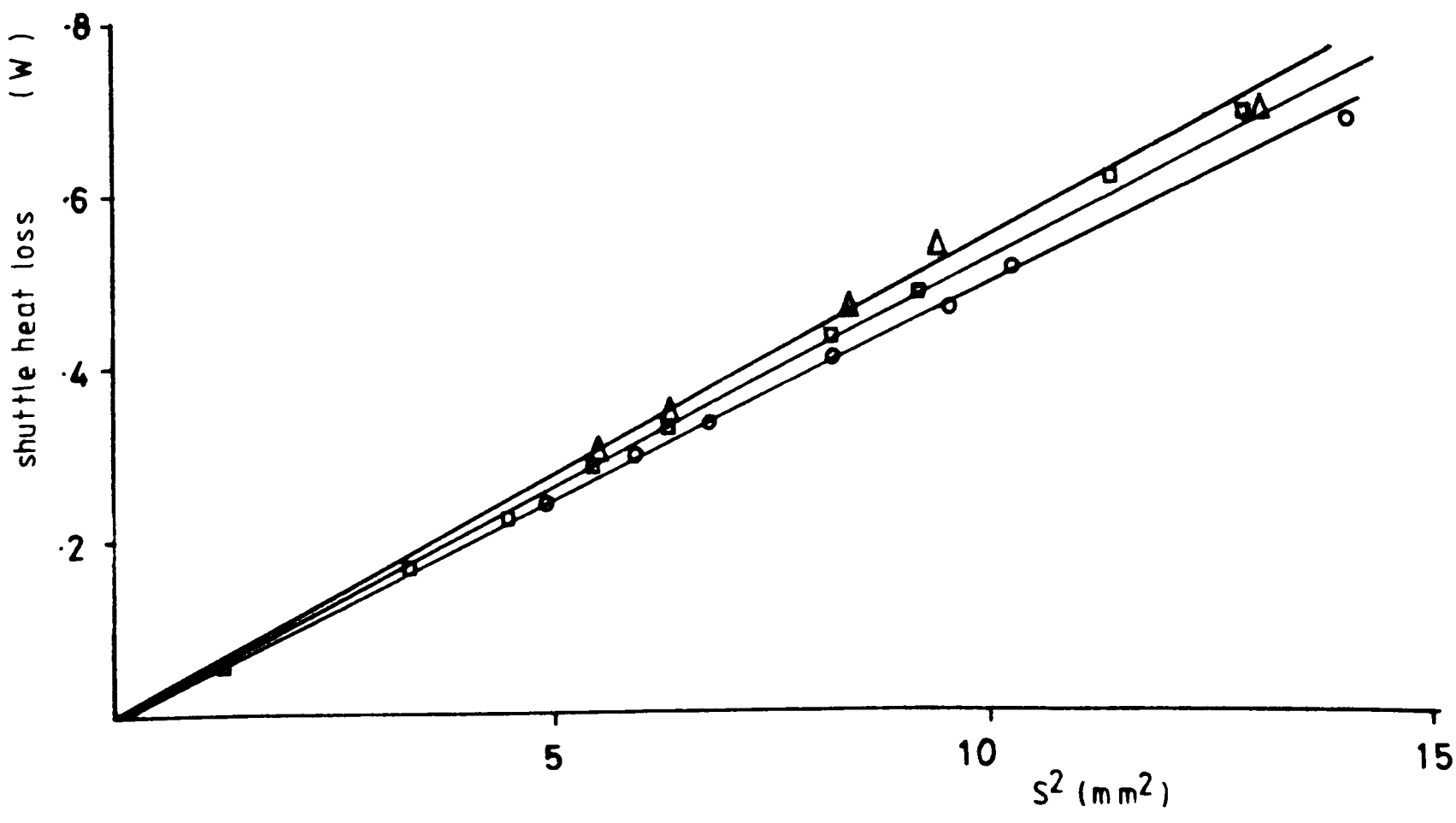

Figure 6.9 Shuttle Heat Loss

40Hz: Δ 72K, o 90K, x 120K
90K: □ 30Hz, • 50Hz
---- equation (3-12)

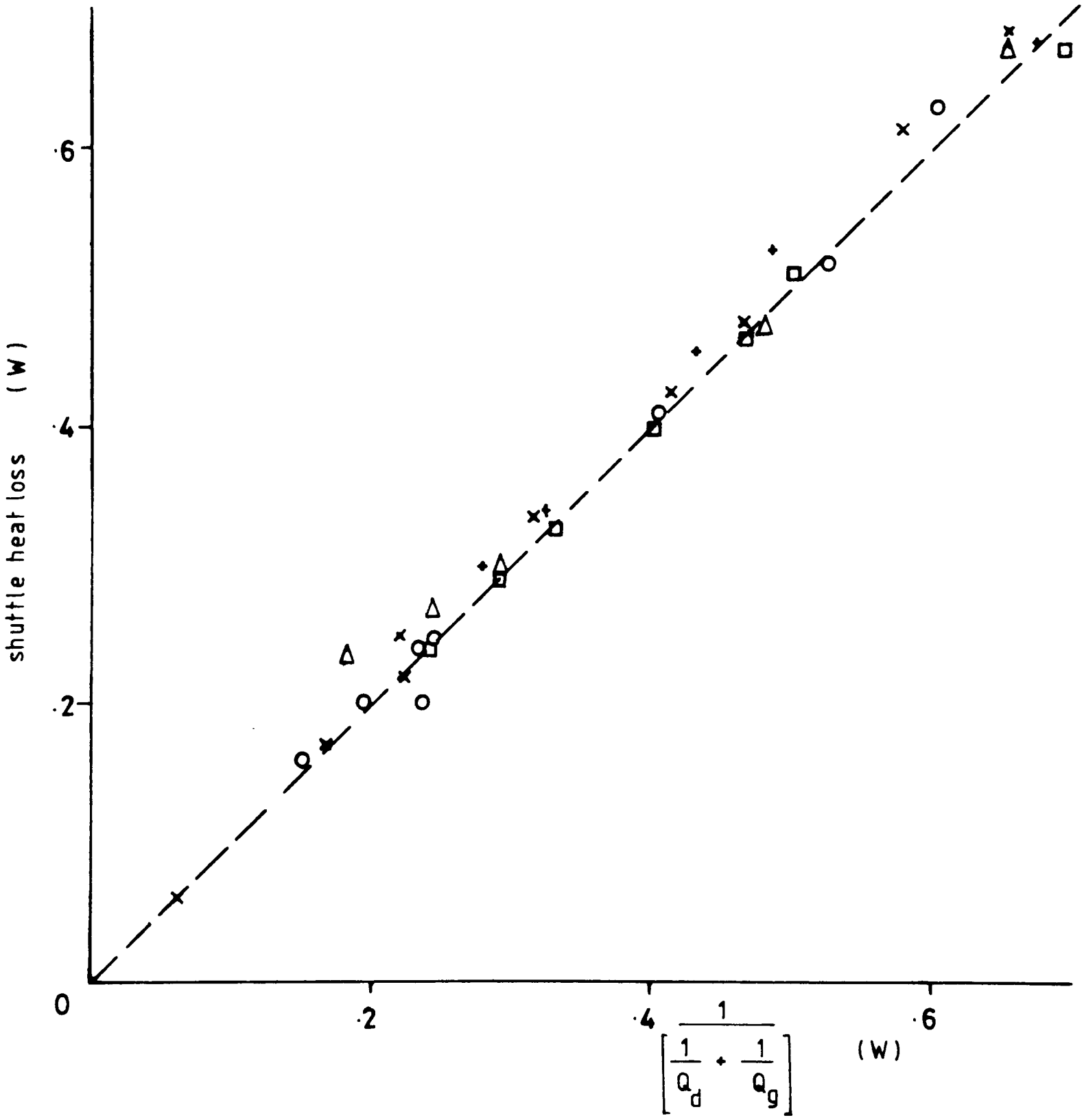

Figure 6.10 Regenerator Loss (Pressure Variation)

40Hz 90K

150 mesh ——: ● 11.6 bar, ■ 10.2 bar, ▲ 8.1 bar
250 mesh ---: o 11.6 bar, □ 10.2 bar, △ 8.1 bar

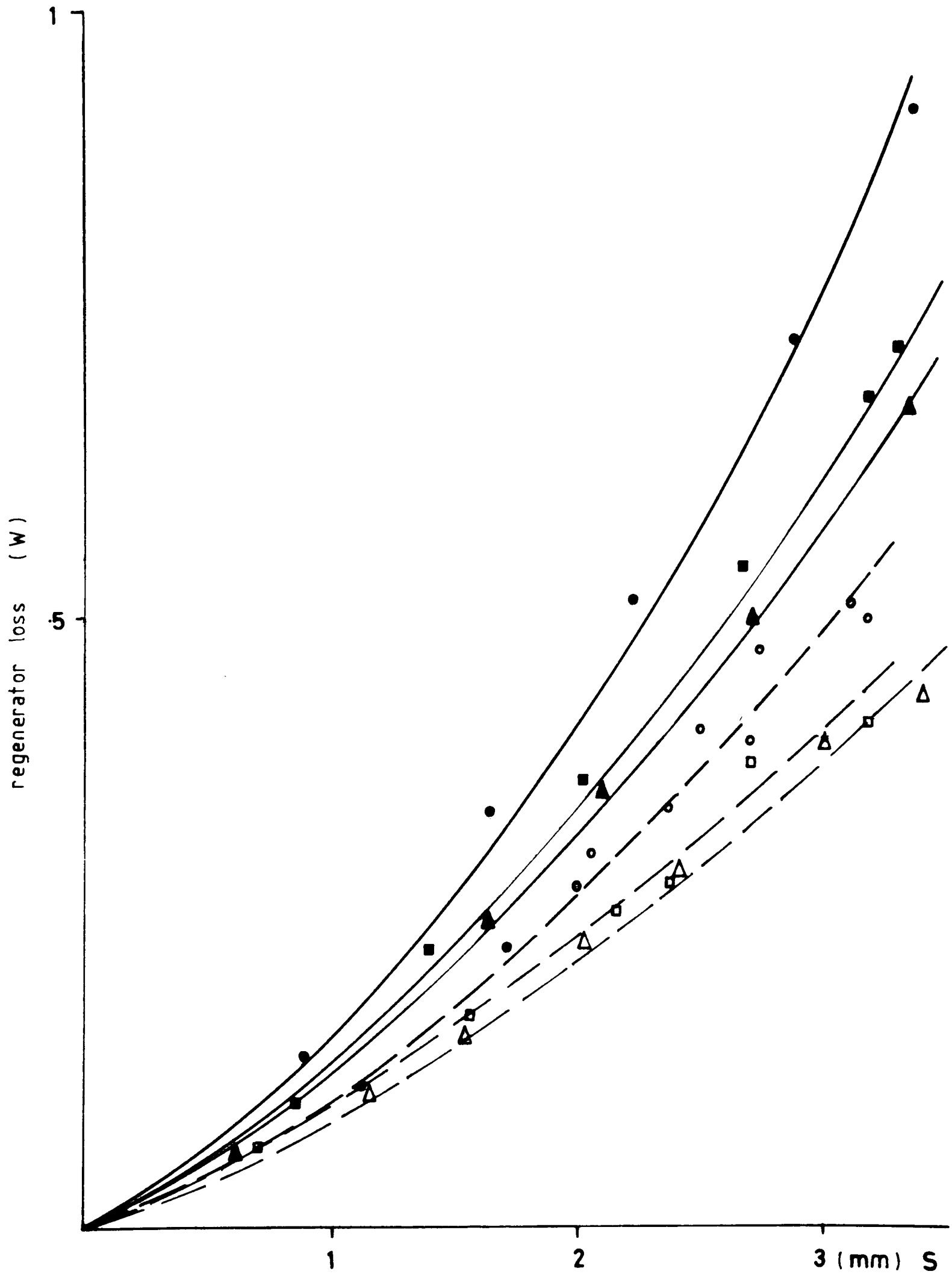

Figure 6.11 Regenerator Loss (Temperature Variation)

40Hz 10·2 bar

150 mesh ——: ● 72K, ■ 90K, ▲ 120K
250 mesh ---: ○ 72K, □ 90K, △ 120K

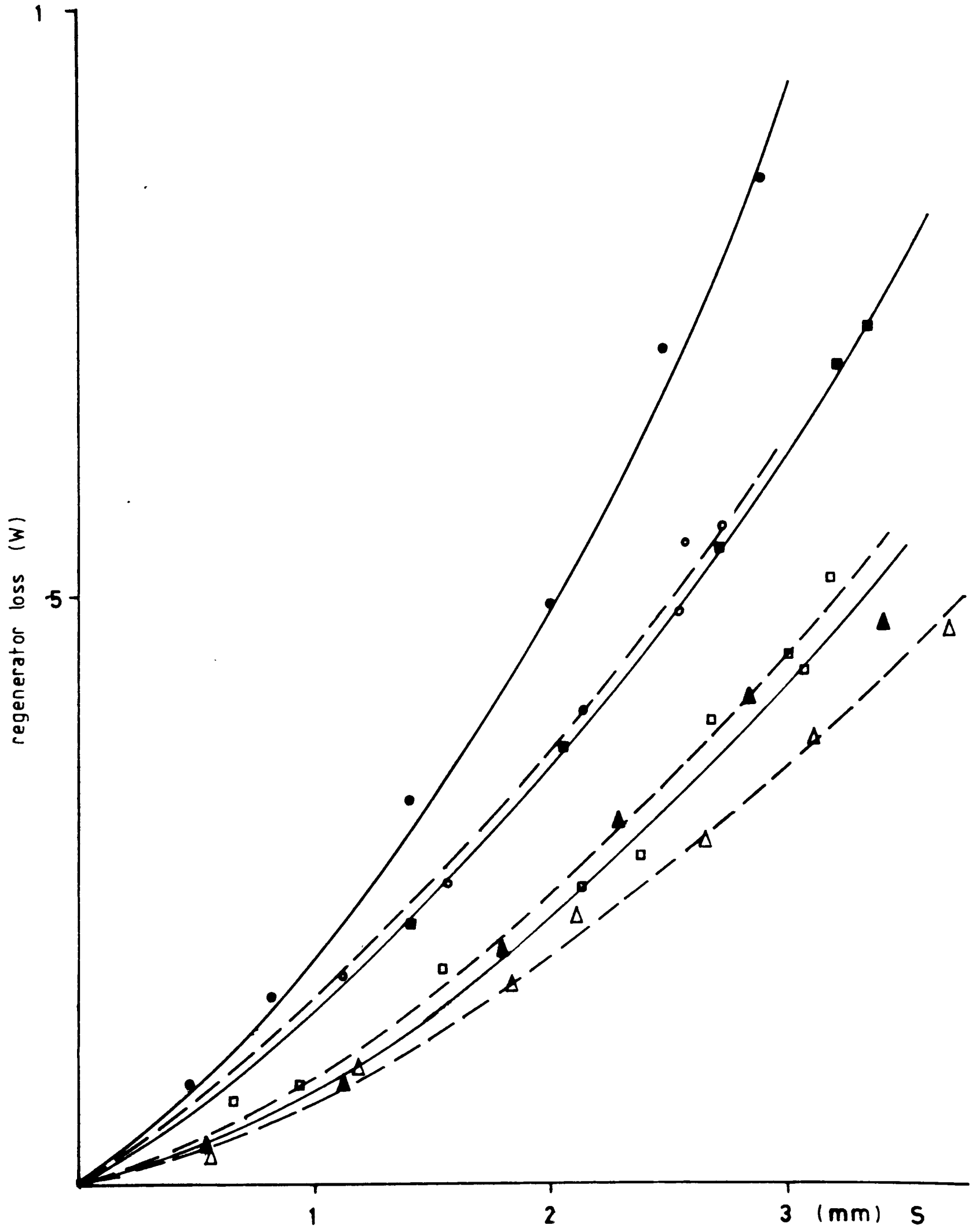

Figure 6.12 Regenerator Loss (Frequency Variation)

90 K 10·2 bar

150 mesh ——: ● 50Hz, ■ 40Hz, ▲ 30Hz
250 mesh ---: o 50Hz, ▫ 40Hz, Δ 30Hz

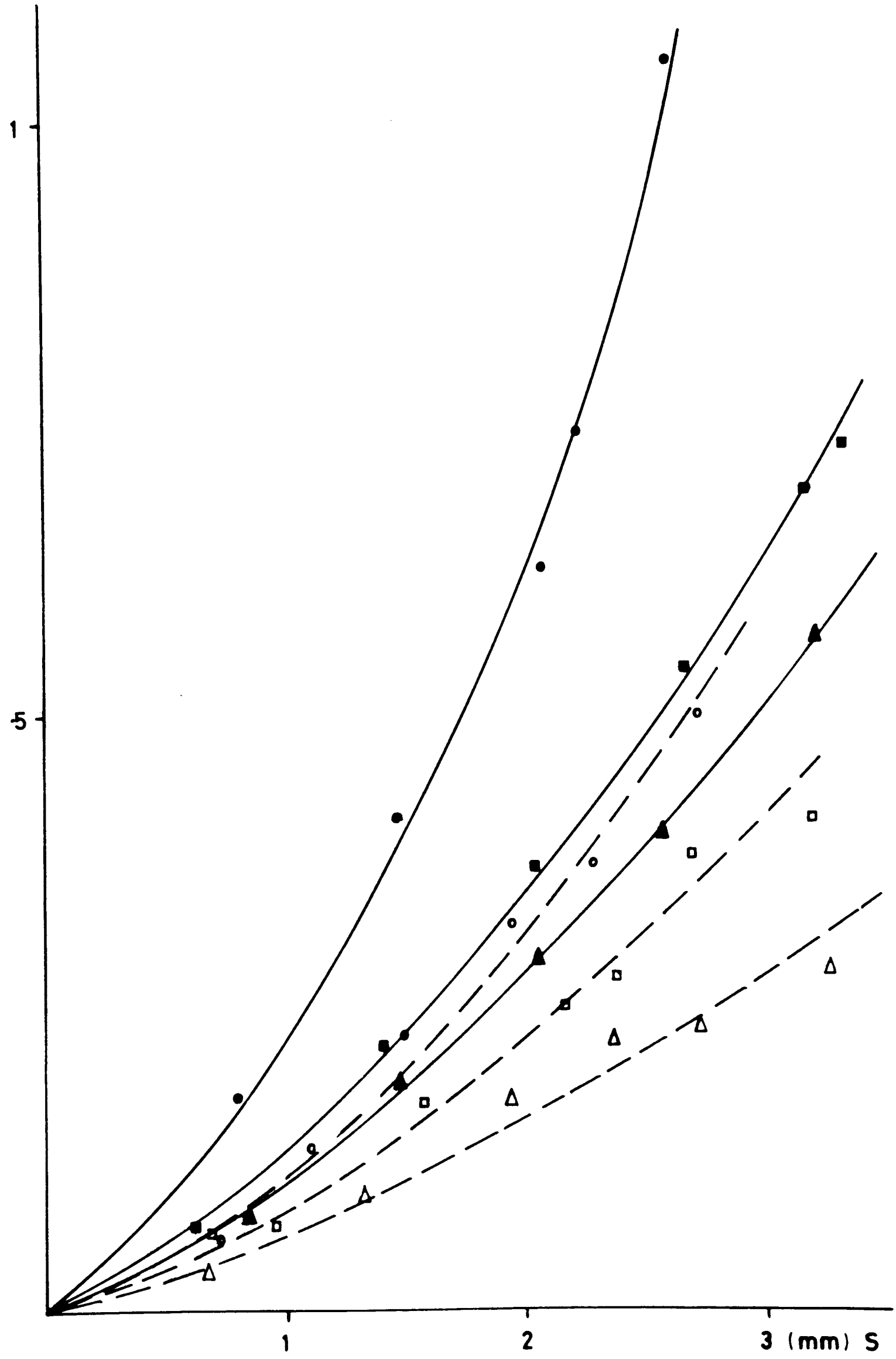

Figure 6.13 Regenerator Efficiency (Pressure Variation)
40Hz, 90K

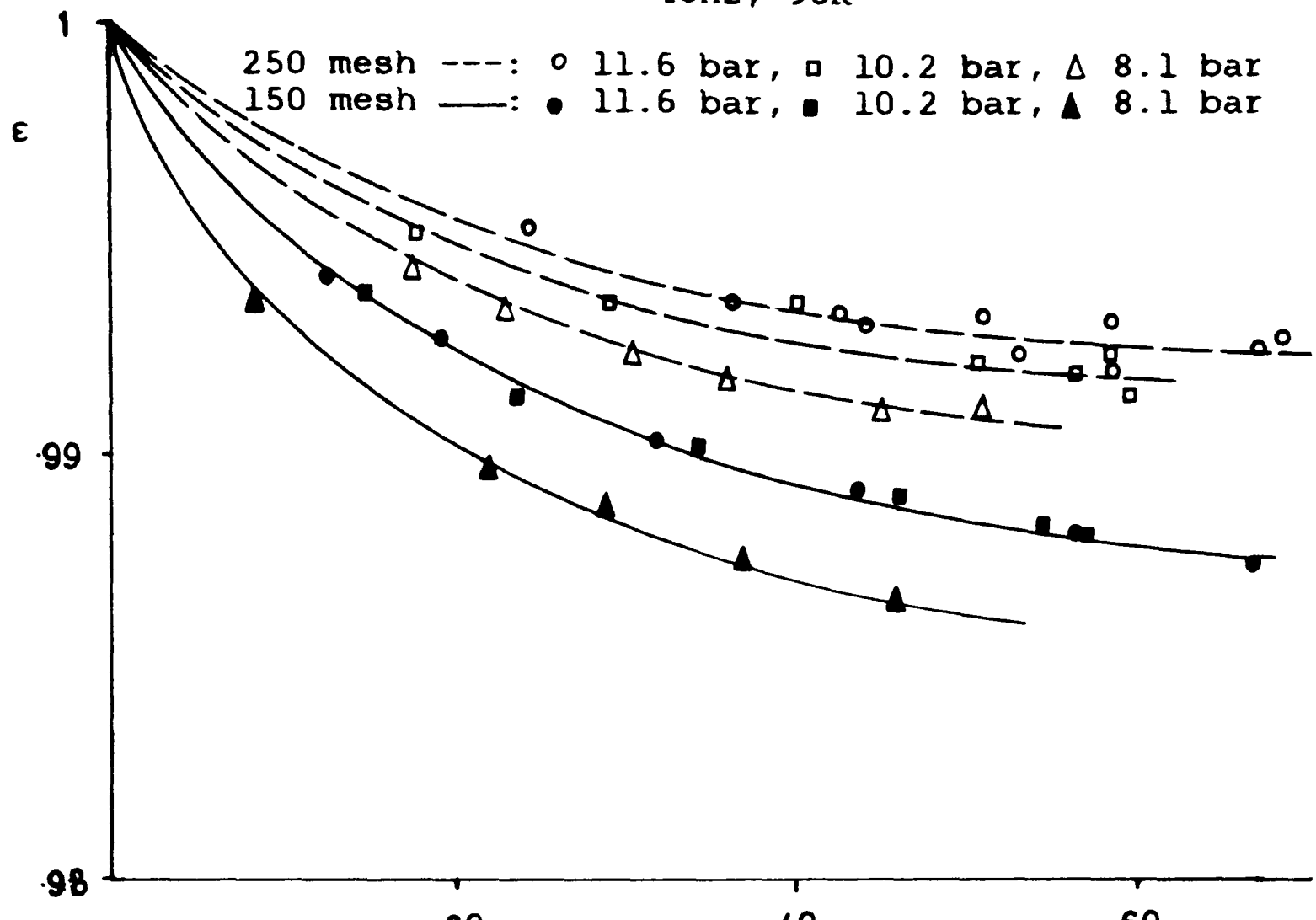

Figure 6.14 Regenerator Efficiency (Temperature Variation)
40Hz, 10.2 bar

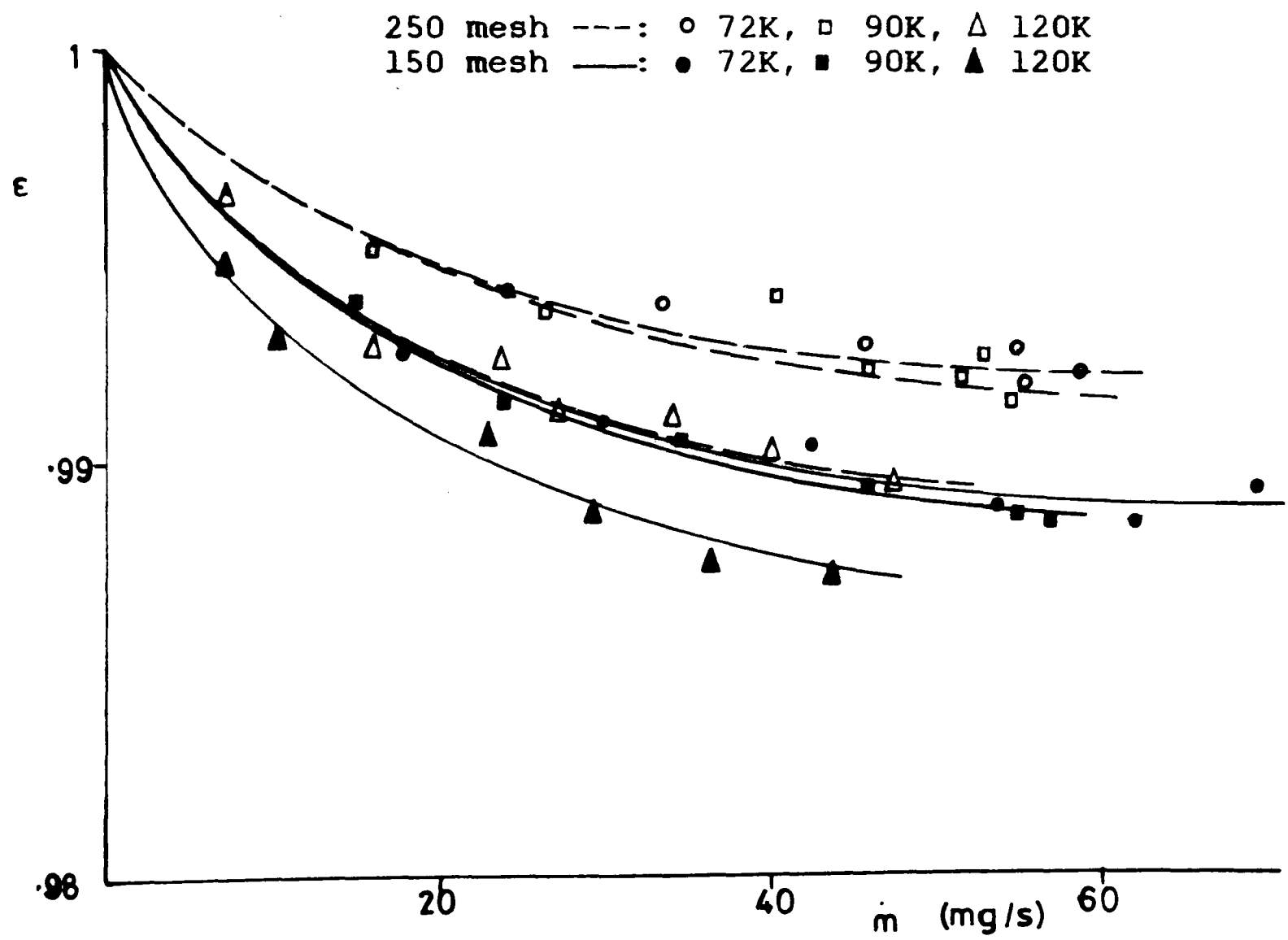

Figure 6.15 Regenerator Efficiency (Frequency Variation)
90K, 10.2 bar

250 mesh ---: Δ 30Hz, ▫ 40Hz, ○ 50Hz
150 mesh ——: ▲ 30Hz, ■ 40Hz, ● 50Hz

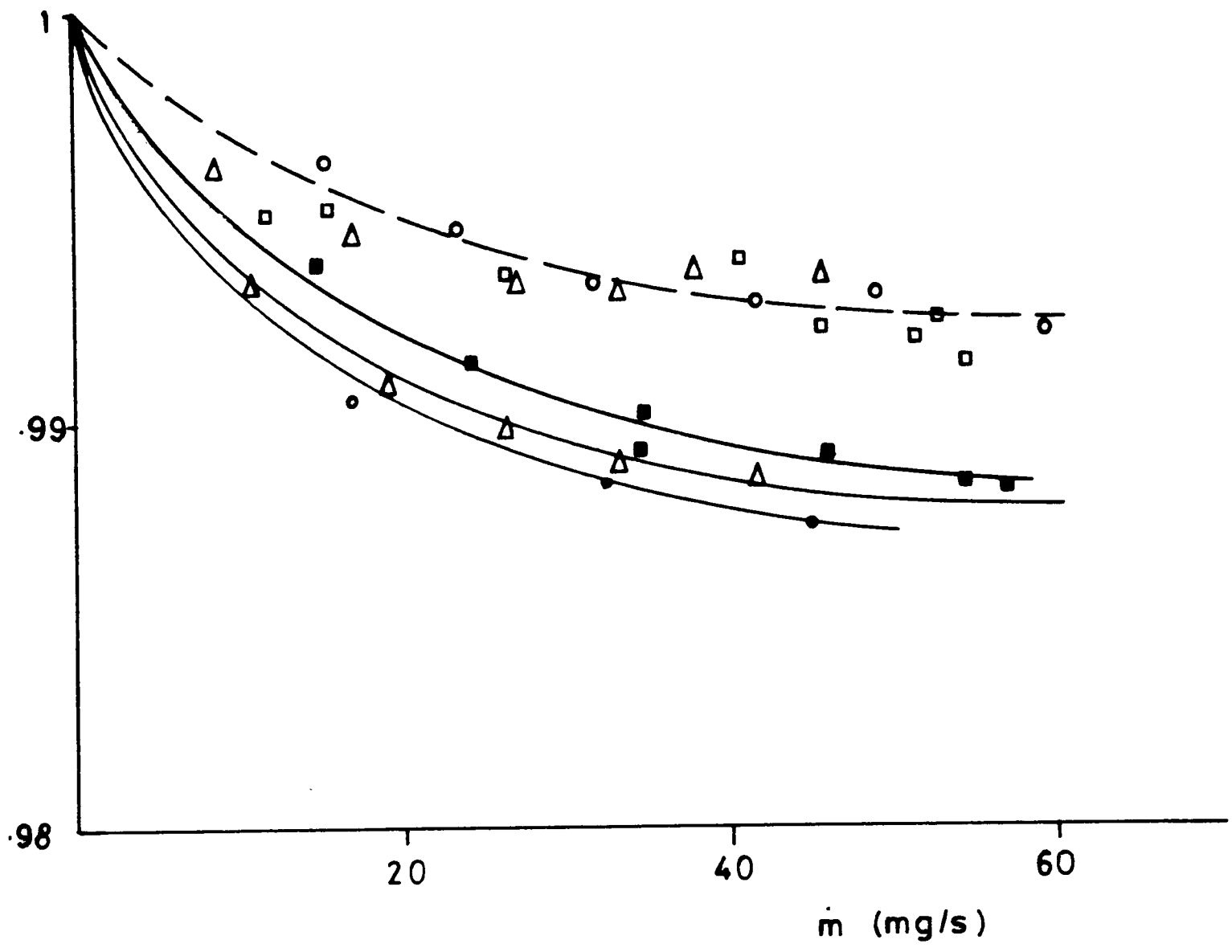

Figure 6.16 Heat Transfer in Regenerator Matrices

250 mesh, 10.2 bar: ▽ 72K, ○ 90K, ◇ 120K
90K: △ 8.1 bar, □ 11.6 bar
150 mesh, 10.2 bar: ▼ 72K, ● 90K, ◆ 120K
90K: ▲ 8.1 bar, ■ 11.6 bar
---- Equation (4-10)

/// range of steady-flow data [Figure (4.7)]

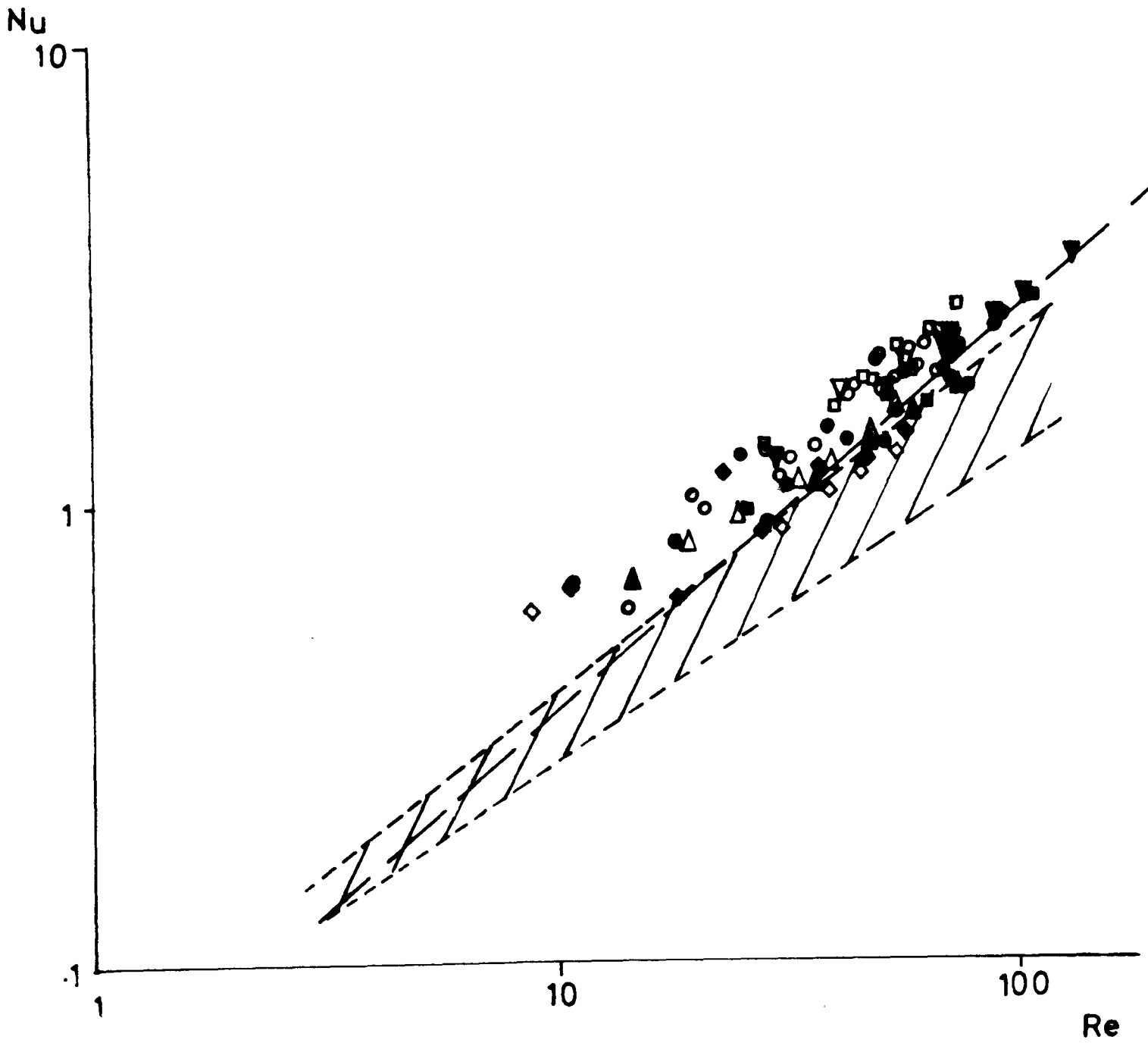

Figure 6.17 Regenerator Inefficiency

250 mesh, 10.2 bar, 40Hz: ▽ 72K, ○ 90K, ✱ 120K
10 2 bar, 90K: ◇ 30Hz, □ 50Hz
40Hz, 90K: × 11.6 bar, △ 8.1 bar
150 mesh, 10.2 bar, 40Hz: ▼ 72K, ● 90K
10.2 bar, 90K: ◆ 30Hz, ■ 50Hz
40Hz, 90K: ⬩ 11.6 bar, ▲ 8.1 bar

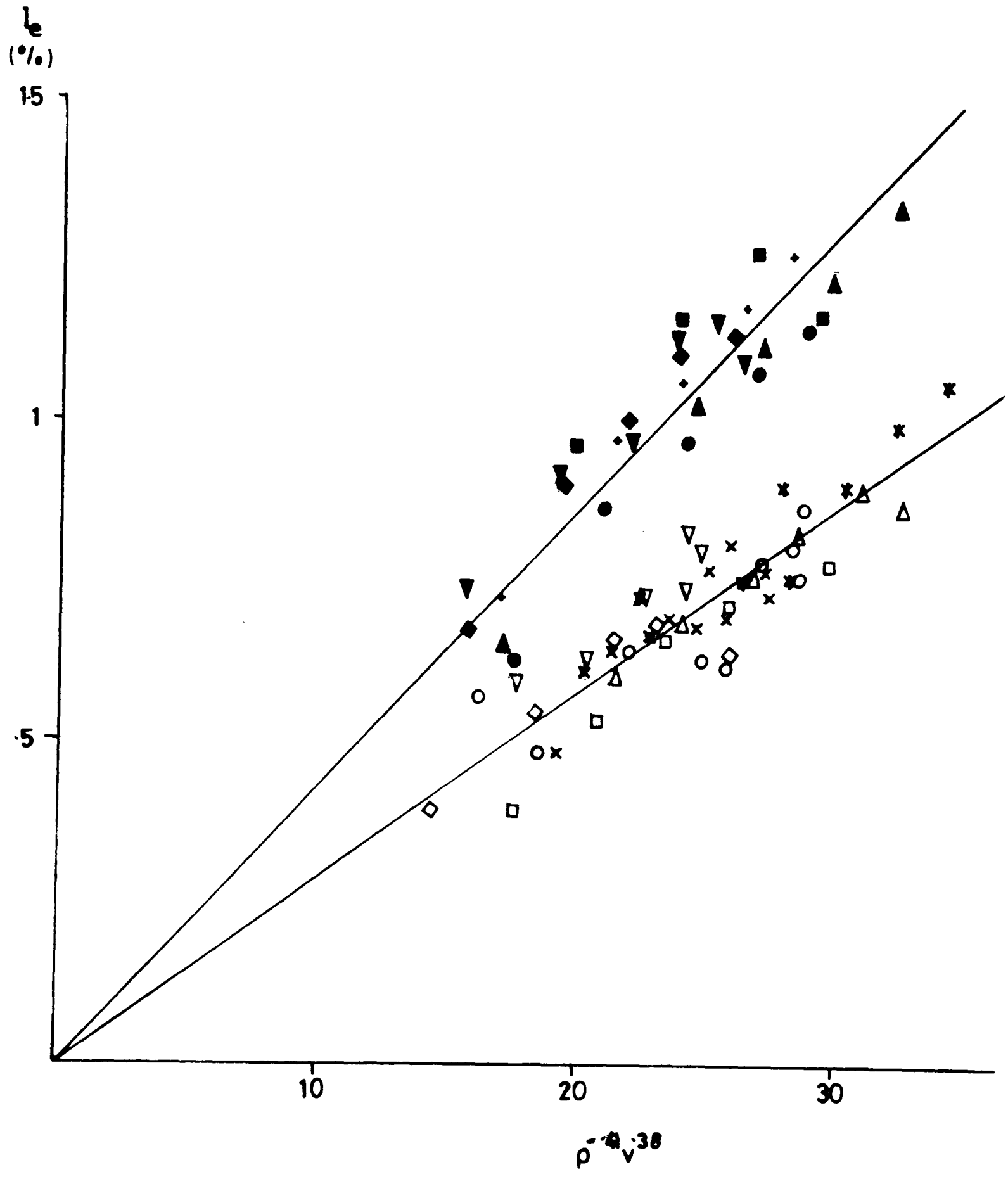

Figure 6.18 Indicated Power (30Hz)

Compression space

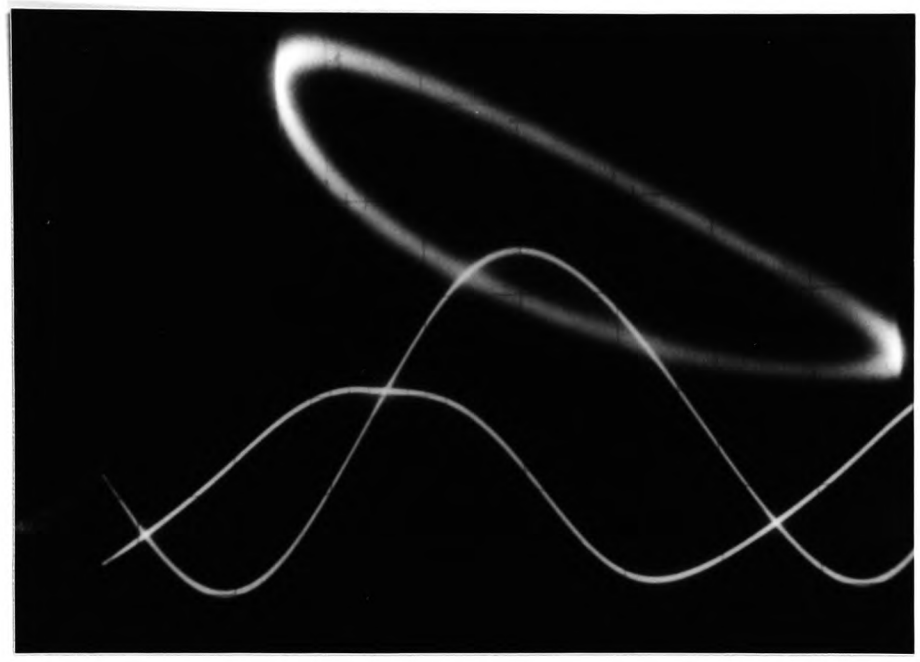

Compression space (displacer stationary)

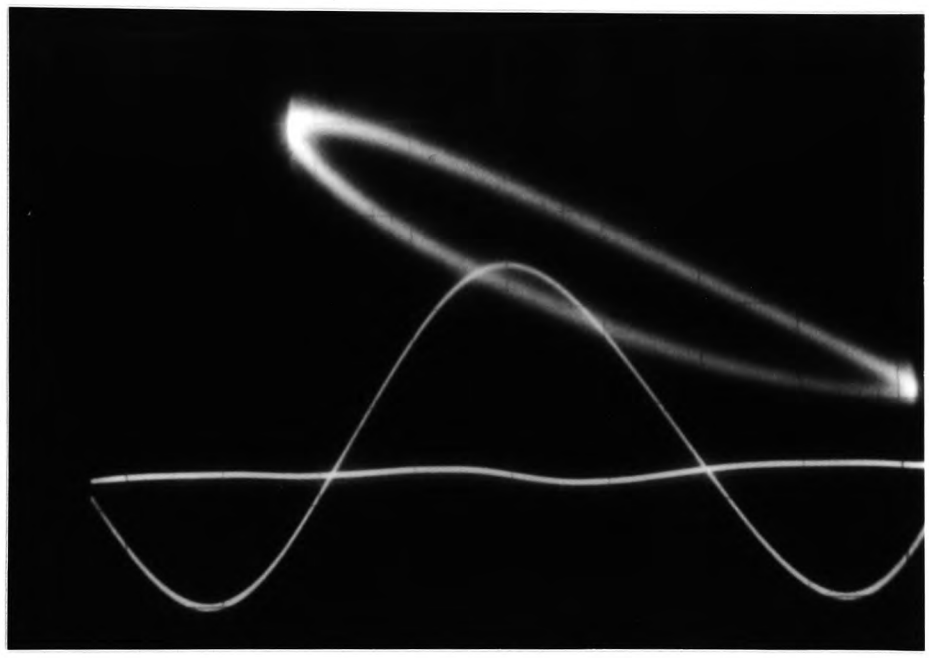

Expansion space

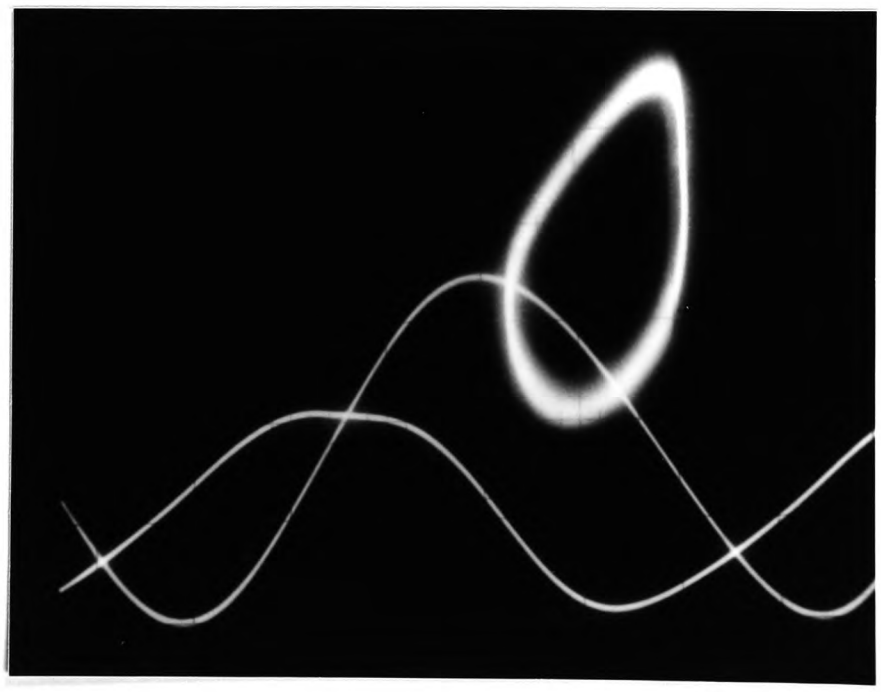

Figure 6.19 Indicated Power (40Hz)

Compression space

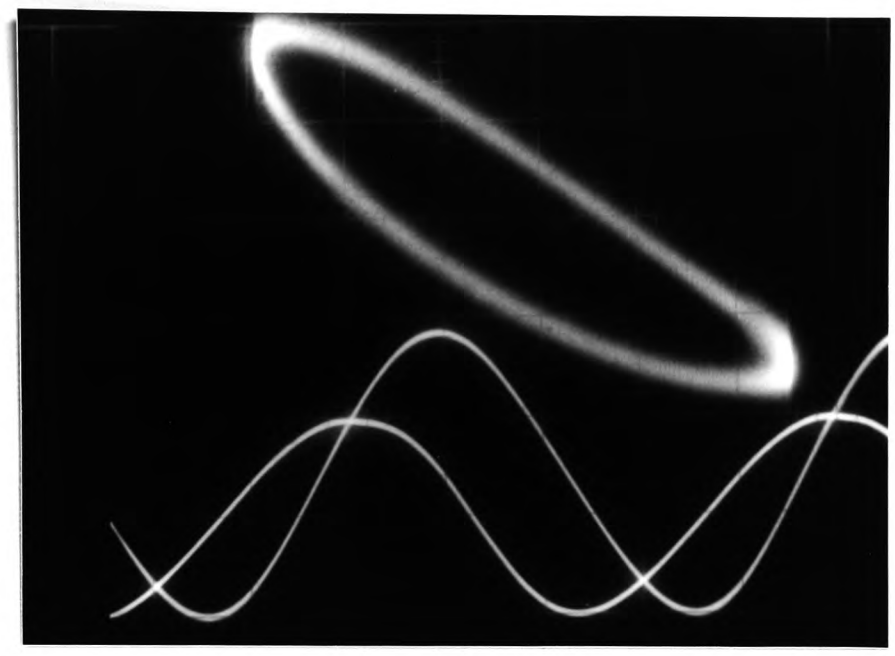

:ompression Space (displacer stationary)

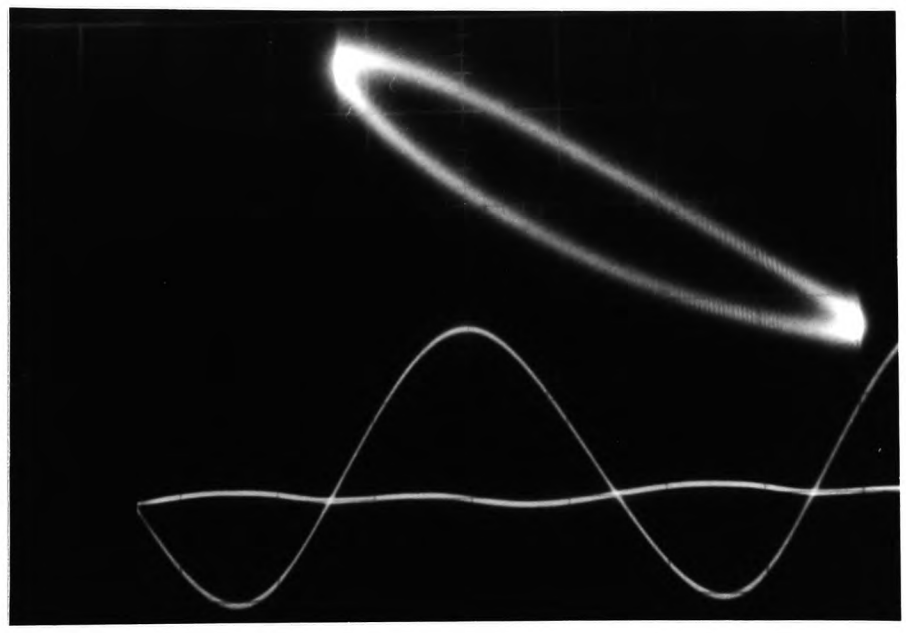

Expansion Space

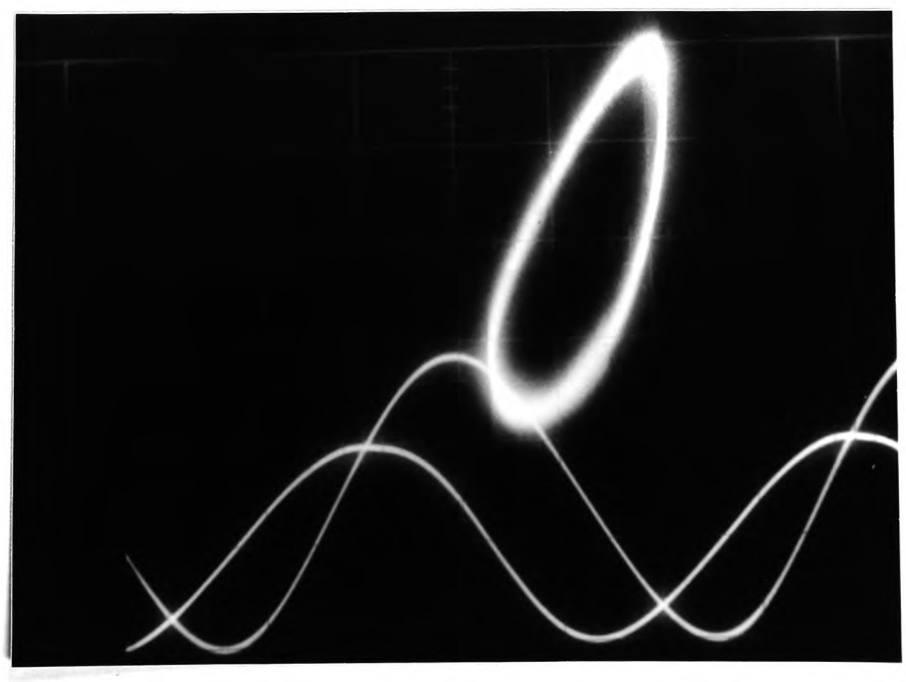

Figure 6.20 Indicated Power (50Hz)

Compression Space

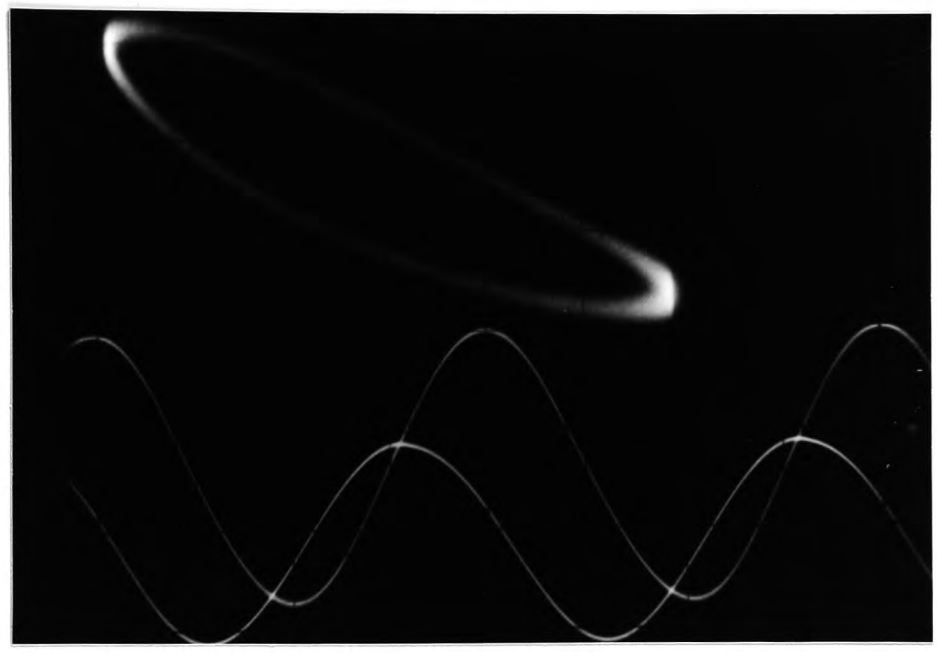

Compression Space (displacer stationary)

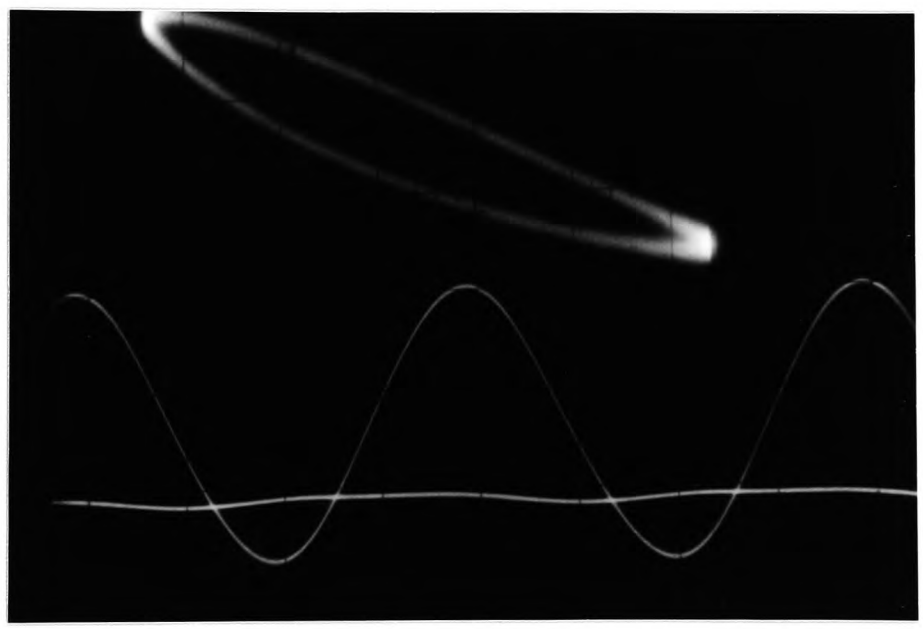

Expansion Space

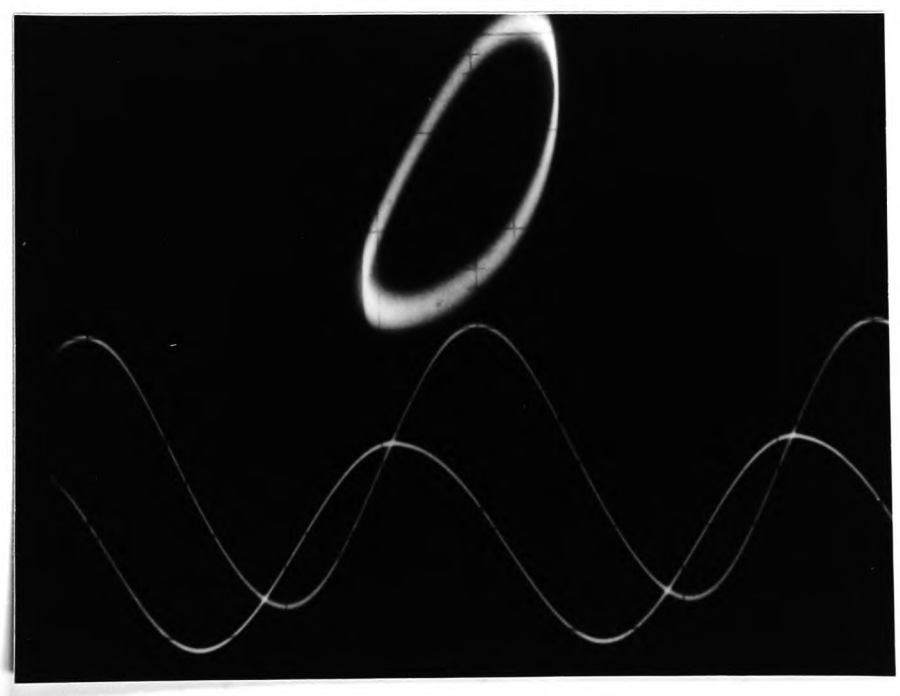

Table 6.1 Refrigerator Performance (250 mesh regenerator)

Frequency Hz	Cold end T K	Filling Pressure bar (abs)	W_{tot} $-I^2R$ W	Wi W	Wg W	Useful Refrig-eration W	Displacer Loss W	Static Losses W	Total Refrig-eration W	Indicated Refrig-eration W	η/η carnot	ΔT_c (to give $\eta_c = \eta$)
30	72	11.6	18.9	11.0	7.9	0.58	.80	.49	1.87	2.17	.87	7.3
30	90	11.6	19.6	12.7	6.9	1.10	.68	.48	2.26	2.43	.82	11.9
30	120	11.6	19.2	13.4	5.8	1.75	.76	.44	2.95	2.92	.76	19.5
40	72	11.6	19.7	11.4	8.3	.60	1.12	.49	2.21	2.36	.90	5.6
40	90	11.6	19.9	12.8	7.1	1.05	.90	.48	2.43	2.54	.83	11.0
40	120	11.6	19.0	13.2	5.8	1.75	.84	.44	3.03	3.09	.80	16.8
50	72	11.6	19.5	10.6	8.9	.58	1.32	.49	2.39	2.65	.94	1.6
50	90	11.6	19.9	11.8	8.1	1.05	1.35	.48	2.88	2.98	.86	9.3
50	120	11.6	19.9	14.0	5.9	1.73	1.28	.44	3.45	3.41	.86	10.1
30	72	10.2	19.6	11.1	8.5	.61	.80	.49	1.90	2.34	.87	7.2
30	90	10.2	18.9	12.2	6.7	1.05	.83	.48	2.36	2.45	.85	9.7
30	120	10.2	18.3	12.9	5.4	1.52	.62	.44	2.58	2.80	.78	17.6
40	72	8.1	20.1	11.3	8.8	.58	.94	.49	2.01	2.44	.88	6.8
40	90	8.1	21.1	14.2	6.9	1.08	.73	.48	2.29	2.60	.88	7.9
40	120	8.1	19.9	15.0	4.9	1.63	.67	.44	2.74	2.70	.83	13.4

Table 6.2 Refrigerator Performance (150 mesh regenerator)

Frequency Hz	Cold end T K	Filling Pressure bar (abs)	W_{tot} $-I^2R$ W	Wi W	Wg W	Useful Refrig-eration W	Displacer Loss W	Static Losses W	Total Refrig-eration W	Indicated Refrig-eration W	η/η carnot	ΔT_c (to give $\eta_c = \eta$)
40	72	8.1	20.4	11.8	8.6	0.56	1.18	.48	2.22	2.42	.89	6.1
40	90	8.1	20.3	13.2	7.1	1.00	.94	.44	2.38	2.46	.81	12.8
40	120	8.1	18.5	13.2	5.3	1.50	.72	.40	2.62	2.67	.76	19.5
40	72	10.2	18.0	9.2	8.8	.49	1.28	.48	2.25	2.46	.88	6.5
40	90	10.2	19.0	11.1	7.9	1.07	1.00	.44	2.51	2.79	.82	11.7
40	120	10.2	18.8	12.4	6.4	1.70	.76	.40	2.86	2.98	.70	24.7
40	72	11.6	20.7	11.7	9.0	.60	1.43	.48	2.51	2.61	.93	4.6
40	90	11.6	19.4	11.8	7.6	1.10	1.10	.44	2.64	2.94	.90	6.3
40	120	11.6	19.4	13.0	6.4	1.85	.87	.40	3.12	3.20	.75	20.0

CHAPTER 7

DISCUSSION AND FUTURE WORK

7.1 DISCUSSION

The performance of miniature refrigerators has been shown to be governed by the heat transfer processes involved in their operation. Any improvement in performance can only be achieved by an understanding of these losses and quantative analysis of their dependence on machine parameters.

In Chapter 3, the sources of heat transfer and pressure drop losses particularly relevant to Stirling cycle refrigerators were described, and it was seen that the existing models of cooler performance require particular knowledge of the heat transfer between the working fluid and the regenerator matrix. Data have been accumulated for various regenerator configurations, much of them for large scale devices for industrial cooling plant and furnaces, and many workers have developed sophisticated transient flow techniques in order to assess the behaviour of rapidly cycled regenerators for cryocooler applications.

The problem common to these techniques, that of accurately measuring transient gas temperatures, was outlined in Chapter 4, where data obtained using a simpler steady flow method was presented. It can be seen that these data give reasonable agreement with those from transient tests, and that there is similar scatter in the measurements.

Pressure drop measurements were also performed and the data obtained give good agreement with the model for flow in a packed bed, equation (4-13). The data obtained for the oscillating flow in the refrigerator also fit with this expression.

Although the heat transfer correlations obtained by these techniques are of use when dealing with problems involving large heat exchangers, and the methods outlined here enable experiments to be performed quickly, they are a far from satisfactory basis for prediction of regenerator performance in miniature refrigerators, where the resolution required for adequate models is much greater. For this reason the techniques described in Chapter 5, which enable measurements of the individual components of losses to be made in a way that is directly relevant to the machine performance, have been developed.

The data presented in Chapter 4 do, however, allow comparison between different matrices, and may be of use in the preliminary selection of new geometries for regnerators, such as the metal foam described here, in order to assess whether trials in a refrigerator would be worthwhile.

The experimental methods described in Chapter 5 include many checks to ensure that the data obtained is self-consistant.

The assumption that the only significant loss in the compressor is that due to Joule heating in the coil is justified both by the fact that the areas of the indicator diagrams in the compression space are almost equivalent to $P_{tot}-I^2R$ under many different conditions, and also from the graph of Figure 5.2, which is a straight line through the origin, implying no frequency dependent losses. The slight discrepancy between the indicated power and that measured from $P_{tot}-I^2R$ can be explained by pneumatic driving and the very small amount of windage in the compressor.

The graph of Figure 5.2 also justifies the assumption that the pressure in the system is uniform. In section 6.2 it was seen that losses due to pressure drop are dependent on the second or third power of the frequency, so that if they were significant the graph would deviate from a straight line. Measurement of the pressure at both ends of the connecting pipe between compressor and displacer, and the pressure drop across the displacer, confirms this result.

Good agreement is obtained for the total refrigeration produced, calculated both from the sum of refrigeration losses and useful refrigeration, and from the area of the P-V loop at the cold end. The discrepancy between this value and that predicted from Carnot can be explained by the existance of a temperature difference between the gas and the cold end flange. The methods used to measure and separate the

displacer losses are validated both by this good agreement between the measured and indicated refrigeration, and also by the shuttle heat transfer data which fit the theory very well. These data are obtained after the pressure drop losses, which also fit theoretical predictions, have been subtracted from the measured displacer losses, and the good agreement with theory obtained implies that the methods used are accurate.

These considerations imply that no significant loss in this refrigerator has been overlooked and therefore that the resulting energy balance given by equation (6-9) is valid for this machine.

The energy balance can be used as a basis of a design model, and also as a powerful diagnostic tool in development work. Unexpected deteriorations (or even improvements!) in performance can be traced using the methods described in Chapter 5.

7.2 FUTURE WORK

The work discussed above could obviously be extended to investigate the effects of phase angle and dead volume, and further detail, particularly with regard to the empirical model of regenerator losses could be added to the energy balance. It would also be of great interest to apply the similar experimental techniques to machines of different design. However the energy balance is at present capable of showing the most profitable areas in which to concentrate development effort.

From the distribution of energy loss given in Tables (6.1) and (6.2), it can be seen that a major loss in this refrigerator is that due to irreversible compression. Any improvement in this area could greatly increase overall efficiency. For example, if the loss due to irreversible compression could be reduced by 1W (approximately 8%), the total refrigeration could be increased by about 0.43W at 90K, (typically 17%), furthermore, if the refrigeration losses were kept approximately constant then the gain in useful refrigeration could be as much as 40%. Improvements could be made by 'isothermalizing' compression, possibly by the inclusion of a heat exchanger inside the piston and/or cylinder, and also by the use of forced convection in cooling the compressor body, where the proposed application allows.

The importance of shuttle heat transfer can also be seen from Tables (6.1) and (6.2). From the data in Figure (6.8) and those given in the text, it can be seen that for this refrigerator, the governing component in the shuttle heat loss is the conduction across the gas gap, so that there is little to be gained by using different displacer and wall materials to change their diffusivities (in any case, there are few materials presently available which have the required wear properties, and most have similar thermal properties) compared with the decrease in shuttle heat loss that would arise from increasing the width of the clearance gap. It is clearly desirable to have the largest clearance possible, commensurate with the gas seal required.

It would appear that overall regenerator performance could be improved by stacking the matrix with fine mesh gauze at the cold end, and coarser mesh at the warm end. In this way the pressure drop across the regenerator could be kept low while allowing a large surface area for heat transfer. Preliminary investigations into such regenerators are being carried out and have yielded promising results.

In this refrigerator, matrix heat capacity is not a problem at the required operating temperature. However for low temperature applications this could become a problem and the most commonly used regenerator in this temperature range, one composed of lead spheres, does not appear to be the ideal solution, both because of the high pressure drop across such a geometry, and because of the low apparent surface area, highlighted in Chapter 4. Research into other geometries for these applications is obviously a priority, and an area in which the methods presented here would be an asset.

It is hoped that future development of miniature cryocoolers will result in significant progress, and that the efficiency, reliability, and simplicity (and therefore cost) of such machines will thereby improve. If these aims can be achieved, it seems certain that there will be a considerably wider range of applications for these machines.

Similar experimental techniques to those described here could be applied to other cyclic machines, such as heat pumps, and bring greater understanding of their real, as opposed to ideal, operation.

REFERENCES

[1] RADEBAUGH, R. "Refrigeration Fundamentals: A View toward new refrigeration systems"
NBS Special Publication 508 (1978)

[2] WALKER, G. "Cryocoolers" Volumes 1 and 2
Plenum Press (1983)

[3] KÖHLER, J.W.L., "The Stirling Refrigerator Cycle"
Scientific American, Vol.212 no.4 (1965)

[4] COLLINS, S.C., "Early History and Development of Cryogenics"
Cryogenic Technology Vol.4 no.4 (1968)

[5] BAILEY, C.A., " Advanced Cryogenics"
Plenum Press (1971)

[6] HASLEDEN, C.G., "Cryogenic Fundamentals"
Academic Press (1971)

[7] FUJITA, T., SUZUKI, M., IKEGEWA, S., OHTSUKA, T., ANAYAMA, T., "High Temperature Operation of Nb_3Ge SQUIDs"
Proceedings ICEC 9, Kobe (1982)

[8] BEASLEY, M.R., "Progress Report on High-T_c Superconducting devices"
NBS Special Publication 508 (1978)

[9] MASON, P.V., "Space Cryogenics in the 1980's"
Proceedings ICEC8, Genova (1980)

[10] VORREITER, J.W., "Cryogenic System for Spacecraft"
Contemporary Physics Vol.21 no.3 (1981)

[11] SHERMAN, A., "National Aeronautics and Space Administrative Needs and Trends in Cryogenic Cooling"
Cryogenics July 1980

[12] WATSON, K. "Geologic Applications of Thermal Infrared Imaging"
Proceedings of the IEEE January 1975

[13] NAKANO, I., EMARA, T.,HOLTA, T.,TOMODA, Y.,NAGANO, H., "Ocean Bottom SQUID Magnetometers"
Proceedings ICEC10 Helsinki (1984)

[14] HUDSON Jr, R. D., HUDSON, J.W., "The Military Applications of Remote Sensing by Infrared"
Proceedings of the IEEE Vol.63 no.1 (1975)

[15] HAYWARD, H.T., "Cryogenic Cooling of Electronic Components for Military Purposes"
Electronic Components June 1980

[16] DAVY, J.R., "Medical Applications of Thermography"
IEE Low Light and Thermal Imaging (1975)

[17] WILLIAMSON, S.J., KAUFMAN, L., "Application of SQUID Detectors in Biomagnetism"
NBS Special Publication 508 (1978)

[18] KLIPPING, G., KLIPPING, I., MIERSCH, J., "Simple Instruments for Cryosurgery"
Proceedings ICEC9 Kobe (1982)

[19] HAARHUIS, G. J., "The Application of Stirling Cryogenerators in Medical Whole Body NMR Scanning"
Proceedings ICEC10 Helsinki (1984)

[20] FUJITA, T., OHTSUKA, T., ISHIZAKI, Y., "Japanese Activities in Refrigeration Technology"
Cryogenics July 1983

[21] VAN DER HOEVEN, B.J.C., ANACKER, W., "Refrigeration Requirements for Potential Josephson Data Processing Systems"
NBS Special Publication 508 (1978)

[22] LUNHOLM Jr, J.G., "NASA Low and Ultralow Temperature Cryogenic Cooler Systems for Space Missions"
ISA Transactions Vol 19 no.1

[23] JENSEN, H.L., NAST, T.C., GLASSFORD, A.P.M., "Closed-cycle Cryogenic Refrigerators for Space Applications"
Applications of Cryogenic Technology 4

[24] DONOHOE, M., SHERMAN, A., "Radiant Coolers - Theory, Flight History, Design Comparisons and Future Applications"
AIAA 13th Aerospace Sciences Meeting (1975)

[25] KISLOV, A.M., SALENKOV, V.Ya., YASTRGEMBSKY, A.L., "Efficiency of Space Radiators for Cooling Shields in Cryostat Insulation"
Proceedings ICEC10 Helsinki (1984)

[26] KARR, G.R., HENDRICKS, J.B., URBAN, E.W., KUTZ, L., LANDNER, D., "Cryogenic Sub-system Performance of the Infrared Telescope for Space Lab 2"
Proceedings ICEC8 Genova (1980)

[27] HIGA, W.H., WIEBE, E., "One Million Hours at 4.5 Kelvin"
NBS Special Publication 508 (1978)

[28] NAES, L.G., NAST, T.C., "Long-life Orbital Operation of Stirling-cycle Mechanical Refrigerators"
Proceedings ICEC8 Genova (1980)

[29] GRENIER, M., "Cryogenic Liquid Production Plant of Large Tonnage"
Proceedings ICEC8 Genova (1980)

[30] JAKOB, M., "Heat Transfer" Volume 2
Wiley and Sons (1957)

[31] MCADAMS, W.H., "Heat Transmission"
McGraw-Hill (1954)

[32] GROSSMAN, D.G., LANNING, J.G., "Aluminous Keatite Ceramic Regenerators"
American Ceramic Society Bulletin Vol 156 no.5

[33] CARNOT, S.M.L., "Réflexions sur la Puissance Mortice du Feu At sur les Machines propres à Développer cette Puissance"
(translation by THURSTON R.H.)
Transactions ASME (1943)

[34] KIRK, A.G.
Minutes Proceedings of the Institute Civil Engineers 37 (1873/4)

[35] RICHARDSON, R.N., "Pulse Tube Refrigeration, an Investigation Pertinent to Cryocooler Development"
D.Phil Thesis Oxford University (1982)

[36] CHELLIS, F., "Design Compromises in the Selection of Closed-cycle Coolers"
NBS Special Publication 508 (1978)

[37] KÖHLER, J.W.L., JONKERS, C.O., "Fundamentals of the Gas Refrigerating Machine"
Philips Technical Review no.16 (1954)

[38] MEIJER, R.J., "The Philips Hot-gas Engine with Rhombic Drive Mechanism"
Philips Technical Review no.20 (1959)

[39] WHITE, R., HASKIN, H., "Development Approaches for Long-life Cryocoolers"
Nbs Special Publication 607 (1980)

[40] DANIELS, A., STOLFI, F., SHERMAN, A., GASSER, M., "Magnetically Suspended Stirling Cryogenic Space Refrigerator"
Advances in Cryogenic Engineering Vol 29

[41] DAVEY, G., "The Oxford University Miniature Cryogenic Refrigerator"
IEE International Conference on Advanced Infrared Detectors and Systems London (1982)

[42] ZIMMERMAN, J.E., RADEBAUGH, R., SIEGWARTH, J.D. "Possible Cryocoolers for SQUID Magnetometers"
Proceedings International Conference on Superconducting Quantum Devices
West Berlin (1976)

[43] MCMAHON, H.O., GIFFORD, W.E., "A New Low Temperature Gas Expansion Cycle"
Advances in Cryogenic Engineering Vol 5 (1960)

[44] DANIELS, A., DU PRÉ, F.K., "Triple Expansion Stirling-cycle Refrigerator"
Advances in Cryogenic Engineering Vol 16 (1970)

[45] ZIMMERMAN, J.E., SULLIVAN, D.B., "A Milliwatt Stirling Cryocooler for Temperatures Below 4K"
Cryogenics March 1979

[46] PRAST, G., "A Gas Refrigerating Machine for Temperatures down to 20K and Lower"
Philips Technical Review 26 (1965)

[47] STUART, R.W., COHEN, B.M., HARTWIG, W.H., "Operation and Application of a Three-Stage Closed-cycle Regenerative Refrigerator in the 6.5K Region" Advances in Cryogenic Engineering vol 15 (1969)

[48] HUNG, C.S., "Cryogenics in China Today" Proceedings ICEC8 Genova (1980)

[49] MYRTLE, K., WINTER, C., GYGAX, S., "A 9K Conical Stirling-cycle cryocooler" Cryogenics March 1982

[50] NAKASHIMA, H., ISHIBASHI, K., ISHIKAZI, Y., "Stirling Cycle Refrigerator Test Result Below 5K" Proceedings ICEC10 Helsinki (1984)

[51] VINCENT, D.A., "Closed-cycle Refrigeration for a Superconducting susceptometer" NBS Special Peblication 508 (1978)

[52] SHERMAN, A., "Crogenic Cooling for Spacecraft Sensors, Instruments, and Experiments" AIAA (1978)

[53] SCHMIDT, G., "Theore der Lehmannschen Calorischen Maschine" Z. Verbdt. Ing. Vol 15 no.1 (1871)

[54] WALKER, G., "Stirling Engines" Clarendon Press (1980)

[55] HALPERN, V., SHTRIKMAN, S., "Comparison of the Theoretical Performance of Regenerative Refrigerators in the Adiabatic and Isothermal Regimes" Cryogenics December 1980

[56] FINKELSTEIN, T., "A Thermodynamic Analysis of Stirling Engines" SAE Paper no.118B (January 1960)

[57] WALKER, G., KHAN, M., "Theoretical Performance of Stirling-Cycle Engines"
SAE Paper no.949A

[58] RIOS, A., SMITH Jr, J.L., QVALE, E.B., "An Analysis of the Stirling-cycle Refrigerator"
Advances in Cryogenic Engineering Vol 14 (1968)

[59] CHELLIS, F.F., HOSMER, T.P., KELLER, E., "Closed-Cycle Refrigeration for an Airborn Illuminator"
Advances in Cryogenic Engineering Vol 16 (1970)

[60] FINKELSTEIN, T., "Computer Analysis of Stirling Engines"
Advances in Cryogenic Engineering Vol 20

[61] WALKER, G., VASISHTA, V., "Heat Transfer and Flow Friction Characteristics of Dense-mesh, Wire-screen, Stirling-cycle Regenerators"
Advances in Cryogenic Engineering Vol 16 (1970)

[62] KIRKLEY, D.W., "A Thermodynamic Analysis of the Stirling cycle and a comparison with Experiment"
SAE Paper 949B
International Automotive Engineering Congress
Detroit 1965

[63] HARRIS, W.S., RIOS, P.A., SMITH Jr,J.L., "The Design of Thermal Regenerators for Stirling-type Refrigerators"
Advances in Cryogenic Engineering Vol 16 (1970)

[64] COPPAGE, J.E., LONDON, A.L., "The Periodic-flow Regenerator, a Summary of Design Theory"
Transactions ASME Vol 75 (1953)

[65] HAUSEN, H., "Wärmeübertragung in Gegenetrom, Gleichstrom und Kreuzstrom"
Springer, Berlin (1950)

[66] NUSSELT, W., "Der Berharrungszustand in Winderhitzer"
Z. Ver. Dt. Ing Vol 27 (1928)

[67] ILLIFE, C.E., "Thermal Analysis of the Contra-flow Regenerative Heat Exchanger"
Proceedings I.Mech.E Vol 159 (1948)

[68] SANDERS, O.A., SMOLENIEC, S., "Heat Transfer in Regenerators"
IME-ASME General Discussion on Heat Transfer,
London (1957)

[69] GRANVILLE, W.H., MACDONALD, W.F., CULTER, P.,
3rd International Heat Transfer Conference Vol 4
Science Press Inc. (1966)

[70] LARSON, F.W., "Rapid Calculation of Temperature in a Regenerative Heat Exchanger having Arbitrary Initial Solid and Entering Fluid Temperatures"
International Journal Heat Mass Transfer Vol 10 (1967)

[71] HARNESS, J.B., NEWMANN, P.E.L., "Digital Computer Simulation of Voidage in a Regenerator"
Advances in Cryogenic Engineering Vol 25

[72] REA, S.N., SMITH Jr, J.L., "The Influence of Pressure Cycling on Thermal Regenerators"
Journal of Engineering for Industry

[73] QVALE, E.B., SMITH Jr, J.L., "An Approximate Solution for the Performance of a Stirling-Engine Regenerator"
Transactions ASME, Journal Engineering for Power
April 1969

[74] RIOS, P.A., SMITH Jr, J.L., "The Effect of Variable Specific Heat of the Matrix on the Performance of Thermal Regenerators"
Advances in Cryogenic Engineering Vol 13 (1968)

[75] DANEY, D.E., RADEBAUGH, R., "Non-Ideal Regenerator Performance - the Effect of Void Volume Fluid Heat Capacity"
Cryogenics September 1984

[76] EDER, F.X., "A Regeneerator with an Iron Whisker Matrix"
Advances in Cryogenic Engineering Vol 23

[77] WALKER, G., "Operations Cycle of the Stirling Engine with Particular Reference to the Function of the Regenerator"
Journal Mechanical Engineering Science Vol 3 (1961)

[78] GIFFORD, W.E., ACHARYA, A., ACKERMANN, R.A., "Compact Cryogenic Regenerator Performance"
Advances in Cryogenic Engineering Vol 14 (1968)

[79] ACKERMANN, R.A., GIFFORD, W.E., "Small Cryogenic Regenerator Performance"
Journal of Engineering for Industry February 1969

[80] GIFFORD, W.E., ACHARYA, A., "Low Temperature Regenerator Test Apparatus"
Advances in Cryogenic Engineering Vol 15 (1969)

[81] BRETHERTON, A., GRANVILLE, W.H., HARNESS, J.B., "Performance of Regenerators at Low Temperatures"
Advances in Cryogenic Engineering Vol 16 (1970)

[82] KAYS, W.M., LONDON, A.L., "Compact Heat Exchangers"
McGraw-Hill (1964)

[83] GUTFINGER, C., ABAUF, N., "Heat Transfer in Fluidised Beds"
Advances in Heat Transfer Vol 10 (1977)

[84] KREITH, F., "Principles of Heat Transfer"
International Textbook Company (1967)

[85] SCHMIDT,F.W., WILLMOTT, A.J., "Thermal Energy Storage and Regeneration"
McGraw-Hill (1981)

[86] WALKER, G., WAN, W.K., "Heat Transfer and Flow Friction Characteristics of Dense-Mesh Wire-Screen Regenerator Matrices at Cryogenic Temperatures"
Proceedings ICEC4, Eindhoven (1972)

[87] BARCLAY, J.A., OVERTON Jr, W.C., STEWART, W.F., SUNIL SARANGI, "Experiment to Determine Properties of Packed Particle Beds and Regenerators at Cryogenic Temperatures "
Advances in Cryogenic Engineering Vol 29

[88] QVALE, E.B., SMITH Jr, J.L., "A simple Correlation for the Heat Transfer Characteristics of a Family of Matrices Subjected to Complex Flow Conditions"
Cryogenics February 1969

[89] ZIMMERMAN, F.C., LONGSWORTH, R.C., "Shuttle Heat Transfer"
Advances in Cryogenic Engineering

[90] HARNESS, J.B., NEWMANN, P.E.L., "A Theoretical Solution of the Shuttle Heat Transfer Problem"
Proceedings ICEC4, Eindhoven (1972)

[91] RADEBAUGH, R., ZIMMERMAN, F.J., "Shuttle Heat Transfer in Plastic Displacers at Low Speeds"
NBS Special Publication 508 (1978)

[92] SCHNEIDER, P.J., "Conduction Heat Transfer"
Addison-Wesley (1955)

[93] SHAH, R.K., LONDON, A.L., "Laminar Flow Forced Convection in Ducts"
Advances in Heat Transfer, Supplement 1
Academic Press (1978)

[94] TONG, L.S., LONDON, A.L., "Heat Transfer and Flow Friction Characteristics of Woven-Screen and Crossed-Rod Matrices"
Transactions ASME Vol79 no.10 (1957)

[95] MIKULIN, E.I., SHEVICH, V.A., "Experimentalnoe Issledovania Teploobmena a Setchatich Matrizach"
Inzh. -Fiz, Zh. XXII (6) (1972)

[96] KAY, J.M., "An Introduction to Fluid Mechanics and Heat Transfer"
Cambridge University Press (1957)

[97] SCHWARTZ, C.E., SMITH, J.M., "Flow Distribution in Packed Beds"
Industrial and Engineering Chemistry
Vol 45 no.6 (1953)

[98] DAVEY, G., Private Communication

[99] ed. TOULOUKIAN, Y.S., BUYCO, E.H., "Thermophysical Properties of Matter"
The TPRC Data Series, IFI/Plenum (1970)

[100] COPPAGE, J.E. The Heat Transfer and Flow Friction Characteristics of Porous Media"
Ph.D. Thesis Stanford University (1952)

[101] GAMSON, B.W., THODOS, G., HOUGEN, O.A.
Transactions AIChE 39 (1943)

[102] WILKE, C.R., HOUGEN, O.A.
Transactions AIChE 41 (1945)

[103] DENTON, W.H., "The Heat Transfer and Flow Resistance through Randomly Packed Spheres"
I.Mech.Eng. and ASME London (1951)

[104] McCUNE,L.H., WILHELM, R.H.
Ind.Eng.Chem. 41 (1949)

[105] MEEK, R.M.G., "The measurement of Heat Transfer Coefficients in Packed Beds by the Cyclic Method"
International Heat Transfer Conference,
Boulder Colorado (1961)

APPENDIX A

THE SCHMIDT ANALYSIS

The following version of the Schmidt analysis has been taken from the comprehensive account of the analysis given by Walker, [2]. The assumptions made in the analysis have been stated in Chapter 3.

A.1 NOMENCLATURE

$A = (\tau^2 + 2\tau\kappa\cos\alpha + \kappa^2)$

$B = (\tau + \kappa + 2S)$

K = a constant

M = total mass of working fluid

N = machine speed

p = instantaneous cycle-pressure

p_{max} = maximum cycle-pressure

p_{mean} = mean cycle-pressure

p_{min} = minimum cycle-pressure

P = engine output

$P_{mass} = P/RT_c$, dimensionless power parameter based on the mass of working fluid

$P_{max} = P/(p_{max}V_T)$, dimensionless power parameter, based on the maximum cycle-pressure and combined swept volume

Q = heat transferred to the working fluid in the expansion space, i.e. the heat extracted

Q_{mass} = Q/RT_C, the dimensionless heat, based on the mass of working fluid

Q_{max} = $Q/(p_{max}V_T)$, the dimensionless heat, based on the maximum cycle-pressure

R = characteristic gas constant of the working fluid

S = $(2X\tau)/(\tau+1)$, reduced dead volume

T_C = temperature of the working fluid in the compression space, generally assumed to be 300K

T_D = temperature of the working fluid in the dead space

T_E = temperature of the working fluid in the expansion space

V_C = swept volume in the compression space

V_E = swept volume in the expansion space

V_D = total internal volume of heat exchangers, regenerator and associated ducts and ports, i.e. dead volume

V_T = $(V_C+V_E) = (1+\kappa)V_E$, combined swept volume

V_W = $0.5V_E(1+\cos\psi) + 0.5V_C[1+\cos(\psi-\alpha)] + V_D$, volume of total working space

V_{Wmax} = maximum volume of total working space

X = V_D/V_E, dead volume ratio

α = angle by which volume variations in the expansion space lead those in the compression space (in fractions of π radians)

δ = $(\tau^2+\kappa^2+2\tau\kappa\cos\alpha)/(\tau+\kappa+2S)$

θ = $\tan^{-1}[(\kappa\sin\alpha)/(\tau+\kappa\cos\alpha)]$

κ = V_C/V_E, swept volume ratio

$\tau = T_C/T_E$, temperature ratio

ψ = crank angle

Lower case subscripts refer to instantaneous values, upper case to maximum (or constant) values.

A.2 BASIC EQUATIONS

Volume of expansion space,

$$V_e = 0.5V_E(1+\cos\psi) \qquad \text{(A-1)}$$

Volume of compression space,

$$V_c = 0.5V_C[1+\cos(\psi-\alpha)] \qquad \text{(A-2)}$$

$$= 0.5\kappa V_E[1+\cos(\psi-\alpha)] \qquad \text{(A-3)}$$

Volume of dead space,

$$V_D = XV_E \qquad \text{(A-4)}$$

Mass of working fluid in expansion space,

$$M_e = (p_eV_e)/(RT_e)$$

Mass of working fluid in compression space,

$$M_c = (p_cV_c)/(RT_c)$$

Mass of working fluid in dead space,

$$M_d = (p_dV_d)/(RT_d)$$

The total mass in the system remains constant, so,

$$M_T = (p_e V_e)/(RT_e)+(p_c V_c)/(RT_c)+(p_d V_d)/(RT_d)$$

$$= (KV_E)/(2RT_c) \qquad (A-5)$$

If the instantaneous pressure is uniform in the system, and equal to p, and if T_e and T_c are constant at T_E and T_C then, substituting for the volumes and eliminating R,

$$K/p=(T_C/T_E)(1+\cos\varphi)+\kappa[1+\cos(\varphi-\alpha)]+(2V_D T_C)/(V_E T_D) \qquad (A-6)$$

If the temperature in the dead space is linear in the axial direction, then the mean temperature is,

$$T_D = T_C+0.5(T_E-T_C)$$

$$= (1+T_E/T_C)(T_C/2)$$

and, since $T_C/T_E=\tau$, then from equation (A1-6),

$$K/p=\tau(1+\cos\varphi)+\kappa[1+\cos(\varphi-\alpha)]+2S \qquad (A-7)$$

where $S = 2X\tau(\tau+1)$, the reduced dead volume.

Equation (A1-7) can be simplified, [2],

$$K/p = (\tau^2+2\tau\kappa\cos\alpha+\kappa^2)\cos(\varphi-\theta)+\tau+\kappa+2S)$$

where $\tan\theta = (\kappa\sin\alpha)/(\tau+\kappa\cos\alpha)$

Introducing the factors A and B, defined above,

$$K/p = A\cos(\varphi-\theta)+B$$

and

$$p = K/\{B[1+\delta\cos(\psi-\theta)]\}$$

The instantaneous pressure is a minimum when $\psi=\theta$, and a maximum when $\psi=\theta+\pi$. Therefore, $p_{min}=K/[B(1+\delta)]$, and $p_{max}=K/[B(1-\delta)]$.

Thus,

$$p = p_{max}(1-\delta)/[1+\delta\cos(\psi-\theta)] \qquad \text{(A-8a)}$$

$$= p_{min}(1+\delta)/[1+\delta\cos(\psi-\theta)] \qquad \text{(A-8b)}$$

and the pressure ratio, $p_r = P_{max}/p_{min}$

$$= (1+\delta)/(1-\delta) \qquad \text{(A-9)}$$

A.3 THE MEAN CYCLE PRESSURE

The mean cycle pressure is given by,

$$p_{mean} = (0.5\pi)\int_0^{2\pi} p \; d(\psi-\theta)$$

$$= (0.5\pi)\int_0^{2\pi} \{p_{max}(1-\delta)/[1+\delta\cos(\psi-\theta)]\} \; d(\psi-\theta)$$

which can be resolved to

$$p_{mean} = p_{max}\,[(1-\delta)/(1+\delta)] \qquad \text{(A-10)}$$

A.4 HEAT TRANSFERRED AND WORK DONE

The processes of compression and expansion are assumed to take place isothermally, so the heat transferred, Q, is equal to the work done, P,

$$Q = P = \int pdV$$

If $V = 0.5V_E(1+\cos\varphi)$,

$$dV = -0.5V_E \sin\varphi \, d\varphi \qquad \text{(A-11)}$$

and if $p = p_{mean}[1-\Delta\cos(\varphi-\theta)]$ (A-12)

approximately†, where,

$$\Delta = 2\delta/[1+ (1-\delta^2)]$$

then

$$Q = -0.5\int_0^{2\pi} \{p_{mean}V_E[1-\Delta\cos(\varphi-\theta)]\sin\varphi\} \, d\varphi$$

$$= -0.5p_{mean}V_E\int_0^{2\pi} [\sin\varphi-\Delta(\cos\varphi\cos\theta\sin\varphi+\sin\theta\sin^2\varphi)] \, d\varphi$$

$$= -0.5p_{mean}V_E \times$$

$$\{-\cos\varphi-\Delta[-0.5\cos\theta\cos2\varphi+\sin\theta(0.5\varphi-0.25\sin^2\varphi]_0^{2\pi}\}$$

$$= -0.5p_{mean}V_E[-\Delta\sin\theta.\varphi/2]_0^{2\pi}$$

$$= -0.5\pi p_{mean}V_E\Delta\sin\theta \qquad \text{(A-13)}$$

A.4.1 Expansion Space

The variation of volume in the expansion space follows the equation,

$$V_e = 0.5V_E(1+\cos\varphi)$$

which conforms with equation (A-11), therefore the heat

†It is possible to obtain the required expressions for heat transferred in the working spaces without invoking this approximation. See Walker, [2].

transferred in the expansion space, from equation (A-13), is,

$$Q = \pi p_{mean} V_E \delta \sin\theta / [1 + (1-\delta^2)] \qquad (A-14)$$

A.4.2 Compression Space

The variation of volume in the compression space follows the equation,

$$V_C = 0.5 \kappa V_E [1 + \cos(\phi - \alpha)]$$

and by a process similar to that above, the heat transferred in the compression space is given by,

$$Q_C = [\pi p_{mean} V_E \kappa \delta \sin(\theta - \alpha)] / [1 + (1-\delta^2)] \qquad (A-15)$$

dividing equation (A-15) by equation (A-14),

$$Q_C/Q = [\kappa \sin(\theta - \alpha)] / \sin\theta$$

$$= \kappa(\sin\theta\cos\alpha - \cos\theta\sin\alpha)/\sin\theta$$

$$= \kappa[(\cos\alpha - \sin\alpha)/\tan\theta]$$

but $\tan\theta = \kappa \sin\alpha(\tau + \kappa\cos\alpha)$, so

$$Q_C/Q = -\tau$$

The heat transferred in the expansion space is of opposite sign to that transferred in the compression space, and is numerically different by the temperature ratio τ. By analogy the work done in the two spaces has the same relationship, $P_C = -\tau P_E$, and the net power is,

$P = P_E + P_C = (1-\tau)Q$

For a refrigerator, $T_E < T_C$, i.e. $\tau > 1$, and

Coefficient of performance = heat extracted/work done

$$= Q/(Q-Q_C) = 1/(1-\tau)$$

$$= T_E/(T_E-T_C) \qquad \text{(A-16)}$$

which corresponds to the Carnot efficiency.

A.5 MASS DISTRIBUTION IN THE MACHINE

From the characteristic gas equation, $M = pV/RT$,

where

$$p = p_{mean}\sqrt{(1-\delta^2)}/[1+\delta\cos(\psi-\theta)]$$

For the expansion space, $V_e = 0.5V_E(1+\cos\psi)$

The instantaneous mass of working fluid in the expansion space is,

$$M_e = \frac{0.5V_E p_{mean}\sqrt{(1-\delta^2)}(1+\cos\psi)}{RT_E[1+\delta\cos(\psi-\theta)]^2}$$

The rate of change of mass of working fluid in the expansion space is,

$$\frac{dM_e}{d\psi} = \frac{V_E p_{mean}\sqrt{(1-\delta^2)}\{\delta[\sin(\psi-\theta)-\sin\theta]-\sin\psi\}}{2RT_E[1+\delta\cos(\psi-\theta)]^2}$$

For the compression space where $V_C=0.5\kappa V_E[1+\cos(\psi-\alpha)]$,

The instantaneous mass of gas in the compression space is,

$$M_C = \frac{0.5\{\kappa V_E p_{mean}\sqrt{(1-\delta^2)}[1+\cos(\psi-\alpha)]\}}{2RT_C\{1+\delta\cos(\psi-\theta)]}$$

The rate of change of mass of working fluid in the compression space is,

$$\frac{dM_C}{d\psi}=\frac{\kappa V_E p_{mean}\sqrt{(1-\delta^2)}\{\delta[\sin(\psi-\theta)+\sin(\alpha-\theta)-\sin(\theta-\alpha)]\}}{2RT_C[1+\delta\cos(\psi-\theta)]^2}$$

For the dead space, $V_D=XV_E$=constant

The instantaneous mass of working fluid in the dead space is,

$$M_d=\frac{[XV_E p_{mean}\sqrt{(1-\delta^2)}]}{RT_D[1+\delta\cos(\psi-\theta)]}$$

The rate of change of mass of working fluid in the dead space is,

$$\frac{dM_d}{d\psi} = \frac{[XV_E p_{mean}\sqrt{(1-\delta^2)}\delta\sin(\psi-\theta)]}{RT_D[1+\delta\cos(\psi-\theta)]^2}$$

The total mass of working fluid, M_T, is a constant, so

$$dM_e + dM_c + dM_d = 0 \text{ and}$$

$$M_T = \frac{V_E p_{mean}\sqrt{(1-\delta^2)}\{\tau(1+\cos\psi)+\kappa[1+\cos(\psi-\theta)]+2S\}}{2RT_c[1+\delta\cos(\Psi-\theta)]}$$

and when $\psi = 0$,

$$M_T = \frac{V_E p_{mean}\sqrt{(1-\delta^2)}[\tau+S+(\kappa/2)(1+\cos\alpha)]}{RT_c(1+\delta\cos\theta)}$$

APPENDIX B

SHUTTLE HEAT TRANSFER THEORY

B.1 GAS CONDUCTION

This derivation is taken from the work of Zimmerman and Longsworth, [89], and Radebaugh and Zimmerman, [91].

The assumptions made in the derivation of the gas conduction component of shuttle heat transfer are as follows,

(1) Estimated average values of properties that greatly vary with temperature are used.

(2) The thermal capacities of the displacer and wall materials are assumed to be infinite.

(3) The effects of gas-pressure are ignored, (i.e. the heat transfer across the gas gap is due to the conductivity of the gas only).

(4) The interaction of longitudinal conduction in the displacer and wall is neglected.

(5) The displacer is at top dead centre for half the cycle and at bottom dead centre for the other half-cycle.

On the basis of assumptions (1) and (4), the temperature gradients in the displacer and wall are assumed to be linear, and when the displacer is in the mid-stroke position, the gradients are matched. The temperature gradient is thus,

$$\frac{(T_{hot} - T_{cold})}{L_d}$$

and the temperature difference between the displacer and the wall when the displacer is at either end position is,

$$\Delta T = \frac{(T_{hot} - T_{cold})}{L_d} \times \frac{S}{2}$$

The heat transferred per half cycle of time $\Delta\tau$, using assumption (3), is,

$$Q = \frac{k_g A \Delta T \ \Delta\tau}{t}$$

where t is the width of the clearance gap, and A is the surface area of the cylinder,

$$A = \pi D_d L_d$$

and the half cycle time is $\Delta\tau = 1/(2f)$

The total heat transfer per half cycle is therefore,

$$Q = \frac{k_g \pi D_d S}{4f} \frac{(T_{hot} - T_{cold})}{t} \qquad (B\text{-}1)$$

The rate at which heat is transferred from the hot end of the cylinder to the cold end depends on,

(i) How much heat is transferred between displacer and wall per cycle.

(ii) How far on average energy is transported during each cycle, $\bar{X}$.

(iii) The cycle rate.

(iv) The distance between the hot and cold ends.

thus the gas conduction component of shuttle heat transfer, Q_s, is given by,

$$Q_g = \frac{Q\bar{X}f}{L} \qquad (B\text{-}2)$$

Substituting equation (B-1) into equation (B-2),

$$Q_g = \frac{k_g \pi D_d S^2}{4t} \frac{(T_{hot} - T_{cold})}{L_d}$$

For sinusoidal displacer motion the heat transferred will be the rms value ($1/\sqrt{2}$) of that with square wave motion, so

$$Q_g = \frac{k_g \pi D_d S^2 \ (T_h - T_c)}{5.66t \qquad L_d}$$

B.2 CONDUCTION INTO DISPLACER

The problem of conduction into the displacer material is one of sinusoidal temperature variations on the surface of a semi-infinite solid, and is treated by Schneider, [92], who gives the heat transferred during one half of the cycle as,

$$Q = 2A\Delta T_o \sqrt{[(k_d c_d \rho_d)/(2\pi f)]}$$

where $\Delta T_o = \frac{dT}{dx} (S/2)$ is the peak of the temperature fluctuation, and $A = \pi D_d S$

During one half cycle the heat transferred will be,

$$Q = D_d S^2 \frac{dT}{dx} \sqrt{[(\pi k_d c_d \rho_d)/(2f)]}$$

The average shuttle heat transfer, with f cycles per second, then becomes,

$$Q_d = fD_dS^2\frac{dT}{dx}\sqrt{[(\pi k_d c_d \rho_d)/(2f)]}$$

$$= D_dS^2\frac{(T_h-T_c)}{L_d}\sqrt{[(f\pi k_d c_d \rho_d)/2]} \qquad \text{(B-3)}$$

assuming a linear temperature gradient in the displacer. This analysis also assumes that the penetration depth, λ, given approximately by,

$$\lambda = \sqrt{[k_d/(f\pi c_d \rho_d)]}$$

is considerably smaller than the thickness of the displacer material. In this case, λ at 40Hz and with a cold end temperature of 90K, is approximately 0.02mm, and the thickness of the Fluorosint of the displacer is over 1.0mm, so that this condition is satisfied.

B.3 TOTAL SHUTTLE HEAT TRANSFER

Considering the two thermal resistances (that of gas conduction, and that of conduction into the displacer) to be in series, the shuttle heat trasnfer, Q_s, is given by,

$$\frac{1}{Q_s} = \frac{1}{Q_g} + \frac{1}{Q_d}$$